



**REPUBLIC OF IRAQ
MINISTRY OF HIGHER EDUCATION
AND SCIENTIFIC RESEARCH**

**AI-FURAT AL-AWSAT TECHNICAL
UNIVERSITY
ENGINEERING TECHNICAL
COLLEGE- NAJAF**

**PERFORMANCE ENHANCEMENT OF
DOUBLE GAIN CHAIN FIBER LASER**

HAIDER YAHYA SAEED

**(M.Sc Communication Techniques
Engineering)**

2022



**PERFORMANCE ENHANCEMENT OF DOUBLE GAIN CHAIN
FIBER LASER**

THESIS

**SUBMITTED TO THE
(COMMUNICATION TECHNIQUES
ENGINEERING DEPARTMENT)**

**IN PARTIAL FULFILLMENT OF THE
REQUIREMENTS FOR THE DEGREE
OF (MASTER OF COMMUNICATION)**

BY

HAIDER YAHYA SAEED

Supervised by

Prof.Dr. Ali Abdul Abas Al Bakri

Lecturer Dr. Husam Noman Mohammed Ali

November /2022

Supervisor Certification

we certify that this thesis titled " **Performance Enhancement Of Double Gain Chain Fiber Laser** " which is being submitted by Haider Yahya Saeed was prepared under our supervision at the Communication Techniques Engineering Department, Engineering Technical College-Najaf, Al-Furat Al Awsat Technical University, as a partial fulfillment of the requirements for the degree of Master of Technical in Communication Engineering.

Signature:

Name: Lecturer Dr. Husam Noman Mohammed Ali
(Supervisor)

Date : / / 2022

Signature:

Name: Prof. Dr. Ali Abdul Abas Al Bakri
(Supervisor)

Date: / / 2022

I submit this thesis for the examining committee's consideration based on the available suggestion.

Signature:

Name: **Prof. Dr. Ahmad T. Abdulsadda**
(Head of comm. Tech. Eng. Dept.)

Date: / / 2022

Committee Report

We certify that we have read the thesis titled “**Performance Enhancement Of Double Gain Chain Fiber Laser**” submitted by Haider Yahya Saeed and as an Examining Committee, examined the student’s thesis in its contents. In our opinion, it is adequate for an award of a degree of Technical Master in Communication Engineering.

Signature :
Name :Prof. Dr. Adheed Hasan Sallomi
Degree: PHd.
(Chairman)
Date: / / 2022

Signature:
Name: Prof . Dr. Faris Mohammed
Ali
Degree: PHd.
(Member)
Date: / / 2022

Signature:
Name: Assistant Prof . Dr. Ali Abdulelah
Noori Al- Naji
Degree: PHd
(Member)
Date: / / 2022

Signature:
Name: Prof. Dr. Ali Abdul Abbas Al
Bakri
Degree: PHd.
(Supervisor)
Date: / / 2022

Signature:
Name: Lecturer Dr. Husam Noman
Mohammed Ali
Degree: PHd.
(Supervisor)
Date: / / 2022

Engineering Technical College-Najaf approval.

Signature :

Name : Assistant Prof . Dr. Hassanain G. Hameed
Dean of Engineering Technical College- Najaf

Linguistic Certification

This is to confirm that this thesis , "**Performance Enhancement Of Double Gain Chain Fiber Laser,**" underwent linguistic evaluation. Its language was changed to conform to the English language style.

Signature:

Name:

Date:

Abstract

Recently, the development of contemporary telecommunications has led to an exponential expansion in information technology. The development of high quality and high speed communications systems is especially dependent upon optical fiber connection. In order to obtain high signaling speeds, optical fibers are now employed not only in telephony systems but also in the Internet and local area networks (LAN).

In the single mode optical fiber, the bending impact on coherent light was investigated. Single mode optical fiber consisting of silica and rotating cylinders of various diameters are used in this thesis. Laser with fiber optics loop mirror double gain has recently become one of the most important subjects. Many researchers have been reported the main problem in this type of systems which is nonlinearity of the amplification properties.

One solution for this crucial issue is using the deep learning and evolutionary searching algorithm. In this thesis, proposed a listed the main evolutionary algorithm of the optical simulation model and demonstrate the simulation results to solve this problem. The author noticed that a software architecture utilizing advancements in adaptive control and machine learning offers the best integration platform for self-tuning optics. In order to implement a training and execution software module capable of self-tuning the laser cavity even in the presence of

mechanical and/or environmental perturbations, servo controllers can be combined with commercially available optical telecom components for mode-locked lasers. This could potentially stabilize a frequency roll. In the algorithm training step, the parameter space is thoroughly searched to identify the optimal performance areas for one or more interesting objective functions. Three activation are used with global optimization techniques, genetic algorithm to find the best and shortest laser pulse duration , it finds the optimal solution 20 generation. The $i_{d1}=5.9$ mA and $i_{d2}=1.9$ mA. The PI controller has been enhancement the performance with optimal angle.

Acknowledgment

First and foremost, I want to give Allah praise for providing me the fortitude, endurance, bravery, and will to do this task. All praise and gratitude are due to the All-Powerful Allah.

My supervisors, Dr. Husam Noman Mohammed Ali and Prof. Dr. Ali Abdul Abas Al Bakri, deserve a particular thank you for your invaluable guidance, counsel, and prompt assistance provided to me throughout my study period. They have been so patient and have given me such helpful input that I have been able to effectively finish my research project and produce this thesis.

Additionally, my college (Department of Communication Engineering, Engineering Technical College/Najaf, Al-Furat Al-Awsat Technical University), which I consider to be a second home, is sincerely thanked. Haidar S. Zaeer Dhaam is to be thanked for any assistance or advice he provided me with about my thesis.

DECLARATION

I hereby declare that the thesis is my original work except for quotations and citations which have been duly acknowledged.

1Nov 2022

HAIDER YAHYA SAEED

TABLE OF CONTENTS	Page
Supervisor Certification	ii
Committee Report	iii
Linguistic Certification	iv
Abstract	v
Acknowledgment	vii
Declaration	viii
Tables Of Contents	ix
List of Tables	xii
List of Figures	xiii
List of Abbreviations/ Nomenclature	xvi
List of Symbols	xvii
List of Publications	xviii
Dedication	xix
Chapter One : Back Ground Theory And Literature Review	
1.1 Introduction	1
1.2 Literature Review	5
1.3 Gaps And Limition Of Literature Review	17
1.4 Problem Statements	19
1.5 Thesis Objectives	19
1.6 Contribution	20
1.7 Organization of Thesis	21
Chapter Two: Mathematical Problem formulation	
2.1 Introduction	22
2.2 Laser Over Fiber Modes	24
2.2.1 Step-Index Multimode	29

2.2.2 Graded-Index Fiber	30
2.2.3 Single-Mode Step-Index	30
2.3 Double Gain Deep Learning Technique	31
2.3.1 Laser-Fiber Nonlinearity	34
2.3.2 Genetic Algorithms	35
2.3.3 Objective Fitness Function In GA	38
2.4 Control Polarization Angle	39
2.4.1 Control Angle Problem Formulation	40
2.4.2 PID Controller And Objective Functions	43
2.5 Summary	45
Chapter Three: Proposed System Design And Implementation	
3.1 Introduction	46
3.2. Single And Multi-Modes	46
3.3. Open Net Program And Used Parameters	50
3.3.1 Introduction	50
3.3.2 OPNET As a Research Tool	51
3.3.3 Features of OPNET	53
3.4. Single Gain Loop with The Genetic Algorithm Proposed System	60
3.5. Multi-Mode With Coupler Gain Loop With The Genetic Algorithm Proposed system	65
3.6. Single And Multiple Mode With And Without Coupler Genetic Algorithm	71
3.7. Polarization Angle Proposed	73
Chapter Four: Simulation Setup And Results	
4.1 Introduction	78
4.2. Simulation Results: Type Of Laser Modes Under Bending Effect	78
4.3 Single Mode Fiber With Coupler Linear	82

4.4 Linear Multi-Mode With Coupler	85
4.5 Linear Single Mode Fiber Without Coupler	87
4.6 Linear Multi-Mode Fiber Without Coupler	89
4.7 Simulation Results Of Genetic Algorithm	90
4.8 PID Controller For Polarization Angles	93
4.9 Simulation Results Of Genetic Algorithm	96
Chapter Five: Conclusions and Future Works	
5.1 Conclusion	97
5.2 Future works	99
References	100
الخلاصة	107

List of Tables	Page
Table 1-1 provided a concise and clear summary of the most pertinent literature review of the earlier publications	6
Table 1.2 a concise and clear summary of the most pertinent literature review of the earlier publications (gaps and limitation)	18
Table 3.1 The component of optisystem in the table that used	55
Table 3-2 A fiber laser schematic showing both of the loops to have two active fiber stretches in single mode	61
Table 3-3 Parameters setup for double gain coupler laser fiber proposed system	66
Table 3-4 Parameters setup for polarization angle laser fiber proposed system	74
Table 4-1 diode current relationship with RF and intensity	83
Table 4-2 illustrated values of the 1 Km fiber linear couple	85
Table 4-3 single mode without coupler	87
Table 4-4 actual value of the intensity and wavelength for multi-mode without coupler	89
Table 4-5 polarization angle changes	93
Table 4.6 Gaps And Limitation Of Thesis	96

List of Figures	Page
Figure 1-1 mirror loop for double gain laser fiber optics	2
Figure 1-2 Schematic diagram for combiner fiber optics laser loop	4
Figure 2.1 type of linear optic	22
Figure 2.2 type of linear optic	22
Figure2-3 Communication system by using laser fiber optics	24
Figure 2-4 Different position laser over fiber pulse shaping	25
Figure 2-5 Schematic diagram of step-index multimode	29
Figure 2-6 Schematic diagram of graded-index mode	30
Figure 2-7 Schematic diagram of step-index single mode	31
Figure 2-8 Illustration of double gain fiber system	32
Figure 2.9 Standard procedure of genetic algorithm	35
Figure 2-10 Single - point crossover	37
Figure 2-11 Mutation process in GA	38
Figure 2-12 Schematic diagram for themode-lockedfiberlaser	41
Figure 2-13 schematic diagram for the polarization angles effects, adapted from	42
Figure 2-14 Schematic diagram of the proposed PID control system	44
Figure 3-1 Single mode Laser generating schematic diagram	47
Figure 3-2 Multi laser modes with bending effects over the fiber	48
Figure 3-3 Schematic diagram with different bending effect (6cm-20cm); (a) bending effect for 6 cm; (b) bending effect of 8 cm; (c) bending effect of (10 cm); (d) bending effect of (12 cm); (e) bending effect of (16 cm); (f) bending effect of (20 cm); (g) no bending with noisy single mode; (h) no bending single mode	49
Figure 3-4 (a) to (e) samples of the temporal waveform and spectral profile of the dissipative solitons produced on demand	50

Figure 3-5 OptiSystem opens and the graphical user interface appears	55
Figure 3-6 Proposed system by using opt-net software.	61
Figure 3-7 transmission part	63
Figure 3-8 The channel part	64
Figure 3-9 Measurements devices	65
Figure 3-10 A fiber laser schematic showing both of the loops to have two active fiber stretches for multimode with coupler	66
Figure 3-11 Transmission part with coupler	69
Figure 3-12 The channel with coupler parts	70
Figure 3-13 The receiving part with coupler	71
Figure 3-14 schematic diagram for optimal selection of pumping laser diode currents (ILD1, ILD2)	72
Figure 3-15 Schematic of angle polarization	73
Figure 3-16 Polarization angle controller system	77
Figure 4-1 Normalized intensity for 12 modes laser	78
Figure 4-2 normalize four mode laser over the fiber with bending effect	79
Figure 4-3 Mode intensity profiles of the five lowest order fiber modes supported by (a) a straight and (b) a bent MMF	80
Figure 4-4 BPM-Matlab numerical simulations of different LP modes' normalized fractional power in a bent MMF excited: (a) LP01; (b) LP03L modes	81
Figure 4-5 show one case of the original signal when both diode current is 300 m amp	84
Figure 4-6 Signals of simulation results when $id1=id2=800$ m amp	84
Figure 4-7signals for the initial value of the currents which is $id1=id2=300$ m amp	85
Figure 4-8 Illustrated simulation signals $id1=id2=800$ m amp., 1 Km	86
Figure 4-9 shows the simulated signals for the linear single mode without coupler	88

Figure 4-10 signals of id=300 m amp., single mode	88
Figure 4-11 shows the details of multi-mode without a coupler for id 300 m amp. Signals	89
Figure 4-12 Genetic algorithms steps	90
Figure 4-13 All try duration pulses..	91
Figure 4-14 target track using genetic algorithm	92
Figure 4-15 Practical op-net and simulated mat lab three objective function using genetic algorithm	92
Figure 4-16 Polarization angle 100	93
Figure 4-17 Simulation results of polarization angle: (a) Normalized objective function vs time; (b) angle vs time.	94
Figure 4-18 Polarization angle with intensity for different fiber optics length	95

List of Abbreviations/ Nomenclature

Abbreviation	Description
ACF	Auto Correlation Function
BPM	Beam Propagation Method
CMT	Coupled Mode Theory
CNLS	Schrödinger Equation is a Linear Partial Differential Equation that Governs the Wave Function
DFB LASER	Distributed-Feedback Laser
DG-ADI	Douglas-Gunn Alternating Direction Implicit
DMD	Deformable Mirror Devices
ESC	Extremum-seeking control
FD-BPM	Finite Difference Beam Propagation Method
FDTD	Finite-Difference Time-Domain
FFT-BPM	Fast Fourier Transform Beam Propagation Method
GA	Genetic Algorithm
LED	Light Emitting Diode
LP	Linearly Polarized
ML	Machine Learning
MMF	Multi Mode Fiber
NALM	Nonlinear Amplifying Loop Mirror
NPE	Nonlinear Polarization Evolution
NPR	Nonlinear Polarized Rotation
PID	Partial Integral Derivative
TM	Transmission Matrix

List of Symbols

Symbol	Definition		
Nm	Bandwidth of fiber laser, wavelength	MHz	Energy
μm	Center, axial resolution, core radius	fs	external grating-pair compression
Ps	Durations	Kw	Power
nJ	ring laser cavities with lengths of creating stable	GHz	Multimode application
Km	Distance	m	core diameter
I	laser intensity pulses	t	the time of peak

List of Publications

Published.

1. Haider Yahya Saeed, Husam Noman Mohammed Ali, Ali Abdul Abas Al Bakri, Haidar Zaeer Dhaam, “Amplification Loop for Laser Mirror Techniques for Deep Learning,” , Journal of Emerging Technologies and Innovative Research (JETIR) ,2022.

Accepted

2. Haider Yahya Saeed, Husam Noman Mohammed Ali, Ali Abdul Abas Al Bakri, Haidar Zaeer Dhaam, “Nonlinear controller for the laser fiber using PID controller,” BOHR International Journal of Business Ethics and CorporateGovernance (BIJBECG),2022.

Dedication

To whom God has bestowed dignity and honour, who taught me how to give and expect nothing in return, and whom I bear his name with pride, your words still show me the way today, tomorrow and forever like stars in pitch darkness. My dear father, may God protect you and keep you a tent for us and to my dear, tender mother, may God Almighty have mercy on you and enter you into his vast gardens. For those with whom I spent the best days of my life and shared the best memories ever, those who feel happiness for me and my success, my brothers and my friends. To my companion, my soulmate, my partner and support in life, my dear wife finally, to my dear children Husseini and Mayar.

Chapter One

Background Theory and Literature Review

1.1 Introduction

Modern engineering systems are getting more and more complex, typically using a lot of networked, working together components to get results that are near to perfect. Due to organization non-linearities sensitive and to a multidimensional parameter space, it is frequently difficult to make quantitatively accurate predictions of system performance, even though It is nevertheless crucial to model and simulate such systems in order to characterize the dynamic behavior and spectrum of potential behaviors [1].

Mode-locked lasers [2-4], whose main physical results have been known for more than 30 years, have proven difficult to explain mathematically. This lack of quantitative agreement highlights the fundamentally delicate nature of human-made stochastically variable variations changes in the networked, non-linear system's physical properties. In fact, it is generally known that in method fiber lasers, the fiber birefringence varies randomly across the fiber it self. The birefringence and the results of the consequent mode-locking can be drastically changed by even little fiber bending or environmental temperature changes. Therefore, to protect performance from weather fluctuations, industrial fiber lasers are fixed to the ground and covered.

The complexity of contemporary engineering systems is growing. Only a few of the numerous factors that contribute to the "complexity and unpredictability of system behavior" include environmental changes, Nonlinear dynamics, noise, and multi parametric operational space. A complex environment additional demands on the design controlling systems in terms of accuracy maintenance, quickly adjust to environmental changes, and shifting operational paradigms. Traditional control techniques usually fail in complex nonlinear systems since they were originally designed for linear systems. The flexible, efficient, and nonlinearity-friendly machine learning (ML)-based methods in this case offer an alternative to conventional control tactics. Machine Learning There has been a great deal of research on (ML)-based control techniques, and it has become clear that these tactics are crucial in systems where there is little to no knowledge of the mathematical models. Recent ground-breaking works by the N. Kutz group [5-6] in the domain of lasers demonstrate that non-linear polarity evolutionary (NPE)-based method lasers are capable of a lengthy, self-tuning operation (shown in Figure 1.1).

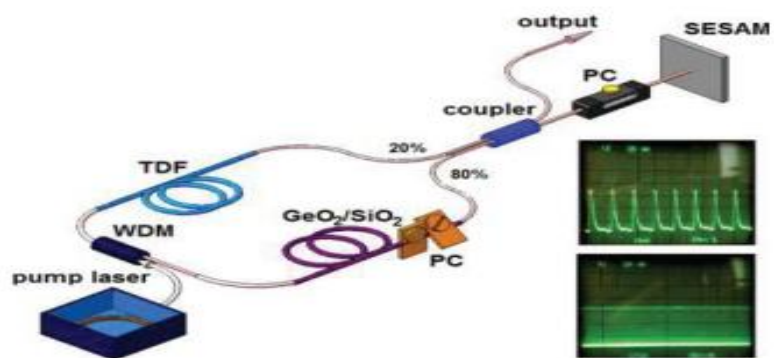


Figure 1.1 The mirror loop for double gain laser fiber optics, adapted from [7].

This is a revolutionary concept because even while Non-linear Polarization Evolution (NPE)-based mode-locked lasers work admirably [8-9], repeatability and control of their process are major technological challenges since the necessary non-linear systems have several operational states [10-11]. Recently, various groups have [5-6,12-19] shown that the showing of (NPE)-based mode-locked fiber lasers may be successfully optimized using ML approaches. The NPE using a non-linear amplification loop mirror as an example, it has been demonstrated that a (NPE) based way of managing pulse limits is compatible with various mode-locking strategies. Self-tuning lasers that are adaptable have the ability to fundamentally alter both the laser business and laser research.

Numerous present and future applications, including micro-machining and metrology (shown in Figure (1.2)), research is always being done to develop new state-of-the-art techniques for cavity design and control of the pulsed regime in fiber lasers for use in spectroscopy, microwave photonics, bio-medical applications, communications, and many other fields. The opposing methods of pulse creation and underlying non-linear physical parameters result in a broad variety of possible lasing regimes. By controlling the non-linearity of fiber lasers, it is feasible to control this unpredictable nature of the output radiation's characteristics. For the feedback-based control to be flexible, cavity settings should be straightforward to alter, either electrically or optically Utilizing electrical control of an electro-optical switch or a semiconductor optical amplifier,

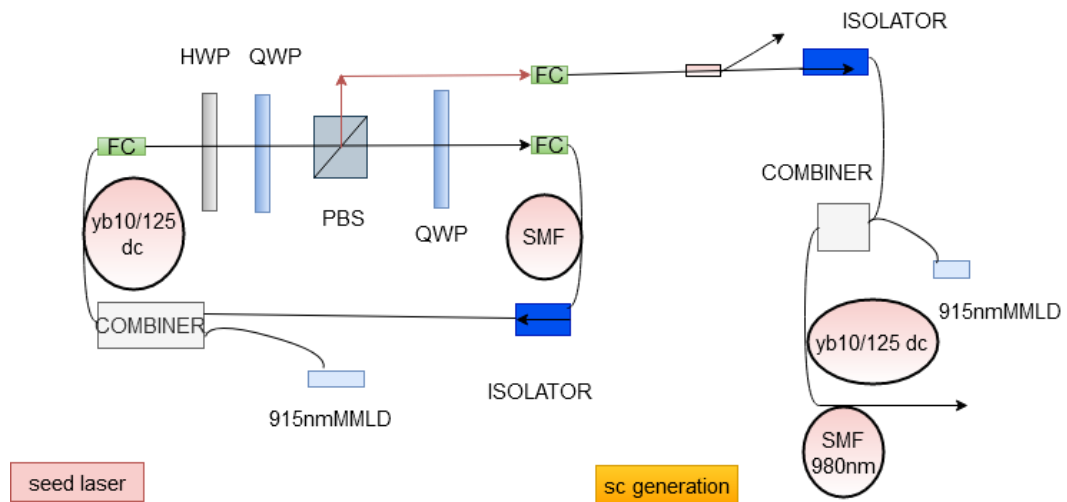


Figure 1.2 Schematic diagram for combiner fiber optics laser loop [20].

recent research has demonstrated unique methods for creating optical patterns [21–22]. But these methods are only applicable to micro-second-scale pulse patterns. Control gets more difficult when Kerr nonlinearity and chromatic dispersion combine strongly to influence the spectrum and temporal characteristics of optical pulses produced.

For example, the continuous formation of classical solitons strongly complies with the balance between non-linearity and chromatic dispersion. Thus, there is a little spectrum and temporal fluctuation in the pulses the solitary waves fiber laser generates. The energy of the (important) solitons produced in method fiber lasers with anomaly dispersion is also constrained to sub-Nano joule levels by the Kelly side-bands instabilities [22,23]. Because laser production pulses have very simple pulse patterns, like Sech or Gaussian waveforms, for example, it is easy to describe them. However, the output laser pulses from non-linear intra-socket

dynamics lasers offer a greater potential for intrigue in terms of their shapes and other features .

1.2 Literature Review

A rapidly growing field that offers a compact and flexible architecture is cavities. Contrarily, the interaction between the configuration of the PCs and the nonlinear transfer function is a very significant problem ,which is made worse by the fact that fiber laser research systems have lumped birefringent effects, which As a result, in the majority of studies, the experimentalist manually spins the three or four integrated PC knobs through a process of trial and error in an effort, for instance, to establish dependable mode locking among a sizable number of devices. for pulse dynamics and effective cavity structures. In order to provide effective background radiation, the gain-aware non-linear amplifying loop mirror (NALM) strongly depends on the input pulse energy of low and intermediate values. Background suppression causes a small decrease in pulse interactions. The NALM provides a second pulse shaping mechanism because of the reflection of its operating strategy. In early thulium-doped mode-locked fiber lasers based on with intra-cavity dispersion control, both ring and linear cavity topologies were shown Table (1.1) provided a concise and clear summary of the most pertinent literature review of the earlier publications.

NO	References	Abstract
1.	Horowitz et al. (1997) [24]	<p>The researchers have described an erbium-doped fiber laser that generates a sequence of strong noise like pulses with a broad spectrum and a short coherence duration. The noise like behavior was seen in both the amplitude and phase of the pulses. The spectral width that could be obtained was 44 nm. Even after transmission over a long dispersive fiber, the light's high intensity and short coherence duration were preserved. According to a theoretical model, this mode of operation may be described by the laser cavity's internal birefringence, a nonlinear transmission element, and the gain response of the fiber amplifier.</p>
2.	Buckley et al. (2005) [25]	<p>It is reported on a set of tests designed to establish the highest pulse energy a femtosecond fiber laser is capable of producing. A Yb fiber laser may produce pulse energy up to 14 nJ by taking advantage of patterns of pulse propagation that prevent</p>

		<p>wave breaking. The pulses' peak strengths can be chirped to be less than 100 fs long, resulting in 100 kW of peak power. It is addressed how much pulse energy is possible to produce.</p>
3.	<p>Kieu et al. (2009) [26]</p>	<p>They described a mode-locked fiber laser that achieves high average power through cladding pumping and dissipative-soliton pulse shaping. With a repetition rate of 70 MHz and an average power of 2.2 W, the laser produces 31 nJ chirped pulses. It is possible to get 80 fs pulses with a peak output of 200 kW after chirping outside the laser</p>
4.	<p>Tian et al. (2009) [27]</p>	<p>They showed a passively mode-locked ultra-long cavity, all-fiber, all-normal-dispersion Yb-doped fiber laser with a semiconductor saturable absorber mirror (SESAM). With the help of the heavily chirped pulse and the nonlinearity-induced spectrum widening, the SESAM performs a filtering-equivalent function without the need of discrete dispersion-compensation components or traditional spectral filters,</p>

		<p>stabilizing the mode locking. The laser produces 4.3 nJ steady mode-locked pulses with a fundamental repetition rate of 397 kHz and a center wavelength of 1068 nm.</p>
5.	<p>Zhang et al. (2010) [28]</p>	<p>They studied the atomic layer graphene has an ultrafast absorption that is wavelength-insensitive and may be used as a "full-band" mode locker. They did experimentally shown that wide range 1570-1600 nm continuous wavelength adjustable dissipative solitons might develop using the broad band absorption band of graphene, in an erbium filled fiber laser modes locked with very few layer graphene.</p>
6.	<p>Chichkov et al. (2010) [29]</p>	<p>They showed that an erbium-doped fiber oscillator that exclusively has positive dispersion fibers, is mode locked via nonlinear polarization evolution, and is stabilized with a birefringent filter, can provide output pulse energies of 20 nJ. With a center wavelength of 1550 nm, the fiber oscillator works at a repetition rate of 3:5. The output pulses are positively chirped, and they last 53 ps for a total of 750 fs.</p>

		Dissipative soliton functioning is indicated by the output pulses' strong positive chirp and the pulse spectrum's
7.	Chichkov et al. (2011) [30]	They demonstrated an all-normal dispersion, mode-locked ytterbium fiber oscillator with pulse energies more than 0.5 J. Non-linear polarization rotation is used to mode-lock the oscillator, and internal spectrum filtering allows for steady single-pulse operation. At a repetition rate of 4.3 MHz and a maximum pulse width of 760 fs, the oscillator produces output pulses that are substantially chirped.
8.	Lecaplain et al. (2012) [31]	They presented an experimentally, high optical intensity rare events are seen at the production of a mode-locked fiber laser that generates chaotic multiple pulses in a severely dissipative zone. These intensity variations' probability distribution, which is heavily influenced by the cavity parameters, has a lengthy tail. The nonlinear interaction and constant relative mobility of pulses inside a temporally confined multi-solution phase are what cause the recorded intensity variations.

9.	Grelu et al. (2012) [32]	<p>These issues include nonlinearity, dispersion, and/or diffraction. Dissipative solitons are localized variations of an electromagnetic field that are maintained in balance by an energy exchange with the environment. It is amazing how frequently they are utilized in the field of passively mode-locked lasers since the concept of a dissipative soliton provides a solid framework for understanding complex pulse dynamics and motivates creative cavity designs. A wonderful opportunity to investigate the unusual dynamics of dissipative solitons and test the underlying theory is offered by the research of mode-locked lasers. Basic definitions of dissipative solitons are given in this review, along with an overview of their implications for the creation of high-energy mode-locked fiber laser cavities, a discussion of striking new dynamics like dissipative soliton molecules, pulsations, explosions, and rain, and an outlook on dissipative light bullets.</p>
10.	Erkintalo et al. (2012) [33]	<p>They described a 1030 nm large chirp oscillator that is stable in the environment.</p>

		<p>Their system proposed to be able to extract pulse energies greater than 10 nJ from a reliable all-PM cavity without the usage of free-space components by using a nonlinear amplifying loop mirror as the mode-locker. Numerous computer simulations show that just enlarging the cavity with a single-mode fiber in the proper location can increase the output oscillator's energy and duration. At 10, 3.7, and 1.7 MHz with associated pulse energies of 2.3, 10 and 16 nJ, we experimentally established environmentally stable mode-locking utilizing various cavity lengths. It has been consistently shown that external grating-pair compression occurs below 400 fs.</p>
11.	Bednyakova et al (2013) [34]	<p>According to their study, induced Raman scattering can affect chirped dissipative solitons (DSs) produced in a long cavity fiber laser (SRS). In this article, we offer theoretical and experimental research on the DS creation and development under intense SRS. The findings show that the increasing noisy Raman pulse (RP), rather of acting as</p>

		<p>just another route for the DS's energy dissipation, can actually promote it, leading to the creation of a complex of bonded DS and RP with a similar energy and duration. The DS allows for amplification of the RP inside the complex. The DS is stabilized by the RP by temporal-spectral filtering. All-fiber ring laser cavities with lengths of create stable 25 nJ SRS-driven chirped DS pulses.</p>
12.	<p>Yi-Jing et al. (2015) [20]</p>	<p>They presented ultrahigh- resolution optical coherence tomography using a proposed high-power super continuous light source based on noise-like pulses created by a rare earth doped fiber laser. The bandwidth that got around of 420 Nanometers and a center of about 1.3 micrometers, the super continuum spectrum is flat. The light source has been successfully used in time-domain optical coherence tomography, with an axial resolution of 2.3 micrometers. Bio-tissue imaging with high resolution fiber-based spectral-domain optical coherence tomography was also shown.</p>

13.	<p>Brunton et al. (2016) [21]</p>	<p>They demonstrated how an adaptive control and machine learning-based software architecture may serve as an appropriate foundation for the integration of self-tuning optics. A training and execution software module can be implemented using commercially available optical mobile communications components in conjunction with servo controllers to self-tune the laser cavity even in the presence of structural and/or environmental instabilities, potentially trying to stabilize a frequency comb for mode-locked lasers. In this algorithm training step, an exhaustive search of parameter space is used to find the optimum performance areas for one or more objective functions of interest. The execution step starts with a sparse sensing method to recognize the parameter space, then quickly goes to a nearly optimum solution and maintain it via an extremum seeking control plane. The process is reliable.</p>
-----	---------------------------------------	-------------------------------------------------------------------------------------------------------------------------------------------------------------------------------------------------------------------------------------------------------------------------------------------------------------------------------------------------------------------------------------------------------------------------------------------------------------------------------------------------------------------------------------------------------------------------------------------------------------------------------------------------------------------------------------------------------------------------------------------------------------------------------------------------------------------------------------------------------------------------------------------------------------------------------------------

14.	Boscolo et al. (2019) [35]	They presented statistically characterize the performance of a newly reported architecture of a flexible laser with two independently pumped active fiber segments in its bidirectional ring using three-dimensional adjustable cavity settings. they illustrated how a regression model based on a neural-network algorithm space of mode-locked.
15.	Alexey et al. (2019) [36]	With the parameters available on demand, they created systems. The reverse laser design challenge that has been putting out is to choose the system structure that permits the development of the necessary laser output Direct back propagation techniques are challenging for reverse issues in nonlinear systems because these problems are typically sensitive to the calculation of the gradients of a target (fitness) function. To build a fiber 8- laser cavity that is independent of fitness task gradients, we employ a particle swarm optimization strategy. This method might be used to identify laser cavity topologies that are best for producing on-demand pulses with

		<p> durations of 1.5-105 Psec and spectral widths of 0.1-20.5 nm. The recommended design optimization method may be used to several laser applications and, more generally, to numerous engineering systems with adaptable setups and demand-driven factories.</p>
16.	<p>Fathi et al . (2021) [37]</p>	<p>Fiber laser technology has shown to be a flexible and dependable method for producing laser sources, with a wide range of applications in industries ranging from science to business. Single-fiber laser systems have encountered a number of fundamental restrictions in terms of power/energy scaling. Combining the output powers of several lasers has emerged as the main strategy for doing so, both to overcome them and to increase the power/energy level even more. The coherent beam combining of fiber amplification channels, which equips ultra-high-power/energy lasers with nearly diffraction-limited beam quality, is the most promising combining technique. The development of coherent beam combining for</p>

		<p>both continuous-wave and ultrafast fiber lasers is thoroughly reviewed in this study. Coherent beam combining is discussed, covering everything from its fundamental principles to its precise needs, difficulties, and solutions. Some useful topologies for continuous and ultrafast fiber lasers are also reported.</p>
17.	<p>Mirza et al. (2022) [38]</p>	<p>With the help of the multi-stage pumping technique, the performance of doped fiber amplifiers can be greatly improved, provided that many crucial pumping parameters, such as their optical power and wavelength, are optimized. We discuss the improvement in performance of a ytterbium doped fiber amplifier (YDFA) for the 1.02-1.08 μm spectral area using an optimized design built on a brand-new dual-stage in-band asymmetrical pumping method. At an optimized length of Ytterbium-doped silica fiber and an optimized doping concentration of Yb^{3+}, a record peak gain of about 62.5 dB and output power of 4.5 W are obtained for a signal wavelength of 1.0329 μm. This is</p>

		<p>accomplished by precisely adjusting the optical power and wavelength of pumps in both stages. Additionally, at a signal wavelength of 1.0329 μm at the optimal parameters, a minimum noise figure (NF) of 4 dB is seen. Similar to this, the impact of utilizing high and low pump powers at the first and second stages, respectively, on the NF of the amplifier is also examined at various signal power values. It has been found that utilizing a high pump power at the first stage and a low pump power at the second stage considerably boosts the value of (nf).</p>
--	--	--------------------------------------------------------------------------------------------------------------------------------------------------------------------------------------------------------------------------------------------------------------------------------------------------------------------------------------------------------------------------------------------------------------------------------------------------------------------------------------------------------------------------------------------------------------------------------------------------------

1.3 Gaps And Limition Of Literature Review

No	Reference	Gaps	Limition
1.	Kutz et al (2015) [8]	the toroidal search learning algorithm which explores parameter space can be evaluated using as many objective functions as desired. For mode-locked lasers and frequency comb applications, this may mean looking for the shortest pulses, most energetic pulses, or most	The ESC is then used to make adaptive adjustments to the mode-locked laser in order to keep it optimally tuned

		stable phase-locking between round trips If a suitable objective function can be constructed, then self-tuning can be achieved.	
2.	Boscolo et al (2019) [35]	the NALM contains two sections of ytterbium-doped fibre, YDF1 and YDF2, of respective lengths 5.3m and 5.0m, separated by a 12.4 m-long section. of NDF The cavity group-velocity dispersion (GVD) is 0.58 ps ²	dual-pump nonlinear amplifying loop mirror mode-locked fibre laser
3.	Horowitz et al. (1997) [24]	Yb-doped fiber laser with a semiconductor saturable absorber mirror (SESAM)	Machine Learning Methods for Control of Fibre Lasers with Double Gain Nonlinear Loop Mirror
4.	Tian et al . (2009) [27]	Used circulator and coupler 50/50 ,WDM coupler, passively mode-locked fiber lasers (PMFL)	Yb-doped fiber laser and single mode fiber

Table 1.2 a concise and clear summary of the most pertinent literature review of the earlier publications (gaps and limitation)

1.4 Problem Statement

In previous studies in Optical Fiber, several problems were found that affect the amount of information received and output from it, the bending in the optical cable and the angle at transmission side, in addition to the effect of the source on the transmission and the intensity of the transmitted information. And a specific stream as well, The demonstration, and analyze the laser over the fiber optical especially when its bending and solve the nonlinearity problem by using global optimization techniques (genetic algorithm(GA)). Below we have listed the main problems that have been considered:

Firstly: considering the problem of converting the single band laser that is being used to transmit and receive data through the complex laser closed loop communications system to multi band with different wavelengths of laser light.

Secondly: Finding the actual wavelength of the receiving signal which is one of the most challenging here and is one of the most problems.

Thirdly: Finding the optimal polarization angle which is another problem by using an automatic PID controller system.

1.5 Thesis Objectives

Going to the understanding of the laser mode through the fiber laser, with double gain fiber loop using a genetic algorithm for different objective functions, for specific brief description of the objectives which are summarized as follows:

- Defining the mathematical formulation, the multi band nonlinear control laser system that is using in communication to solve nonlinearity problem by using a GA.

- Defining the range by using opti-system by Single-Parameter-Single-Result Optimization.
- Building the Matlab Simulink and designing PID controller to find the optimal polarization angle. The virtual schematic diagram for sending and receiving multi-band laser with short wave length.

1.6 Contributions

- In this thesis conducting a study, analyzed and implemented the system using an optic net of the types of lasers and the types of optical fibers that are meant by mods, and the effect of bending.
- Solved the problem of the source, the best value of the current for lasers, so that he could work on a solution for physical nonlinearity in optical fiber. Finding optimal current i_{d1} and i_{d2} for the laser diode.
- Designed a control system, that is combined the control with the polarization angle to find the best value for the polarization. In this case, It will be solved a problem of gain and give it the best value for the signal transmitter from transmitter to receiver.

1.7 Thesis Organized

This thesis is divided into five chapters, the description of each chapter has been described as follows:

Chapter Two: describes the mathematical model of the single and multi-laser over the fiber optics, effecting of the bending, the nonlinearity problem formulation and how polarization mirror angle control the dynamic laser, finally all details about the optimization techniques have been described in this chapter.

Chapter Three: schematic algorithms that are needed for all cases which have been described as a flowchart of the simulation opt net system (multi-mode, genetic, controller, and opt net).

Chapter Four: All simulation setup has been presented in this chapter then demonstrated the proposed system by showing the results.

Chapter Five: summarization of all findings as a ratio and all the demonstration results, the lack points in the proposed system have been discussed in conclusion chapter, and proposed the future plan for this thesis.

Chapter Two

Mathematical Problem Formulation

2.1 Introduction

This chapter is divided into three main sections: Laser mode limited equations by bending condition, Multiband laser fiber machine learning modeling, and lastly, Polarization angle PID control system. Multimode fibers are those with core diameters more than or equal to 50μ and the capacity to support a large number of propagating rays or modes, Figure (2.1) illustrated all type of linear optic and Figure(2.2) shown nonlinear optic mode .

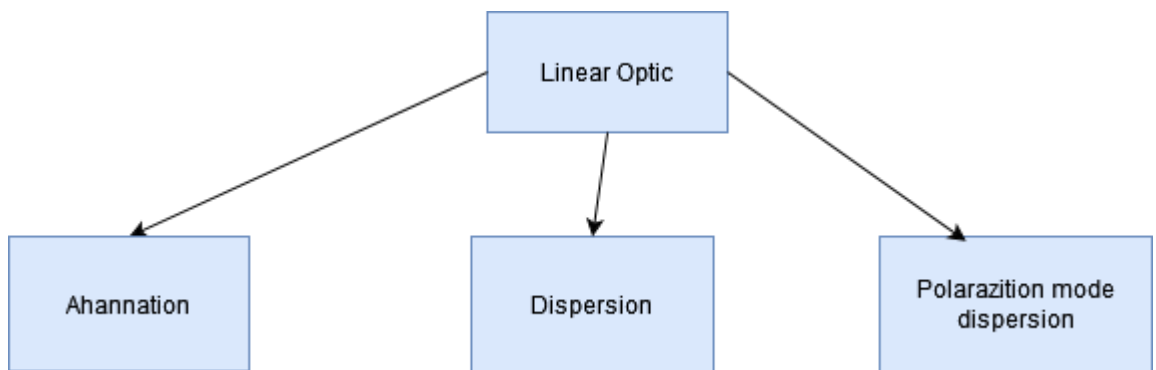


Figure 2.1 Type Of Linear Optic

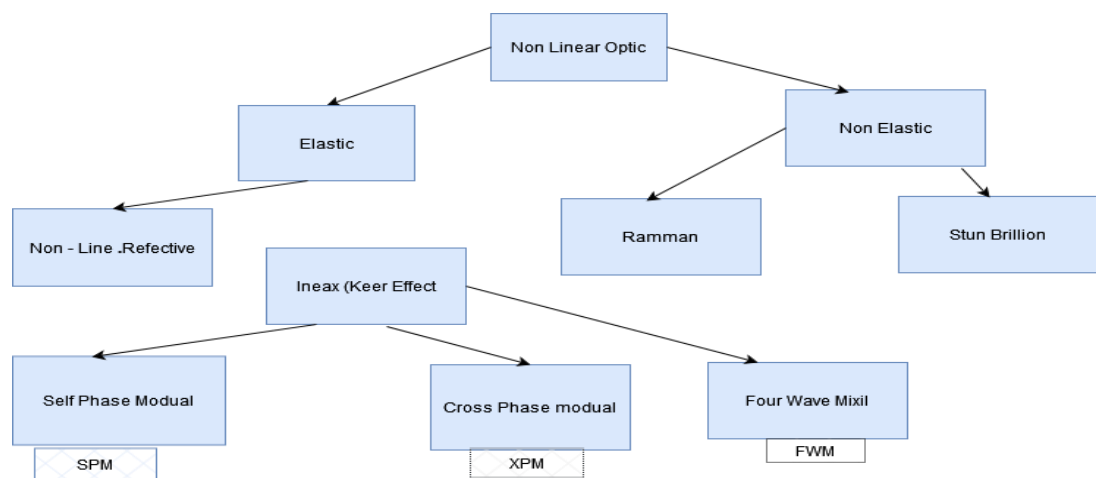


Figure 2.2 Type Of Non -Linear Optic

The two primary types of fiber are also provided by the variations in the material composition of the cladding and core. First, the core's refractive index is constant throughout and abruptly changes (or ceases) at the cladding border. Step-index fiber is the name given to it. The major case in the second Refractive index of an item is influenced by its radial distance from its center. According to this , a fiber has a graded index.

The author was examine a specific mode-locked laser model in more detail to illustrate how deep learning and given in control are used. Given that recreating the birefringence has stayed difficult even after many years, the model is perfect for highlighting the important ideas advocated here.

First-principles modeling is eventually unachievable since the birefringence highlights the sensitivity to a particular stochastic parameter even more. Although a specific model is proposed for the research, the approaches are independent of this model and are applicable to any mode-locking configuration; in other words, the methods are equation-free and do not require any understanding of the specific physics of the laser under study. In reality,one of the beneficial aspects of the approach that makes it so appealing is the fact that The algorithm's learning module explores the parameter space and selects the best parameter settings that are compatible with the built-in objective functions. Finally, Figure (2.3) shows the main communication system based on laser fiber optics.

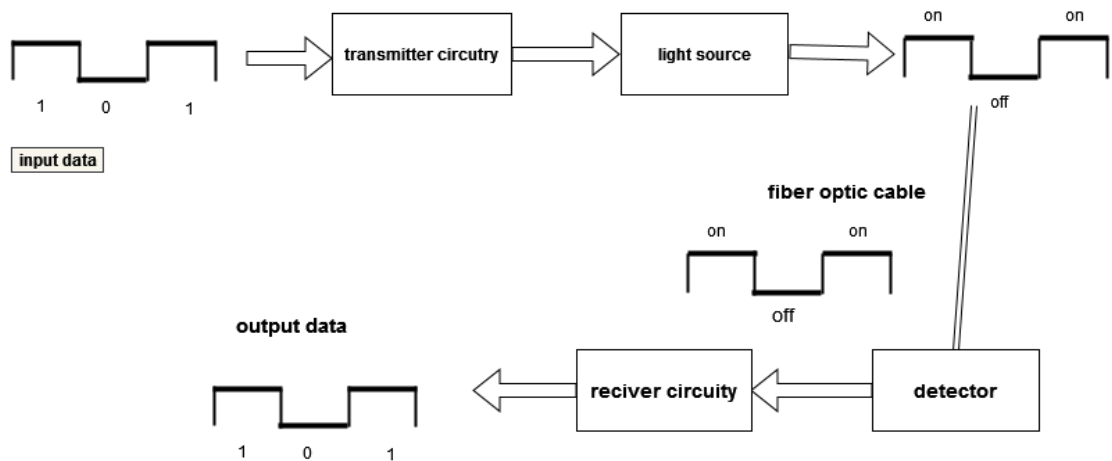


Figure 2.3 Communication system using laser fiber optics and adapted from [39].

2.2 Laser Over Fiber Modes

The usage of ultra-short pulses in technology has a big influence on both business and research. Mode-locked lasers must be the main source of power for ultrashort pulses. In order to generate ultrashort pulses, mode-locked lasers lock many axial modes in the laser cavity because the first mode-locked laser with extremely brief pulses was developed in the 1990s. Both commercial and scholarly research have made substantial use of technologies including frequency metrology, thin film characterisation, multiphoton imaging, and others. Recent decades have seen an increase in the difficulty of using fiber-based mode-locked lasers because they are more reasonably priced and smaller than their solid state counterparts. Although they are based on fiber, fiber-based mode-locked lasers cannot match the performance of solid state lasers. Because of its benefits, it has been successful in applications like precise and endoscopic material processing. Three parameters affect the pulse quality: NPR, cavity structure, and noise or input pulses. (NPR) generate pulses with higher pulse energy and shorter pulse length. The technique of pulse shaping is shown in Figure (2.4).

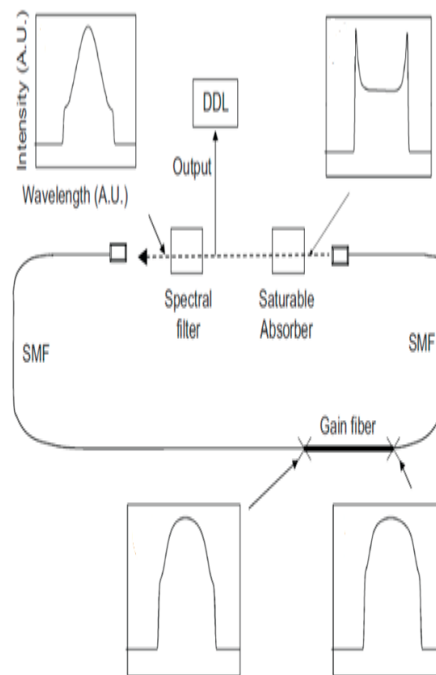


Figure 2.4 Different position laser over fiber pulse shaping [40].

For numerical calculations, It is done using the Douglas-Gunn Alternating Direction Implicit (DG-ADI) and Finite Difference Beam Propagation Method (FD-BPM) finite difference techniques. "The radiative transfer method (BPM) is used to answer the paraxial Helmholtz equation for the spatial distribution of the difficult and complicated electric field $E(x, y, z)$ at any plane along z in the case where the electric field distribution at the input plane, $E(x, y, z=0)$ The approximate paraxial theory is adequately satisfied as long as the angles between the local k -vectors and the z -axis are least, which is the case for weakly guiding materials such fibers with a

little difference in refractive index between the core and the cladding. An alternative method to solve the Helmholtz neutralization for beam spread is coupled mode theory (CMT), although the result depends on the Eigen modes of the waveguide [41,42]. The need to understand guided modes of waveguides makes it difficult to model beam propagation using non-trivial refractive index profiles and CMT. BPM is advantageous in this aspect since it propagates the field in the space domain without decomposing it into modes. Another popular numerical method for beam spread is the finite-difference -time-domain (FDTD) approach [43]. This method solves the time-dependent Maxwell's curl equations. Due to the need to grid the whole three-dimensional model structure and record the field data across the total volume for each time step, FDTD is incredibly computationally inefficient for modeling beam propagating in the space- and time-domains. In the case of the BPM, which only models a steady-state solutions for an electric field distributed in the spatially or frequency domains [41], the two-dimensional field data across one transverse cross-section must be saved. The two primary methods that might be utilized to develop a BPM algorithm are the Finite Difference Beam Spread Method and the Fast Fourier Transform Beam Propagation Method. (FD-BPM) is typically preferred over (FFT-BPM) when simulating light spread in integrated optical elements because it can simulate wave guiding structures with discontinuities in the refractive index, variability in grid point spacing, increased accuracy and computational speed, and operational comfort [44–49]. The explicit FD-BPM [50] approach yields unstable outcomes, such as checkerboard patterns [47,51], if the step size z in the longitudinal path is too big. The un-conditional stability of the Crank-Nicolson scheme in finite difference approximation provides more exact solutions in contrast to the explicit method [47]. Since it limits the systems coupling in each

phase to only one transverse dimension at a time, the DG-ADI transcends the Crank-Nicolson technique even further and provides significantly improved computation efficiency without a significant fineness loss. In contrast, the mode image is frequently used to observe the radiating structure during propagation and may be quite helpful. The E-field situation of linearly polarized (LP) modes is described for straight step-index fibers using a patchwork of Bessel jobs. The analytical formulation may be found in various prior studies [52,53]. For more complex fiber geometries and curvature, this visualization requires the ability to detect the grouping of mode for arbitrary-shaped index of refraction profiles. BPM-Mat lab includes an eigenvector solution for the C matrix expressly for this use. It is not necessary to consider the complete equation since the B matrix on the left-hand side of Eq. (2.1) shows the same breeding as C, but as an implicit step rather than an explicit step [52].

$$\mathbf{B} = \begin{pmatrix}
 b & -ax & \dots & -ay & \dots & \dots \\
 -ax & b & \dots & \dots & \dots & -ay \\
 -ay & \dots & \dots & \dots & \dots & -ax \\
 \dots & \dots & -ay & \dots & -ax & b
 \end{pmatrix} \quad 2.1$$

And, therefore

$$\mathbf{B}E^{Z+\Delta Z} = \mathbf{C}E^Z \quad 2.2$$

Then, Eq 2.1 will be [54]

$$\mathbf{C} = \begin{pmatrix}
 c & ax & \ddots & ay & \ddots & \ddots \\
 ax & c & \ddots & \ddots & \ddots & \ddots \\
 \ddots & \ddots & \ddots & \ddots & \ddots & ay \\
 ay & \ddots & \ddots & \ddots & \ddots & \ddots \\
 \ddots & \ddots & \ddots & \ddots & \ddots & ax \\
 \ddots & \ddots & ay & \ddots & ax & c
 \end{pmatrix} \quad 2.3$$

When determining the eigenvectors, this distinction is meaningless because the eigen-vectors of matrix C will be identical to those of the equation as a whole. Using $n'(x,y)$ refractive index profile, shown in equation, bending is taken into account (2.3). In order to find the user-specified variety of modes with eigenvalues in the complex plane that are closest to 1, the Krylov-Schur method [54] is utilized. Next, the eigenvectors are found using the built-in Matlab eigs method using the consumer number of modes.

$$n'(x, y) = n(x, y) \left[1 - n^2(x, y) \frac{x-x_0}{2R} pe \right] \exp\left(\frac{x-x_0}{R}\right) \quad 2.4$$

The inside product integral of the current field with the field dispersal of the mode is used to define the normalized fractional power of the LP modes [55].

$$\eta = \frac{|\iint E(x,y)E_{l,m,p}^*(x,y)dxdy|^2}{\iint |E(x,y)|^2dxdy \iint |E_{l,m,p}(x,y)|^2dxdy} \quad 2.5$$

where $E(x,Y)$ is the electric field dispersion and $E_l(x,Y)$ is the electric field of the modal with azimuthal mode index (l), radial modal index (m), and parity (p) (even or odd). The normalized fragmentary power of the particular mode's overall propagating E-field is represented by equation (2.6) Other directed modes or radiative, unguided modes either lose the remaining power or are used by other guided modes [55].

$$\eta = \frac{|\iint E(x,y)E_{l,m,p}^*(x,y)dxdy|^2}{\iint |E(x,y)|^2dxdy \iint |E_{l,m,p}(x,y)|^2dxdy} \quad 2.6$$

Regardless of the kind of fiber being utilized or the amount of bending present, Beam Propagation Method (BPM-Matlab) can determine and show the normalized fragmented power in any selected set of LP modes during beam propagation.

2.2.1 Step-Index Multimode

Fiber has an index of refraction that is computed from the cladding to the cores to the cladding (see Figure 2.5) profile that steps from low – high – low. This fiber is distinguished by a numerical aperture and a relatively high core diameter. A common multimode fiber used for communication has a core/cladding diameter of 62.5/125 μ , [56]. (a human hair's width or smaller). The possibility of many modes or pathways through the fiber is denoted by the word “multimode.” Step index multimode fiber is used in applications that need high bandwidth (> 1 GHz) across relatively short distances (3 km), including local area networks or campus network backbones. Compared to single-mode fiber, multimode fiber provides a number of benefits, including:

- comparatively easy handling;
- easier light coupling to and from it due to its greater core size;
- usage of both lasers and LEDs as sources; and
- decreased coupling losses
- Multiple modes are allowed to propagate as a result of modal dispersion, which depends on the numerical aperture, core diameter, and wavelength.

Reduced bandwidth, which results in decreased data rates, is the consequence of modal dispersion. For instance, a network system backbone or a local area network, which spans relatively close (3 km) distances [2,56].

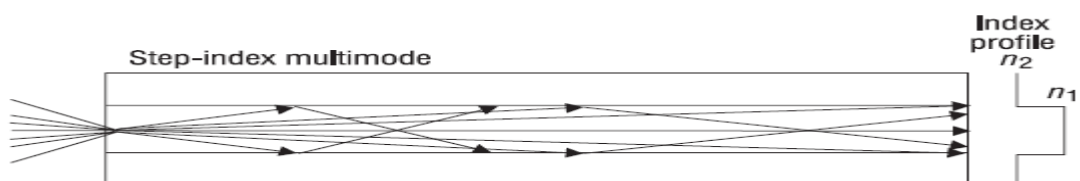


Figure 2.5 Schematic diagram of step-index multimode [2].

2.2.2 Graded-Index Fiber

It is a compromise between the increased bandwidth of single-mode fiber and the large core diameter and N.A. of multimode fiber, as shown in Figure (2.6). Light going through the fiber's center encounters a greater index of refraction than light traveling in the upper modes thanks to the development of a core whose index of refraction drops parabolically from the core center toward the cladding. This implies that the higher-order modes move more quickly compared to the lower-order modes, enabling them to "catch up" with them and lessen modal dispersion, hence increasing the fiber's bandwidth.

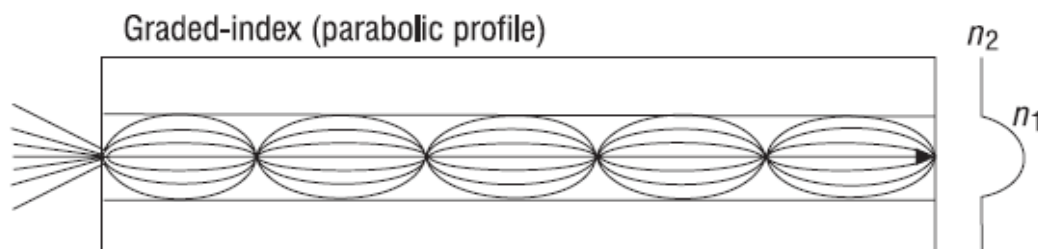


Figure 2.6 Schematic diagram of graded-index mode [2].

2.2.3 Single-Mode Step-Index

Only one path, or mode, of light transport is permitted via fiber. A typical single-mode fiber has a core diameter of 5 to 10 μ and 125 μ cladding. When Low signal loss and fast data rates are required, such as across long distances where the repeater/amplifier spacing must be minimized, single-mode fibers are employed. Single-mode fiber (see Figure (2.7)) can be utilized for applications requiring higher bandwidth since it only permits one mode or ray to travel (being in the lowest order), unlike multimode fiber. Despite the fact that modal dispersion is unaffected by single-mode fiber, chromatic dispersion can still hinder performance at higher data

rates. There are several ways to solve this issue. Transmission options include using an optical source with a very narrow output spectrum, such as a distributed-feedback laser (DFB laser), transmitting at a wavelength where glass' index of refraction is relatively constant (around 1300 nm), using specialized dispersion-compensating fiber, or combining any of these options. Single-mode fiber is primarily utilized in high-bandwidth, cable, and remote applications TV head ends, long-distance telephone trunk lines, and high-speed LAN and WAN backbones. Due to its tiny core, single-mode fiber's main flaw is that it can be challenging to deal with (i.e., splice and terminate). Additionally, due to the large coupling losses associated with LEDs, single-mode fiber is normally only employed with laser sources [2,56].

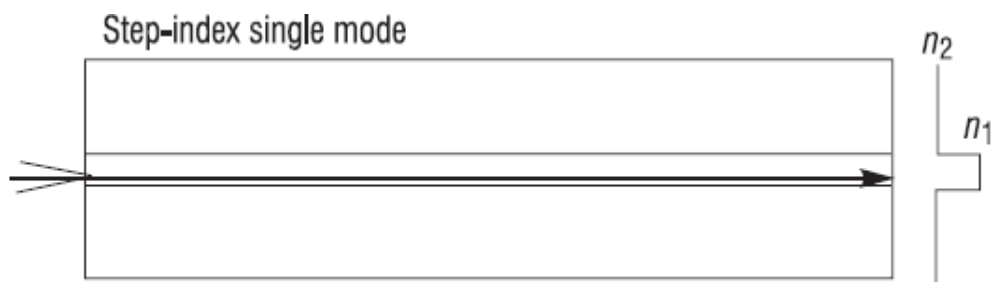


Figure 2.7 Schematic diagram of step-index single mode [2].

2.3 Double gain deep learning technique

The physical challenge of fiber laser operation is difficult. Modeling can offer a theoretic foundation for comprehending several of the characteristics of mode-locked fiber lasers (shown in Figure (2.8)),but due to a limited understanding of the different system factors and model constraints, it is difficult to achieve an individual mapping between numerical modeling and experimentati-ons. It is crucial to realize that although the fiber nonlinearity makes it challenging to comprehend how a laser system operates, it also sets makes mode locking possible and creates the necessary

conditions for it. (ML) methods might offer a means to make good, controlled use of these non-linear effects [57]. .

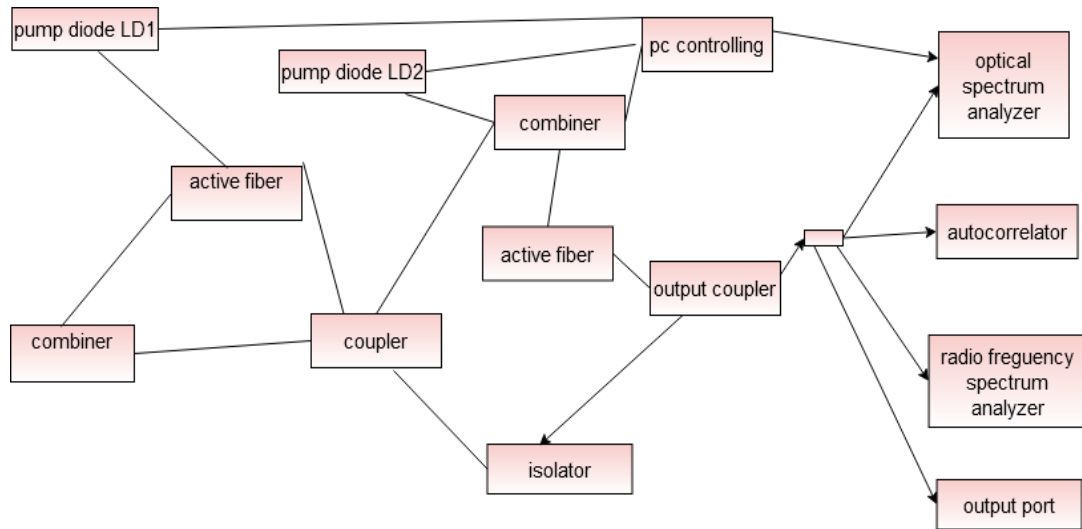


Figure 2.8 Illustration of double gain fiber system [57].

The current study advances NPE-based laser technology by introducing ML-based control to a new class of mode-locked fiber lasers with a double-gain, non-linear amplifying loop mirror (alteration of the fig-eight lasers [58–60]). With this approach, it is possible to combine ML algorithms and goal functions with straightforward electrical domination of the non-linearity and pulse properties.

The author emphasized that the originality of this scheme's use of an ML technique extends beyond scaling up pulse parameters and optimizing laser performance. By selecting the proper goal function, ML approaches may be used to create on-demand, qualitatively novel lasing regimes. Making use of ML approaches can help with the creation of new sophisticated laser organizations in a number of methods.

First, ML can provide a new level of comprehension of the lasing regimes that are available for a certain system configuration and how these regimes will be influenced by a range of potential changes that might dramatically boost a laser's performance throughout the design and testing phases. This new feature cannot realistically be deployed without ML. The ability of ML-based lasers to be self-tuning and incredibly resilient against a variety of environmental perturbations and risks is a second significant new component. This capability is made possible by the streamlined signal processing of the produced signal.

Although further research will be needed to achieve this functionality, the author believe that the current article represents a significant first step in that direction. Here, we regulate the output of a fiber laser with two electronically controlled distributed gain parameters using machine learning approaches for the first time. Thus, we successfully regulate the start of the nonlinear dynamics of optical radiation in the laser cavity and generate pulsed regimes with different durations, energy, optical spectrum widths, and coherence levels. We offer many objective functions that allow us to produce on-demand pulses with the least amount of time, the most amount of energy, and a range of coherence. Further evidence of the suggested laser system's adaptability in terms of applying algorithmic, electronically-driven domination over eradiation mode-locking regimes may be seen in the results.

2.3.1 Laser-Fiber Non-Linearity

Conception of several of the characteristics of mode-locked fiber lasers is possible. Afterward, as a result of ignorance of the many procedure aspects and model restrictions, obtaining a one-to-one mapping between numerical modeling and tests is a challenge. Although fiber non-linearity makes understanding the functioning of the laser system challenging, it is vital to remember that this same non-linearity sets the circumstances for mode locking and makes it feasible in the first place. Machine-learning (ML) approaches may provide a way to harness these non-linear effects in a way that is both controlled and beneficial. The current work extends NPE-based laser control to a modern type of mode-locked fiber lasers with a double-gain, non-linear amplifying loop mirror (alteration of the Figure- (2.8) lasers [57–59]). This approach combines straightforward electrical control of non-linearity and stroke properties [60] with machine learning (ml) methods and goal functions. The originality of utilizing a machine learning technique in this system is not confined to increasing pulse parameters and enhancing laser output. By selecting the proper goal function, machine learning approaches may be used to produce on-demand, qualitatively modern lasing regimes. In a variety of ways, using machine learning techniques to the creation of more sophisticated laser systems can help. First, ML can supply a new degree of understanding of the lasing regimes that are accessible in a certain system setup, as well as how these regimes will be changed by a variety of conceivable alterations that might drastically increase a laser's performance. Without machine learning, this new functionality would be impossible to develop. Second, Machine Learning (ML)-based lasers might potentially be self-tuning and exceptionally resilient to diverse environmental perturbations and risks

because of simplified signal processing. More research will be required to achieve this functionality, but we believe the current article is a significant step in the right direction. For the first time, the author employ machine learning (ml) to regulate the output of a fiber laser with two electronic-managed spread gain parameters. This enables us to successfully regulate the onset of nonlinear dynamics of radiation emitted in the laser cavity as well as produce pulsed regimes with a variable period, energy, laser spectrum length, and coherence level. With our collection of goal functions, we can create on-demand pulsed with the shortest possible length., highest energy, and variable coherence. A further demonstration of the suggested laser method's capability to manage radiation mode-locking regimes algorithmically and electrically is made.

2.3.2 Genetic Algorithms

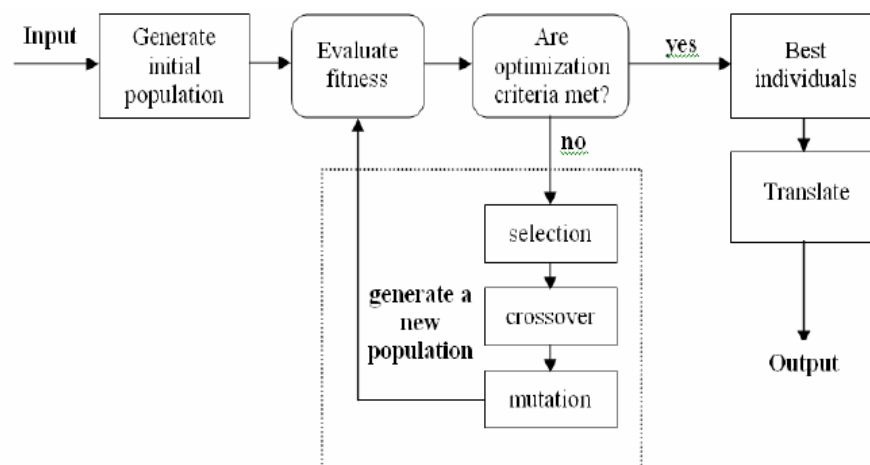


Figure 2.9 Standard procedure of genetic algorithm [61]

Genetic Algorithms are adaptable approaches for solving optimization and search issues. They have their roots in the genetic processes of living things. Natural

populations change over many generations in accordance with the ideas of natural selection and the notion of the fittest. ", as articulated for the first time in Charles Darwin's book *The Origin of Species*. Genetic algorithms can evolve by simulating this process "If properly encoded, solutions to real-world issues can be found. GAs can be used to design bridges with the optimum strength-to-weight ratio or to identify the cloth cutting pattern that uses the least amount of fabric.

The author was also be utilized for real-time process control in a chemical plant or load balancing on a multiprocessor computer system. GAs make use of a natural analogy. They are in charge of a group of people ", each of which represents a potential solution to a particular problem. A fitness score is given to each individual "based on how good of a problem-solving solution It is the strength/weight ratio for a certain bridge design, for example, could be the fitness score. (In nature, this is the same as evaluating an organism's ability to compete for resources.) By cross-breeding with other highly t individuals, the highly t individuals are provided chances to reproduce.

For many problems, like service optimization, it is obvious what the (fitness) function should measure—it should just be the function's value. However, in some cases, such as combinatorial optimization, this is not always the case. Many performance metrics may be optimized in a practical bridge design work, including strength/weight ratio, span, width, maximum load, cost, and construction time or, more likely, a combination of all of these. Reproduction Individuals from the population are chosen and recombined during the GA's reproductive phase, resulting

in off-spring that will make up the following obetetrics. Parents are chosen at random from the population, with more t individuals being given preference. Good people are likely to be chosen multiple times in a generation, while poor people are unlikely to be chosen at all. Following the selection of two parents, their chromosomes are recombined utilizing crossover and mutation mechanisms. These operators come in a variety of forms, the most basic of which are: crossover divides two people into two "head" segments and two "tail" segments by cutting their chromosomal strings at a random location. Two new full-length chromosomes are created by swapping the tail regions (Figure (2.10)). Each parent's genes are passed on to the offspring. Singular point crossover is the term for this. Crossover is not always used for all mating pairings. The likelihood of crossover is normally between 0.6 and 1.0, thus a random pick is made. If no crossover is used, offspring are simply duplicated from their parents. This allows each person to pass on their genes without having to worry about the crossover. Each offspring receives a different mutation after crossing. Each gene is altered at random, and the likelihood of success is extremely low (typically 0.001). Figure (2.11) shows the Mutation of the f^{th} gene on the chromosome (2.8). Generally speaking, the more important of the two methods for quickly scanning a portion of the search field. A small bit of randomness is added to the search through mutation, which also makes sure that no chance to do the search is missed [61-63].

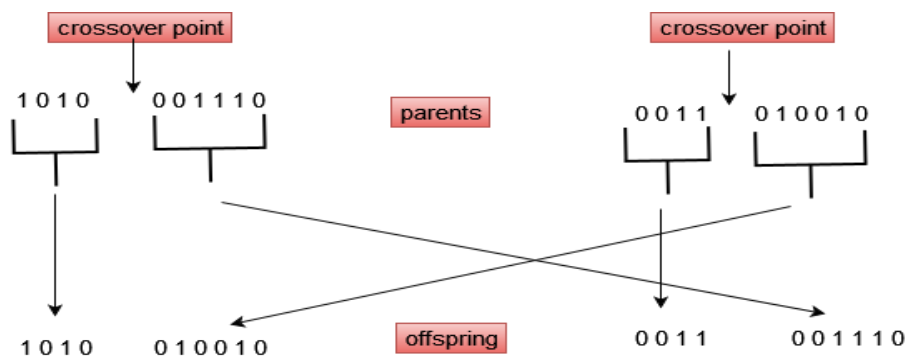


Figure 2.10 Single - point crossover [61].

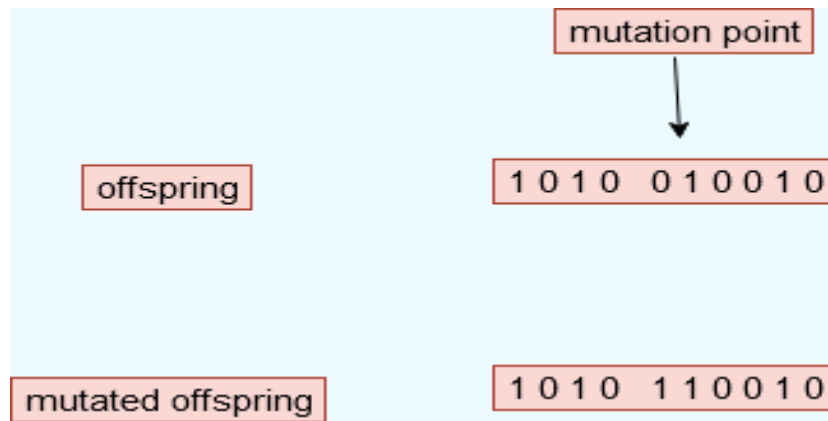


Figure 2.11 Mutation process in GA [61].

Convergence. If the GA is successfully applied, the population will evolve over subsequent generations, bringing the best and average individuals closer to the global optimum. The process of achieving greater homogeneity is known as convergence. When 95 percent of the population has the same value for a gene, it's called convergence [61]. When all of the genes in a population converge, it is said to have converged.

2.3.3 Objective Fitness Function In GA

All types of the objective function are defined as follows:

- Production of the Minimum Pulse: We began by using our evolutionary algorithm-based method to identify the smallest pulsed for our fixed laser cavity.

The functional form we used for this task was as shown in [61].

$$\Psi_1 = \text{RF contrast} + (1/\text{ACF duration})$$

2.7

We added the RF contrast term to the function to ensure the efficacy of the mode-locked regime.

- In a variety of circumstances, either (ps) space-time lumps with (fs) scale sub-pulses or (ns) scale waveforms with (ps) scale vibrations may be required to produce the double scale pulses.

applications, such as optical coherence tomography [62] and the effective generation of the second harmonics [61].

$$\Psi_2 = \frac{1}{\text{ACF envelop}} + \text{Coherence spike contrast} \quad 2.8$$

- Production of the Pulses with a Maximum Power : Finally, in order to identify the pulsed regime with the highest power, we created an objective function.[61,62]

$$\Psi_3 = \text{Power} + \text{RF contrast} \quad 2.9$$

2.4 Control Polarization angle

get a performance that is close to ideal. Although modeling and analysis of such organizations are crucial for defining the underlying variables and range of potential behaviors, organizations' nonlinearities and feeling for a multidimensional parameter space typically make it difficult to make quantitatively precise system performance forecasts. This is particularly true for mode-locked lasers [64], where the primary physical effects have been well-understood for more than three decades, but a quantifiable predictive performance theory has evaded researchers. This quantitative discrepancy emphasizes the underlying and very sensitive characteristics of man's stochastically fluctuating variations in physical elements that engage with the

networked, nonlinear architecture. It is well known that fiber birefringence changes randomly across its length. Consider mode-locked fiber lasers as an illustration.

Environmental temperature variations as well as physical changes to the fiber might affect refraction and the ensuing mode-locking show (bending). To retain performance, fiber lasers intended for industrial usage are networked together and then protected from changes in the environment. As an alternative to environmental shielding, it is possible to use a laser with a robust control mechanism that can detect parameter changes and adaptively modify the parameter site to achieve near-optimal display. In the sections that follow, the author went over how employing adaptive control and machine learning techniques could create a brand-new paradigm for intelligent, self-tuning systems with equation-free architectures. This study's automated system achieved self-tuning and near-optimal performance in a method-locked laser. The learning module explores parameter space with rigor. Identifying areas of optimal performance and building a collection of these parameter rules .

2.4.1 Control angle Problem Formulation

Among other things, the intra-cavity dynamics of the mode-locked laser of interest should be used to account for the different polarization dynamics and energy equilibration that start the mode-locking process. Figure (2.12) illustrates of a cavity construction that has been used in tests to produce stable and long-lasting mode-locking [64]. Incorporating chromatic dispersion, Kerr nonlinearity, absorption, and bandwidth-limited, saturating gain, the other physical properties of the laser cavity are combined into an average total propagation equation [65–71]:

$$i \frac{du}{dz} + \frac{D}{2} \frac{d^2u}{dt^2} - Ku + (|u|^2 + A|v|^2)u + Bv^2u^* = ig(z) \left(1 + \Omega \frac{d^2}{dt^2}\right)u - i\Gamma u \quad 2.10$$

And,

$$i \frac{dv}{dz} + \frac{D}{2} \frac{d^2v}{dt^2} - Ku + (A|u|^2 + |v|^2)v + Bu^2v^* = ig(z) \left(1 + \Omega \frac{d^2}{dt^2}\right) v - i\Gamma v \quad 2.11$$

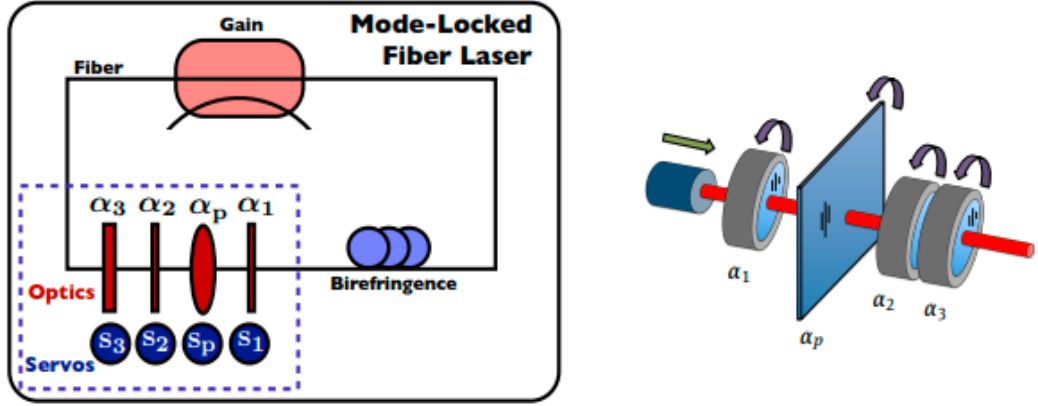


Figure 2.12 A schematic for a fiber laser that is mode-locked [72].

There are two related nonlinear Schrödinger equations on the left side of this equation (CNLS). This system simulates the non-dimensionalized averaged propagating of two orthogonally polarised electric field envelopes over a birefringent optical fiber, with the u and v fields being orthogonally polarized electric field components [73-76]:

$$g(z) = \frac{2g_0}{1 + \frac{1}{E_0} \int_{-\infty}^{\infty} (|u|^2 + |v|^2) dt} \quad 2.12$$

linear attenuation, in addition to (cavity losses). models the distributed loss of the fiber laser cavity caused by the output coupler, fiber attenuation, interconnections, and splicing. In this equation, g_0 and E_0 stand for the gain (pump) strength and cavity saturation energy, respectively. The width of the gain medium is determined by

this parameter. For instance, erbium-doped fiber has a gain bandwidth of around 20–30 nanometers. This paper aims to identify an effective cavity birefringence proxy by utilizing complex data methodologies, such as machine learning methods. A pulse may have a numerical average across a wide range of distances, but in contrast to optical communications, the dynamics of a laser cavity are controlled by a single realization of a stochastic change in birefringence (see Figure 2.13). The cavity becomes disturbed by bends, twists, orthotropic strain, and/or ambient temperature, leading to the development of a new understanding. It is crucial to precisely characterize or detect fiber birefringence in order to enhance performance and, for example, to determine the wave plate and polarizer settings that have the maximum energy efficiency. The ultimate objective of our individual learning subsystem is not to copy or mimic the unique birefringence, but rather to evaluate the impact of birefringence on performance and discover the most suited operating regimes given it.

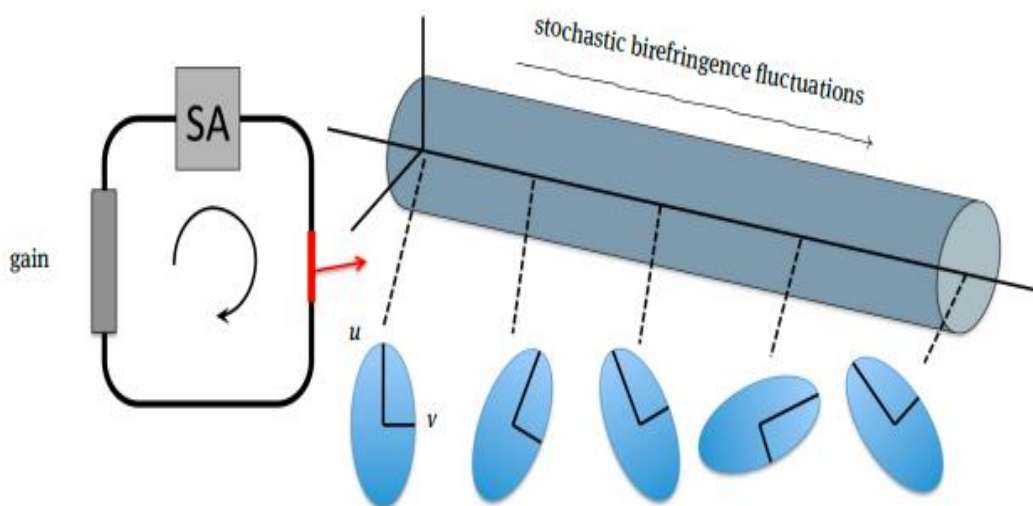


Figure 2.13 impacts of polarization angles, adapted from [77].

2.4.2 PID controller and objective functions

Finding all of the input restrictions that can be utilized to control and alter the behavior of the system is the first stage in the toroidal search. The mode-locked fiber laser used in the trial setup has a polarizer and three wave plates that can be rotated from 0 to 2, creating a 4-torus parameter space. Additionally, polarization ears that may modify cavity birefringence can be included. The author was assume the average birefringence is set to an unknowable value for the time being. Surprisingly, the approach suggested here could be the sole feasible choice for training several NPR laser cavities to achieve ideal, high-capacity performance. This requires sampling or data mining of the generated parameter. One develops a spiral search algorithm (4N-torus). The author will want 4N time series made up of" if we want to examine this 4N-dimensional torus: [76]

$$\theta_j(t) = w_{jt} + \theta_{j_0} \tag{2.13}$$

The input is the angle of the half wave plate, as seen in Figure (2.14). Then, the later-introduced objective function is measured. Additionally, a high-pass filter allows just the variance of the measured objective function to pass. After that, a sin signal with the same frequency as the fluctuation in the input is multiplied by the high-pass filter's output. To guarantee that the PID controller has the highest efficiency possible, the phase is employed to compensate for the additional phase shift induced by the high-pass filter and the integrator is simple to compute

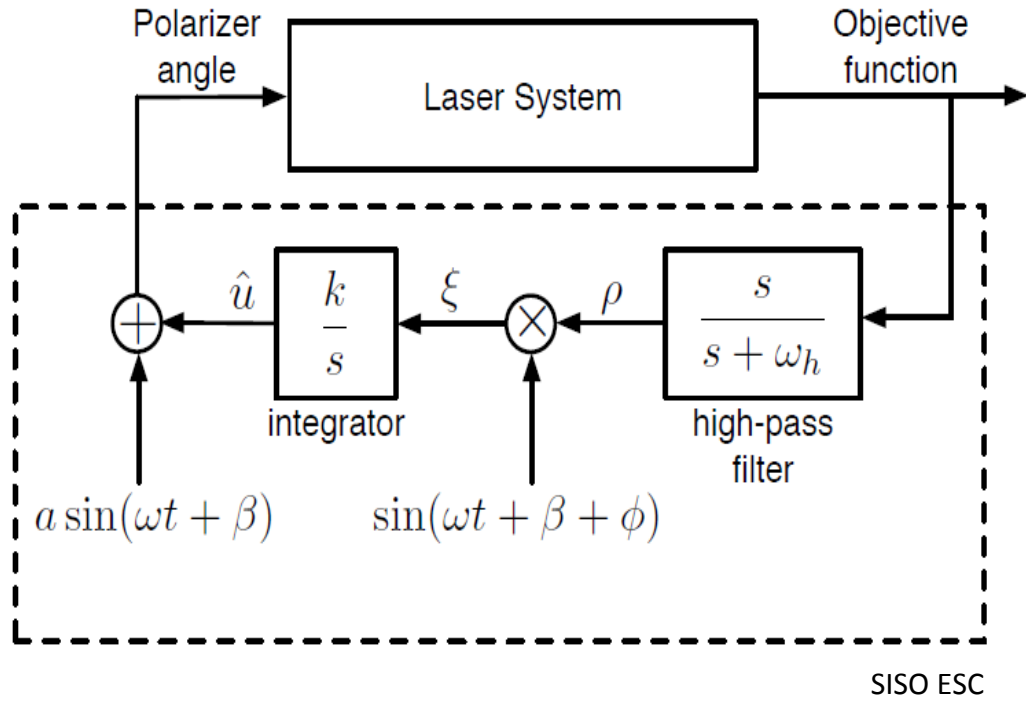


Figure 2.14 Schematic diagram of the proposed PID control system [76].

identified the value of "objective function" as a performance indicator for the system. In this thesis, an objective function for the laser output pulses is defined. Higher pulse energy and shorter pulse length pulses are preferred for the lasers. To ensure that the ESC is as efficient as possible, we define objective function as monitoring phase shift caused by high-pass filter and integrator. It is simple to compute [76] :

$$f(\alpha_3) = \frac{E}{M_4} \quad 2.14$$

Where E is the energy, and M4 is the fourth component of the angler momentum.

It is defined as[76]:

$$M_4 = \int I(t)(t-t_0)^4 dt \quad 2.15$$

Where I is the laser intensity pulses, and t_0 is the time of peak.

2.5 Summary

In the second chapter, the author worked on the mathematical representation with equations to lasers, types of modes, and signal propagation in the Optical Fiber and, discussed the technique of increasing the gain and explained a summary of the nonlinear properties. The author discussed and studied the genetic algorithm with its equations and worked on getting the best angle to receive an exact signal with equations and mathematical representation. To establish a master for each case.

Chapter Three

Proposed System Design and Implementation

3.1 Introduction

In this chapter, the different main three categories that have been explained in chapter 2 will be designed based using the Simulink Matlab and opt-net software.

3.2 Single and multi-mode fiber

The intriguing possibility of not requiring optical components at the fiber output arises when light is specifically delivered through optical fibers, opening up possibilities for miniaturized light delivery in a variety of applications, including endoscopy , telecommunication, item processing, remote sensing, and more [78-88]. Endoscopy has shown useful for minimally invasive in vivo image-based medicine, helping to lower mortality and morbidity rates. The area of optical communication is flourishing by exploiting using a variety of characteristics of light, such as polarization, wavelength, electric field amplitude, and phase. Optical fibers are used for faster and better data transmission rates [82,89]. The entire potential of such techniques must be realized, which calls for a complete understanding of how a shaped beam moves through a certain fiber.

One may determine the light propagation through the fiber by experimentally obtaining its Transmission Matrix (TM) [90,91]. This experimental Transmission Matrix (TM) must be updated whenever the fiber's bending or twisting changes significantly; otherwise, it is only accurate if the fiber conformation stays constant. Theoretically, using perturbation theory [92], the TM for a precisely defined bending may be calculated. The memory effect [93], a mechanism that relates the random patterns made at the distal end of stationary fibers to those made at the ends of fibers bent at various angles, aids in dynamically predetermining the TM.

Recently, digital phase conjugation for multicore fibers or real-time wave front shaping in multimode fibers has both been shown using fast binary deformable mirror devices (DMD) [94,95]. In Figure (3.1), the Simulink implantation for the single mode laser across the fiber is depicted .

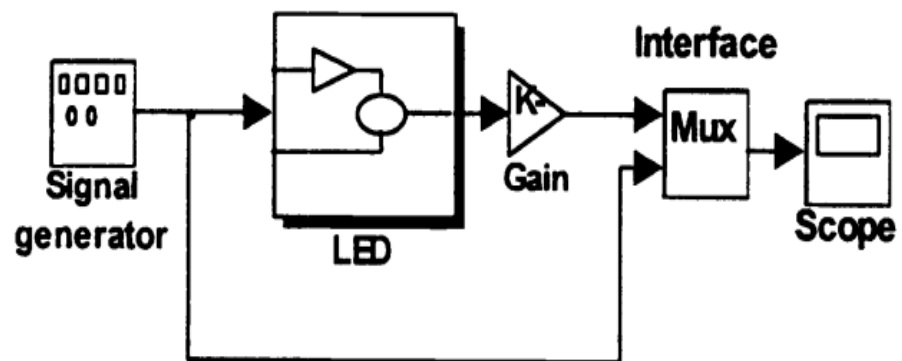


Figure 3.1 Single mode Laser generating schematic diagram [94].

Figure (3.1) illustrates the LED block alongside other blocks, such as a signal generator and scope. The settings of an LED block may be readily changed by the user. The blocks that are presented can be used to mimic a variety of optical

connection topologies since the positioning of the blocks relies on the user's system construction. This example has just educational objectives and will use a point-to-point topology. The simulated connection, which is mounted only using blocks from the five groups, as shown in Figure (3.2).

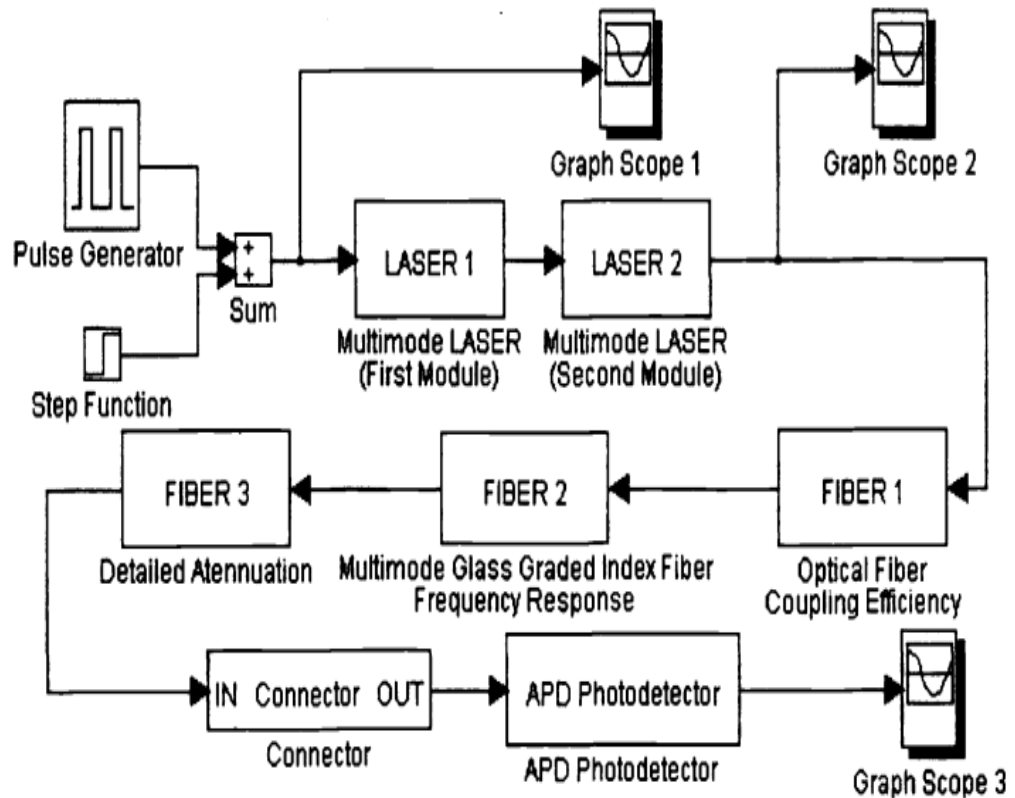


Figure 3.2 Multi laser modes with bending effects over the fiber [95].

However, numerical techniques must be utilized in addition to these theoretical methods, especially for complex fiber configurations and circumstances where perturbation theory may no longer be applicable, to measure the memory effect and precisely anticipate beam propagation. The scientific community frequently uses the Finite-Difference Eigen mode solver and the Eigen mode Expansion propagator for optical fiber modeling techniques based on the Beam Propagation Method (BPM). These modeling tools are not free nor expressive (library), yet they can reproduce a wide variety of free-space applications, waveguides and non-linear optics regimes.

Additionally, many of these tools limit the complexity of arbitrary structure designs by assuming the symmetry of the fiber/component geometry by modeling just a subset (for example, a half or a quarter) of the required geometry. Figure (3.3) shows a different type of laser beam caused by using one single laser pumping with two mirrors and one coupler loop. Generally, from Figure (3.2), the bending effect started from 8cm till 20 cm, the wavelength of the laser pulses is 1526 till 1544. The power is -60 dB till -20 dB. The bending would be made the center of the maximum power peak shift from one wavelength to another .

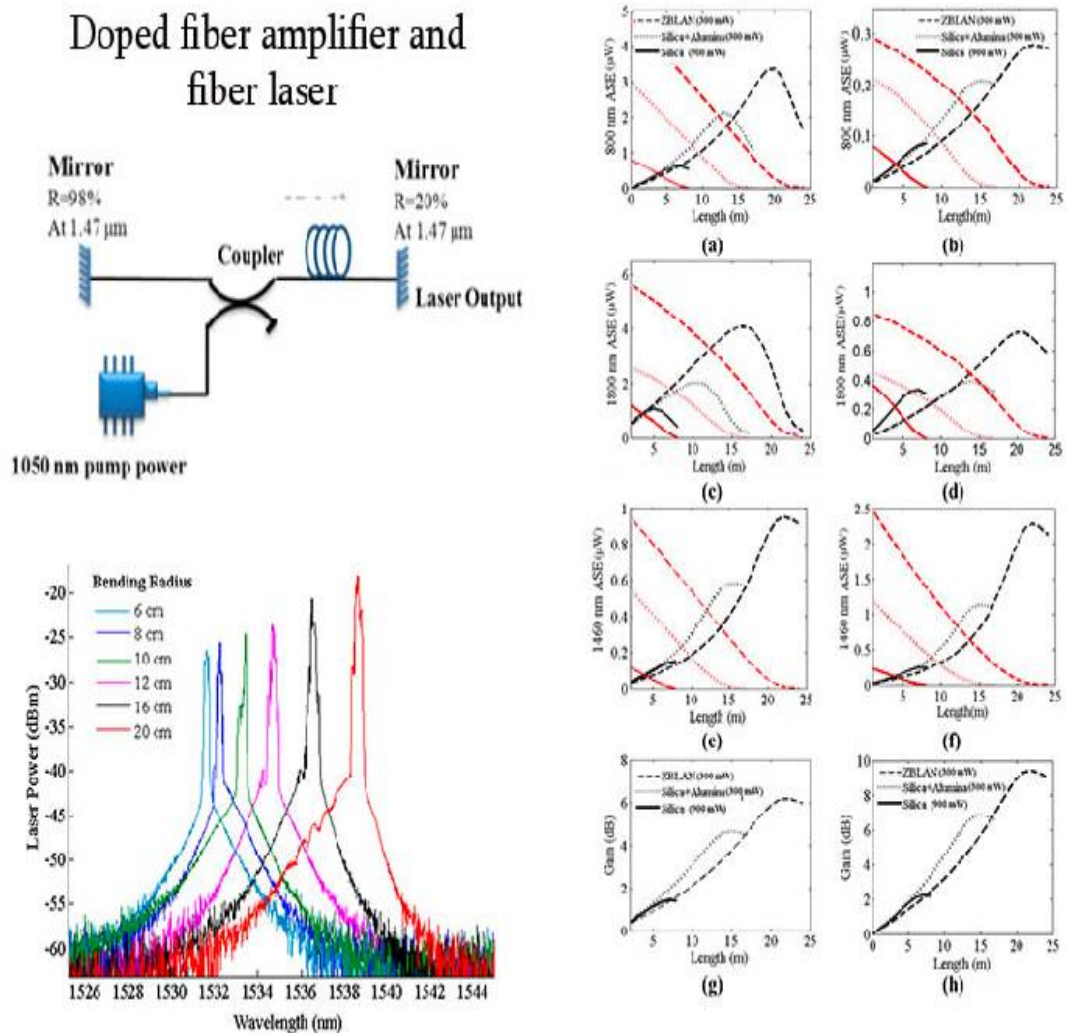


Figure 3.3 Schematic diagram with different bending effect (6cm-20cm); (a) bending effect for 6 cm; (b) bending effect of 8 cm; (c) bending effect of (10 cm); (d) bending effect of (12 cm); (e) bending effect of (16 cm); (f) bending effect of (20 cm); (g) no bending with noisy single mode; (h) no bending single mode [95]

The second main attention is how the pulse of the laser looks like in the fiber traveling, and essentially when the duration of the pulses is narrow that means it is a constraint and it keeps the information receiving without loss. Figure (3.4) shows samples of the main common shape of the laser pulse which is depends up on the wavelength.

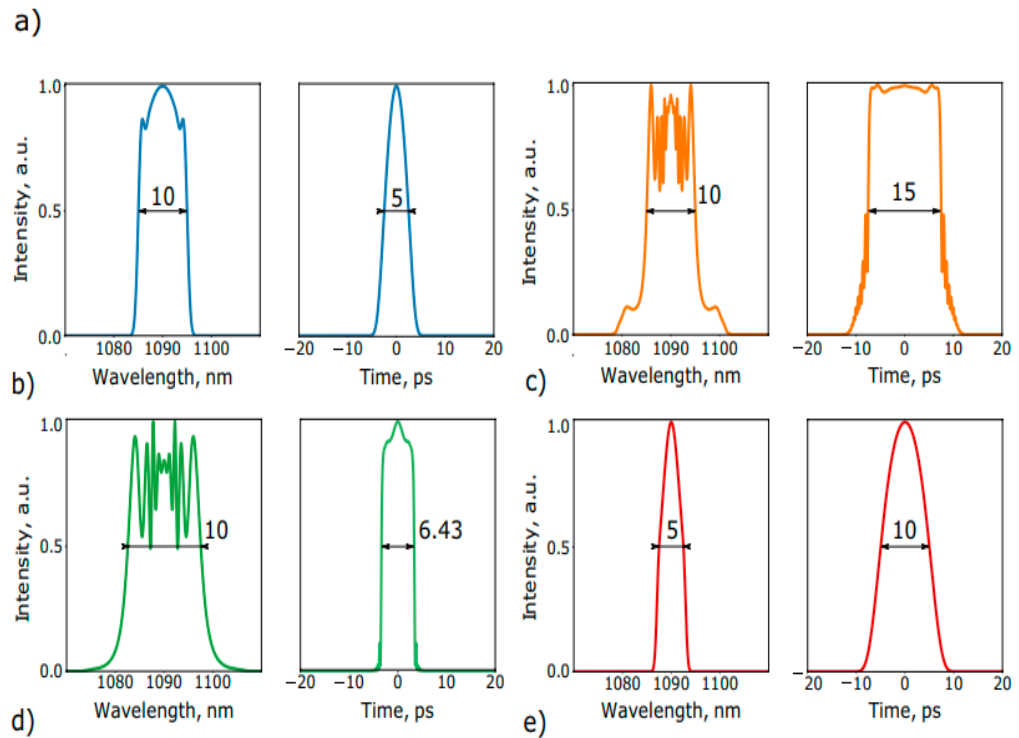


Figure 3.4 (a) to (e) samples of the temporal waveform and spectral profile of the dissipative solitons produced on demand [94]

3.3. Open Net Program And Used Parameters

3.3.1 Introduction

One of the most popular evaluation approaches in the field of computer networks is without a doubt network simulation. In order to get a practical touch with reality in communication and networking, whether it be wired or wireless, practical understanding in modern networking is therefore a requirement for every network engineer. Many simulators, including REAL, NetSim, Harvard Simulator, NS-2,

OMNeT++, and others, have been created by academic community students and researchers because to their usefulness and power in enabling the capacity to quickly experiment with many design possibilities in the design space. The author have specifically chosen OPNET (Optimized Network Engineering Tool) as a simulator in this study and have provided a thorough analysis of its features and application. Additionally, we have made an effort to condense the important elements that various user groups find particularly interesting. First, we'll demonstrate how OPNET may be utilized as a practical research instrument to improve network engineers' technical proficiency. This paper's analytical modeling and simulation of a few projects, which are thought to be crucial components of an advanced course on telecommunication networks, is another significant contribution. The objective of analytical modeling is to carry out some straightforward calculations of various parameters (such as Delay) on a condensed network configuration that will serve as the network performance. To do this, we must first establish a representative topology and add the desired traffic to it; as a result, the traffic from the new services was implemented as explicit traffic while the traffic from already-existing services was defined as background traffic. Using individual statistics, we extract the outcome from the simulation and display it graphically [96].

3.3.2 OPNET As a Research Tool

Researchers need to use effective hardware platforms, flexible methodologies, simulators, and other tools to meet the high computational needs of current state-of-the-art application domains. Because it can simulate a broad range of networking protocols, OPNET is considered to be highly helpful in this situation as a simulator.

It also permits modeling of the complete network, including its servers, routers, switches, protocols, and the various applications they support. The direct access to the source code and user-friendly front end are two features that make OPNET a communications-oriented simulation language. Three main model levels, including the process layer, the node layer, and the network layer, make up OPNET models. The ability to construct process models using finite state machines encourages a modular strategy because large networks may be divided into individual states, and each state can then be separately described and executed. Node models, which can be either preset OPNET artifacts or user-defined models, are employed at the next level of abstraction. A hierarchy of sub-networks may be represented by the network model, which is found above this in the hierarchy. The tool has been found to be a great help in enhancing student learning and bringing student interest to computer network courses because it is used to help the students and researchers critically analyze, evaluate, and explain the behavior and operation of contemporary data communication systems at a high level. The simulation tool also offers the researchers the chance to investigate the interoperability and performance issues related to homogeneous and heterogeneous data communications environments as well as to design, simulate, and evaluate suitable networking solutions to a variety of real-world data communication issues. Through modeling and experimenting, this low-cost active learning environment helps students and researchers gain a deeper knowledge of the network. Thus, the researchers gain useful hands-on experience that enables them to conceive in terms of practical applications, i.e., the recommendations to choose the best among the different feasible design possibilities in reality. The usage of communications and networking systems is widespread nowadays, with applications in the military, health care, education, and other fields.

In these contexts, OPNET is a strong and adaptable instrument that is undoubtedly the preference of business. In light of its effectiveness and thorough modeling, OPNET may thus prove to be a helpful tool for researchers [96].

3.3.3 Features of OPNET

Modeling, simulating, and analyzing are the three basic tasks that OPNET is typically capable of performing. It offers a very basic yet complete graphical framework for modeling, allowing for the creation of various protocols models. Additionally, the simulation uses three distinct but cutting-edge simulation methods and can be used to a variety of investigations. The displayed data from the simulation results can be easily evaluated for analysis purposes. The user-friendly graphs, charts, data, and animations that OPNET can provide make the simulator development environment very accessible. Simply put, OPNET is incredibly practical for its users and has established itself as a crucial tool for system design. Additionally, using OPNET for modeling enables users to offer design specifications with confidence that save time and money from the very start of the design lifecycle. The following list includes a few more OPNET features [96]:

- Source code offers a large number of components in its library
- Modeling based on objects (Object Oriented Modeling)
- Graphical user interface supports 32-bit and 64-bit
- Parallel simulation kernel supports 32-bit and 64-bit.
- Graded or ordered modeling environment.
- Wireless modeling is also customizable.

- Scalable wireless simulation support.
- Also support grid computing.
- Hybrid, discrete event and analytical simulation • Open interface for integrating external component libraries.
- Comprehensive development environment.
- GUI-based debugging.
- Discrete event simulation can be used to examine the behavior and efficiency of modeled systems.
- Its object-oriented design with clearly defined interfaces; modifications made to one module have little to no impact on the functionality of the other nodes. As a result, the entire model continues to function as intended simply by maintaining an adequate interface.

To start OptiSystem, perform the following procedure:

Starting OptiSystem

StepAction

1. On the Taskbar, click Start.
 2. Select Programs > Optiwave Software > OptiSystem 7 > OptiSystem.
- OptiSystem opens and the graphical user interface appears (see Figure 3.5).

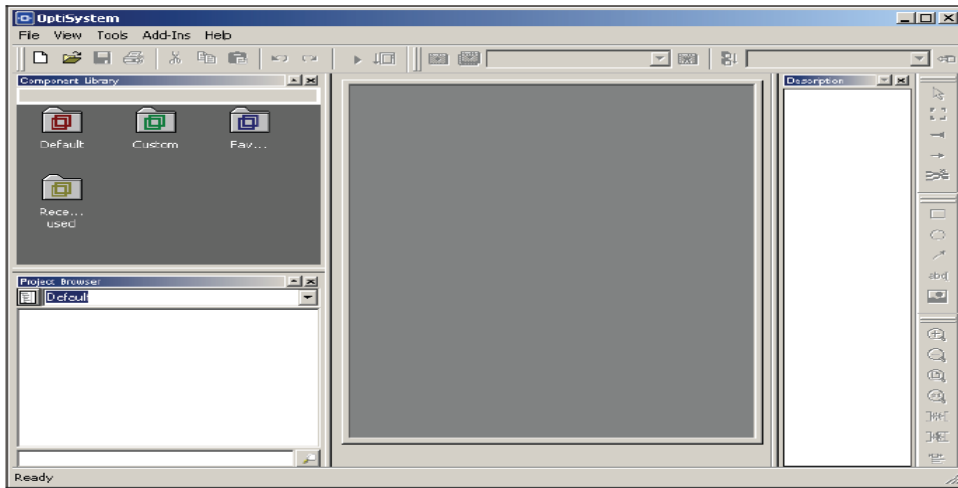


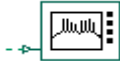
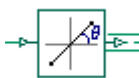



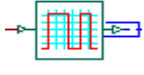
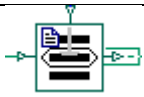
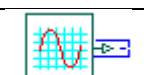

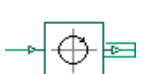
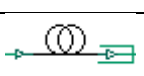
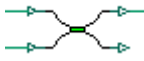
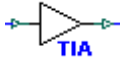

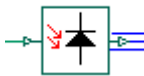
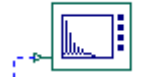


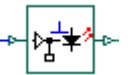
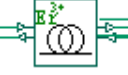
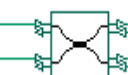
Figure 3.5 OptiSystem opens and the graphical user interface appears

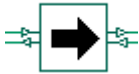
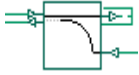



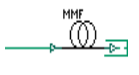
Table 3.1 The component of optisystem in the table that used

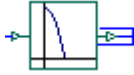
No	Component Name	Description	Icon
1.	User-Defined Bit Sequence Generator	Generates a bit sequence that is user-defined	
2.	Spatial LED	This component is an LED that includes transverse mode profiles in the optical output. It is a subsystem built using the LED component and the Multimode Generator	
3.	optical spectrum analyzer	Input/output optical	
4.	Linear Polarizer	Simulates an ideal linear polarizer	
5.	Polarization analyzer	Lower and upper frequency limit	

6.	Oscilloscope visualizer	Output	
7.	Optical time domain visualizer	Optical output	
8.	NRZ Pulse Generator	Generates a Non Return to Zero (NRZ) coded signal	
9.	Dual Drive Mach-Zehnder Modulator Measured	Simulates a Mach-Zehnder modulator with dual-drive modulation using measured parameters	
10.	Sine Generator	Generates an electrical sine waveform signal	
11.	Power Splitter 1x2	Ideal power splitter - splits an optical input signal into two output signals	
12.	Circular Polarizer	Simulates an ideal circular polarizer	
13.	Optical fiber	The optical fiber component simulates the propagation of an optical field in a single-mode fiber with the dispersive and nonlinear effects taken into account by a direct numerical integration of the modified nonlinear Schrödinger (NLS) equation (when the scalar	

		case is considered) and a system of two, coupled NLS equations when the polarization state of the signal is arbitrary. The optical sampled signals reside in a single frequency band, hence the name total field. The parameterized signals and noise bins are only attenuated.	
14.	X Coupler	Cross coupler for combining or splitting optical signals	
15.	Transimpedance Amplifier	This component is an electrical transimpedance amplifier with user defined noise figure. It has linear gain and additive thermal noise	
16.	Low Pass Butterworth filter	Optical filter with a Butterworth frequency transfer function	
17.	Photodetector PIN	PIN photodiode	
18.	RF Spectrum analyzer	Frequency output	

19.	Controlled Pump Laser	<p>This component is a pump laser that can be controlled by an electrical analog signal. It allows the design and simulation of automatic gain control schemes for optical amplifiers, such as control loops for the pump laser current.</p>	
20.	Erbium Doped Fiber	<p>This component simulates a bidirectional Erbium doped fiber considering ESA, Raleigh scattering, ion-ion interactions, and temperature dependence effects. The component solves numerically the rate and propagation equations in the steady-state case, assuming a two-level Erbium system for an inhomogeneous and homogeneous approach</p>	
21.	Coupler Bidirectional	<p>This component is a cross-coupler for combining or splitting the optical signal. It is bi-directional, with wavelength dependent coupling, insertion loss and return</p>	

		loss	
22.	Isolator Bidirectional	This component is an isolator. It is bidirectional, with wavelength dependent isolation, insertion loss and return loss	
23.	Pump Coupler Counter-Propagating	Equivalent to a subsystem where you can control the attenuation of the signal and pump independently	
24.	3R Regenerator	This component regenerates an electrical signal	
25.	Ber Analyzer	Bit error rate	
26.	Optical Null	Generates a zero-value optical signal	
27.	Linear Multimode Fiber	This component is a multimode fiber. The component has two modes of operation. The first one assumes the fiber has sufficient mode mixing due to imperfections or splices; in this case the modal transfer function approaches a Gaussian function. The second one allows the user to load measured modal delays and	

		power-coupling coefficients. The component also includes first- and second-order chromatic dispersion	
28.	Low Pass Gaussian filter	Optical filter with a Gaussian frequency transfer function	

3.4 Single Gain Loop With Genetic Algorithm Proposed System

look at the design of the mode-locked (shown in Figure (3.6)), figure-eight fiber laser cavity (section (2.3)). The cavity is made up of two unidirectional and bidirectional fiber loops on the left and right, which are coupled together by a 40/60 coupler. Amplifying portions are pumped by multi-mode laser diodes in both loops of the laser resonator. Only polarization-maintaining components make up the laser cavity, preventing problems related to nonlinear polarization development. The radiation that is produced as a result is linearly polarized. The two pump diodes' currents may be independently controlled, which allows for extensive variation in the pulsed regimes' Average output power, radio-frequency contrast, time spent in the Autocorrelation performance and coherence level. The parameters of the pulsed generating regimes were thoroughly measured using an automated system for laser controller, data gathering, and processing (section (2.3)). The power was mostly derived from the autocorrelation readings for diagnostics. It should be verified that the usage of certain radiation in the feedback loop is not having an impact on the performance of the system as a whole .

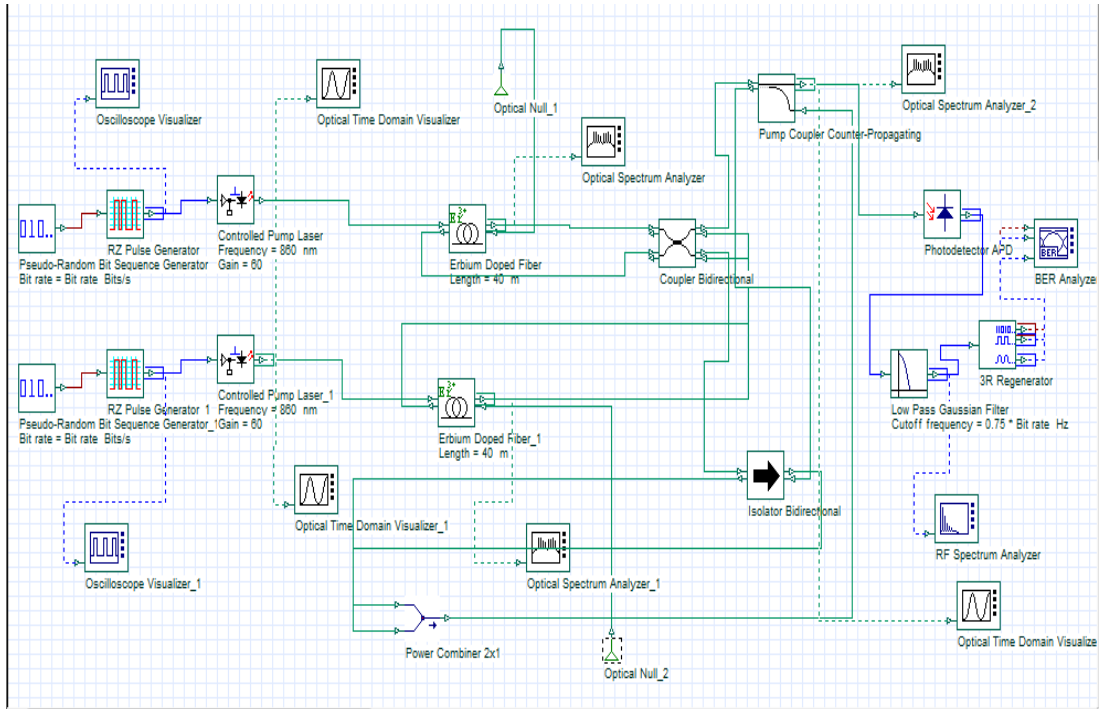


Figure 3.6 The Proposed system based on single opt-net software.

A fiber laser schematic shows both of the loops to have two active fiber stretches for single mode with coupler. The transmission part of a fiber laser schematic showing both of the loops to have two active fiber stretches in single mode contains two generates a Pseudo Random Binary Sequence (PRBS) according to different operation modes. The bit sequence is designed to approximate the characteristics of random data. The proposed system setup parameters are illustrated in Table (3.2) .

Table 3.2 A fiber laser schematic showing both of the loops to have two active fiber stretches in single mode

No	No. of Parameters	Value
1.	Pseudo-Random Bit Sequence Generator	Bit rate
2.	Oscilloscope visualizer	Automatic range(amplitude)

3.	RZ Pulse Generator	Exponential
4.	Controlled Pump Laser	860nm
5.	Optical time domain visualizer	Automatic range(power)
6.	Erbium Doped Fiber(single mode)	40m
7.	Optical Null	Iterations
8.	Power Combiner 2x1	0db
9.	Optical spectrum analyzer	Automatic range(power)dbm
10.	Coupler Bidirectional	Independent
11.	Isolator Bidirectional	Independent
12.	Pump Coupler Counter-Propagating	Signal attenuation (0db)
13.	Photodetector APD	Gain (3)
14.	Low Pass Gaussian filter	Cutoff frequency (0.75 * bit rate)
15.	RF spectrum analyzer	Automatic range(power)dbm
16.	3R Regenerator	Reference bit rate (Bit rate)
17.	BER Analyzer	Time (bit period) Max. Q. Factor

They are responsible for two for generating random data coded as a return to zero (RZ). Oscilloscope visualizer from output of (RZ) which appears the

information. The part of a two-pump laser that an analog electrical signal can operate. It enables automated gain control systems for optical amplifiers, like control loops for the pump laser current, to be designed and simulated. Two Optical Time Domain Visualizer to visualize optical signals in time domain with an Optical Time Domain Visualizer. Two component simulates a bidirectional Erbium doped fiber considering ESA, Raleigh scattering, ion-ion interactions, and temperature dependence effects. The component solves the rate and propagation equations in the steady-state case, assuming a two-level Erbium system for an inhomogeneous and homogeneous approach, Ideal power combiner - combines two optical input signals. Optical Null Generates a zero-value optical signal. Using an optical spectrum analyzer and a bidirectional coupler, one may see optical signals in the frequency domain. For combining or dividing the optical signal, this component functions as a cross-coupler. It is bi-directional, with wavelength dependent coupling, insertion and returns losses

IsolatorBidirectionalIsolator best describes this component. It has wavelength-dependent isolation, insertion loss, and return loss, and is bidirectional, as illustrated in Figure (3.7).

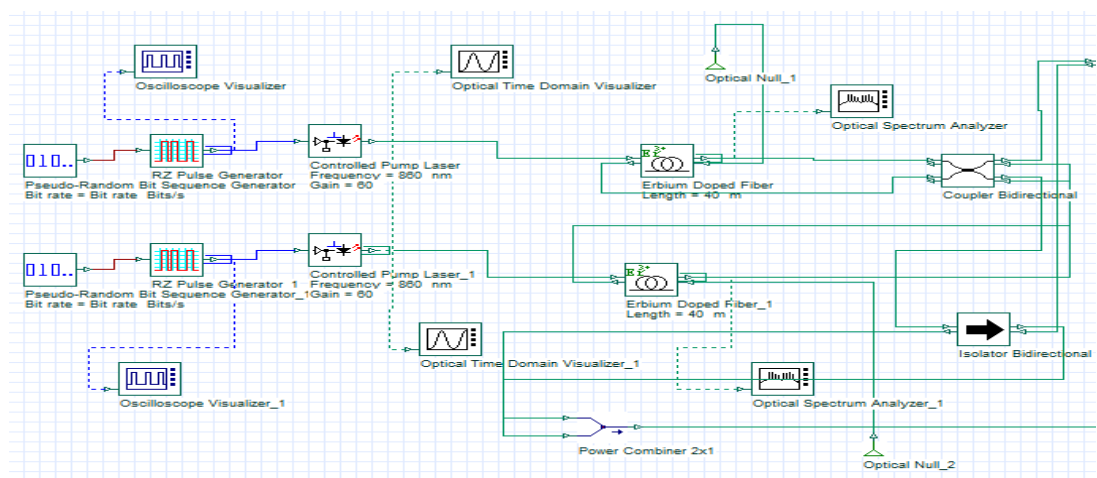


Figure 3.7 Transmission part.

The channel section of Figure (3.8) has two erbium-doped fibers that "This component simulates a bidirectional erbium-doped fiber taking into account ESA, Raleigh scattering, ion-ion interactions, and temperature dependency effects." The component assumes a two-level Erbium system for both an inhomogeneous and homogeneous approach and numerically solves the rate and propagation equations in the steady-state situation. Creates an optical signal with a value of zero. Optical Time Domain Visualizers are used to view optical signals in time using two such devices.

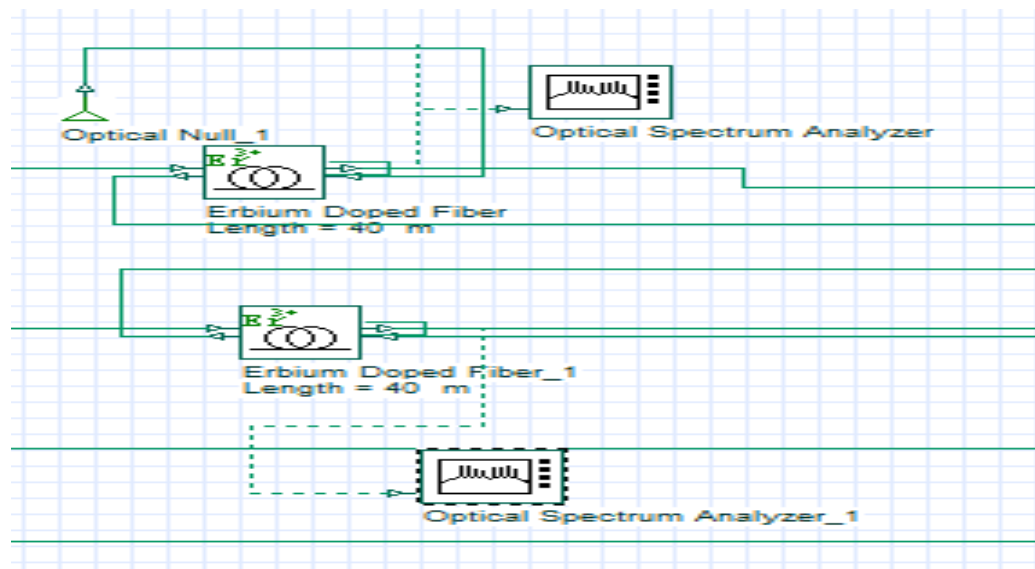


Figure 3.8 The channel part.

The receiver part of a fiber laser schematic shows both the loops to have two active fiber stretches in single mode containing Pump Coupler Counter-Propagating Equivalent to a subsystem where controlling the attenuation of the signal and pump independently, Photodetector APD Filter with a square cosine roll off frequency transfer function. Low Pass Gaussian filter Optical filter in the presence of a Gaussian frequency transfer function . The RF spectrum analyzer is used after the

PIN in order to display the laser frequency response. This component regenerates an electrical signal. BER Analyzers display the Eye Diagram, Q-factor curve, Min BER, Threshold, Eye Height, and BER Patterns represents the optimal point as shown in Figure (3.9).

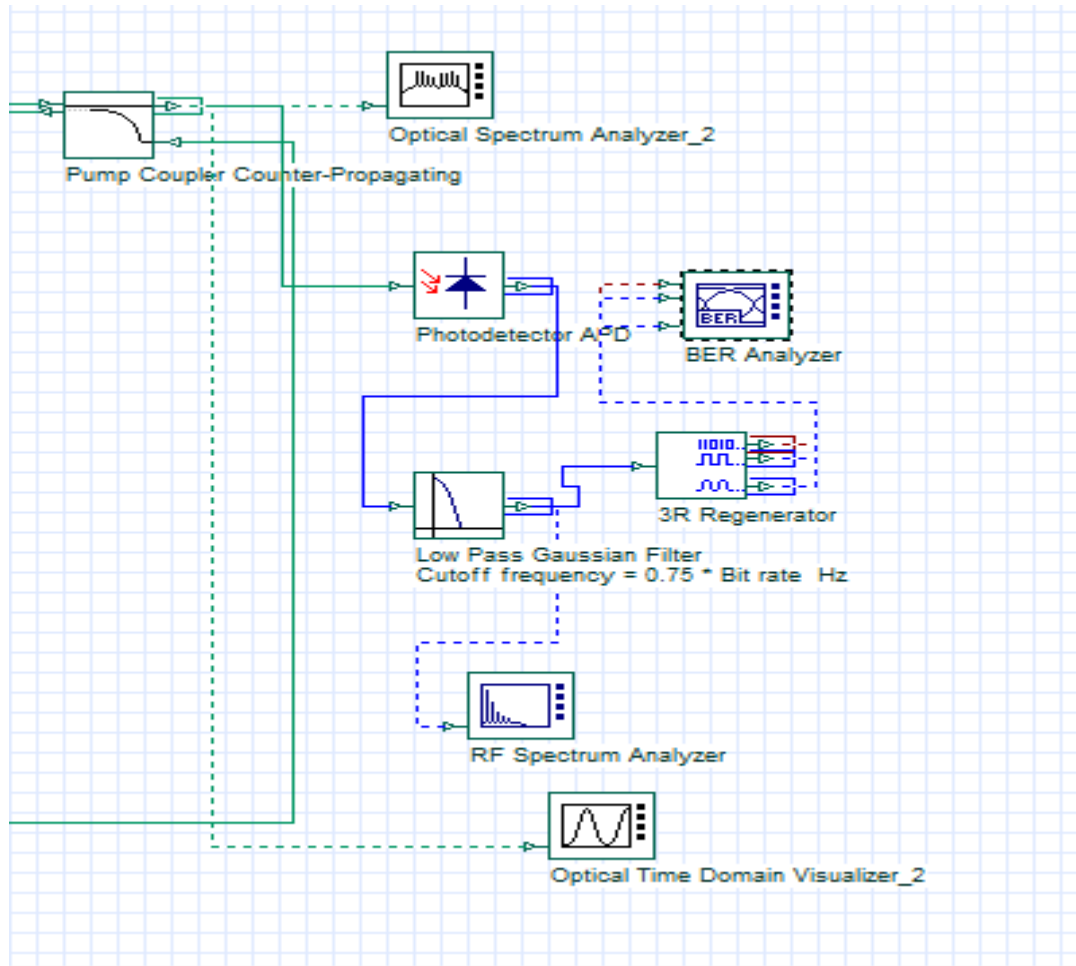


Figure 3.9 Measurements devices.

3.5 Multi-Mode With Coupler Gain Loop With Genetic Algorithm Proposed System

The transmission part (Figure (3.10)) of a fiber laser schematic shows both of the loops to have two active fiber stretches in single mode containing two Generates a Pseudo Random Binary Sequence (PRBS) according to different operation modes. The bit sequence is designed to approximate the characteristics of random data. They

are responsible for two generating random data coded as a return to zero (RZ). Oscilloscope visualizer from the output of (RZ) which shows the information. For Spatial Laser Rates Transverse mode profiles are included in the optical output of this laser-based component, and Table (3.3) shows the setup requirements for this kind of coupler fiber.

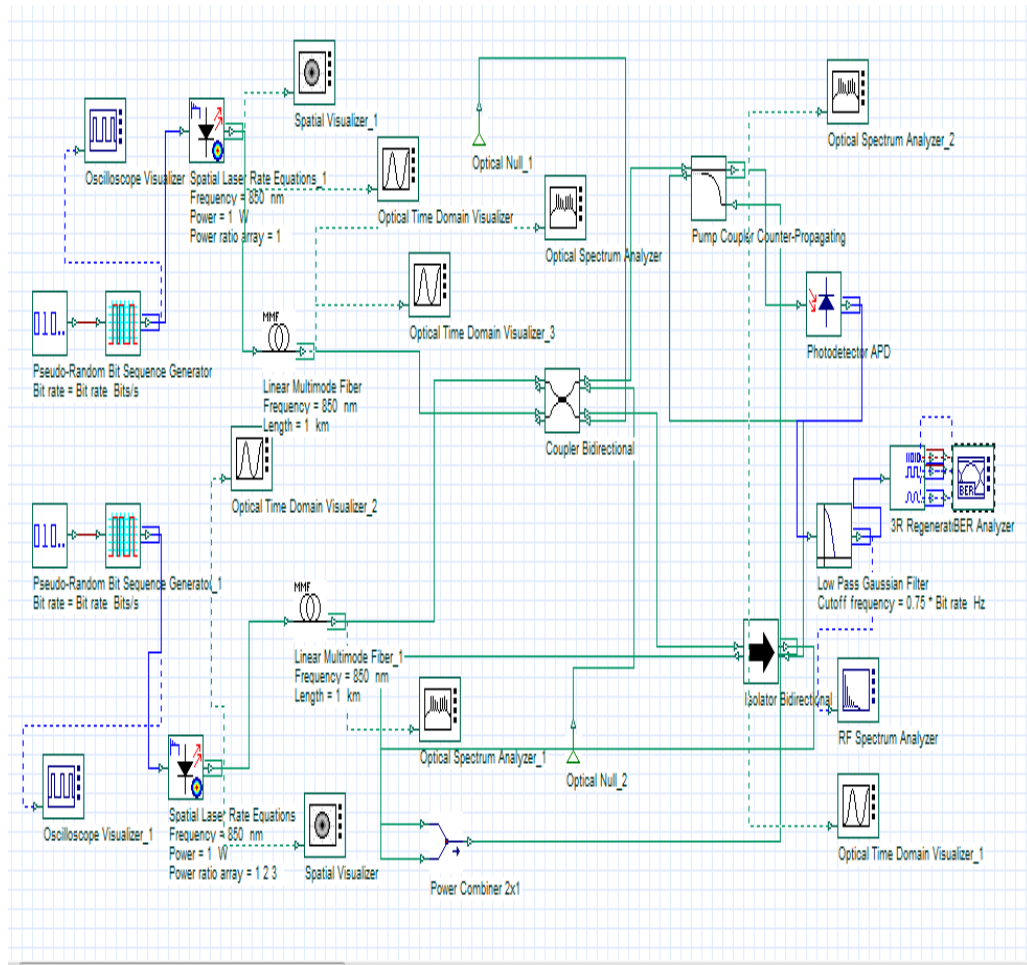


Figure 3.10 A fiber laser schematic showing both of the loops to have two active fiber stretches for multimode with coupler.

Table 3.3 Parameters setup for double gain coupler laser fiber proposed system.

No	No. Parameter	Value
1.	Pseudo-Random Bit Sequence Generator	Bit rate
2.	Oscilloscope visualizer	Automatic

		range(amplitude)
3.	RZ Pulse Generator	Exponential
4.	Controlled Pump Laser	850nm
5.	Optical time domain visualizer	Automatic range(power)
6.	Erbium Doped Fiber(single mode)	1km
7.	Optical Null	Iterations
8.	Power Combiner 2x1	0db
9.	Optical spectrum analyzer	Automatic range(power)db.m
10.	Coupler Bidirectional	Independent
11.	Isolator Bidirectional	Independent
12.	Pump Coupler Counter-Propagating	Signal attenuation (0db)
13.	Photodetector APD	Gain (3)
14.	Low Pass Gaussian filter	Cutoff frequency (0.75 * bit rate)
15.	RF spectrum analyzer	Automatic range(power)db.m
16.	3R Regenerator	Reference bit rate (Bit rate)

17.	BER Analyzer	Time (bit period) Max.Q.Factor
18.	Spatial Laser Rate Equations	Measurements mode ,sum, weights

It is a subsystem created utilizing the Multimode Generator and the Laser Rate Equations component. Optical Time Domain Visualizers, two using an optical time domain visualizer, one may see "optical signals in the time domain, Multimode fiber that is Imflt is a multimode fiber in this part. The component operates in two different modes. The modal transfer function in the first scenario is close to a Gaussian function since it is predicted that the fiber has adequate mode mixing as a result of flaws or splices. The user can load measured modal delays and power-coupling coefficients using the second one. The First- and second-order chromatic dispersion are also included in the component. The element, which assumes a two-level Erbium system for both an inhomogeneous and homogeneous approach, numerically solves the rate and propagation equations in the steady-state situation. Ideal power combiner - combines two optical input signals. The Spatial Visualizer and the profile of each mode supplied at the visualizer input port may be seen using the spatial visualizer. The user may choose the graph's polarization (X or Y), format (Polar or Rectangular), and other options (Power, Phase, Real or Imaginary part). Optical Null produces an optical signal with a zero value. Using an optical spectrum analyzer and a bidirectional coupler, one may see optical signals in the frequency domain. Figure (3.11) shows a cross-coupler for combining or dividing an optical signal.

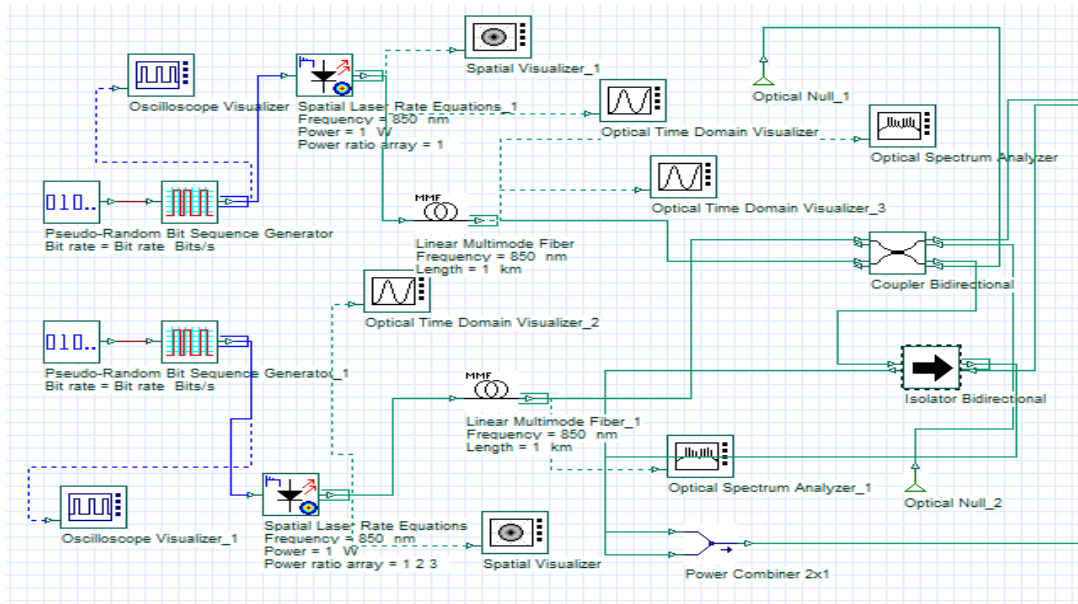


Figure 3.11 Transmission part with coupler.

It is bi-directional, with wavelength dependent coupling, insertion loss and return loss. Isolator Bidirectional This component is an isolator. It is bidirectional, with wavelength dependent isolation, insertion loss and return loss. The channel part (Figure (3.12) contains two Linear Multimode Fibers. This component is a multimode fiber. There are two ways that the component can operate. In the first, it is assumed that the fiber has enough mode mixing as a result of flaws or splices; in this scenario, the modal transfer function resembles a Gaussian function. With the second, the user may load actual modal delays and power-coupling coefficients. Additionally, the component has first- and second-order chromatic dispersion. To visualize the laser frequency response, utilize an RF spectrum analyzer.

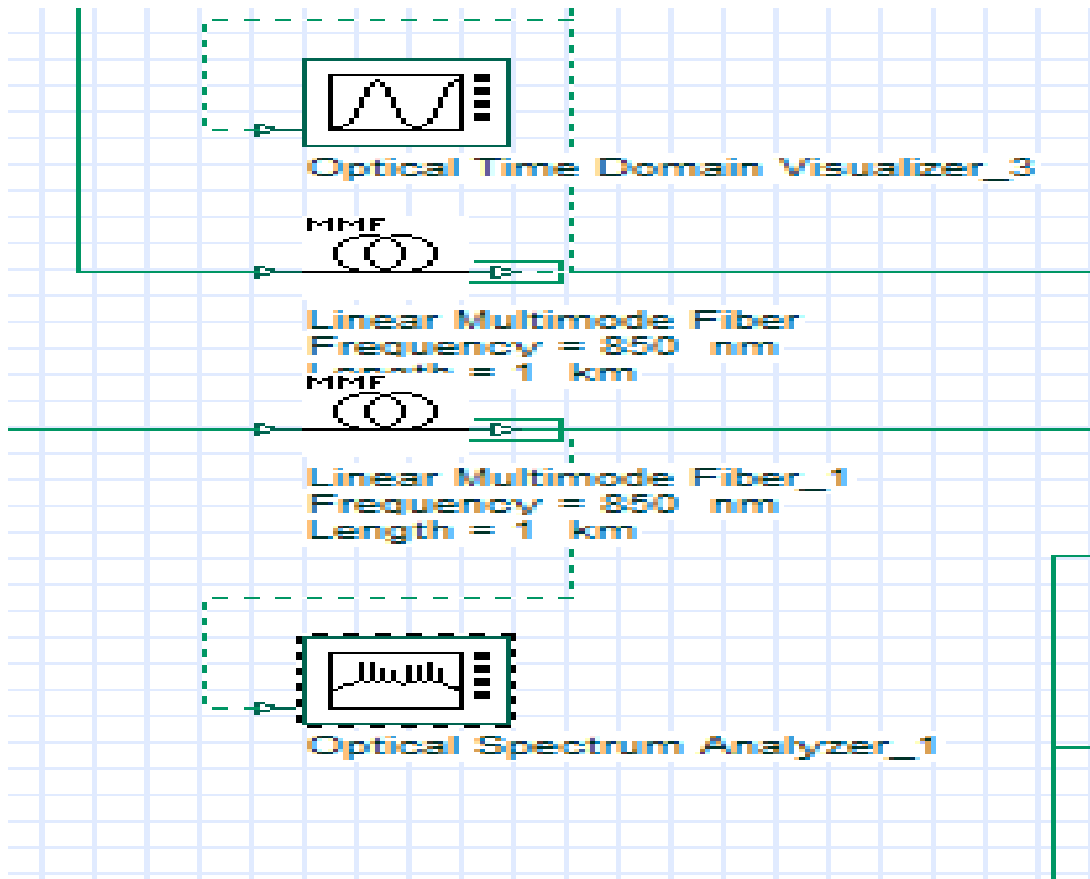


Figure 3.12 The channel with coupler parts.

The receiver part (see Figure (3.13)) of a fiber laser schematic showing both of the loops to have two active fiber stretches in single mode contains Pump Coupler Counter-Propagating Equivalent to a subsystem where you can control the attenuation of the signal and pump independently, Photodetector APD Filter with a square cosine roll off frequency transfer function. Low Pass Gaussian filter Optical filter with a Gaussian frequency transfer function. The RF spectrum analyzer is used after the PIN in order to display the laser frequency response. This component regenerates an electrical signal, BER Analyzers display the Eye Diagram, Q-factor curve, Min BER, Threshold, Eye Height, and BER Patterns that representing the optimal point.

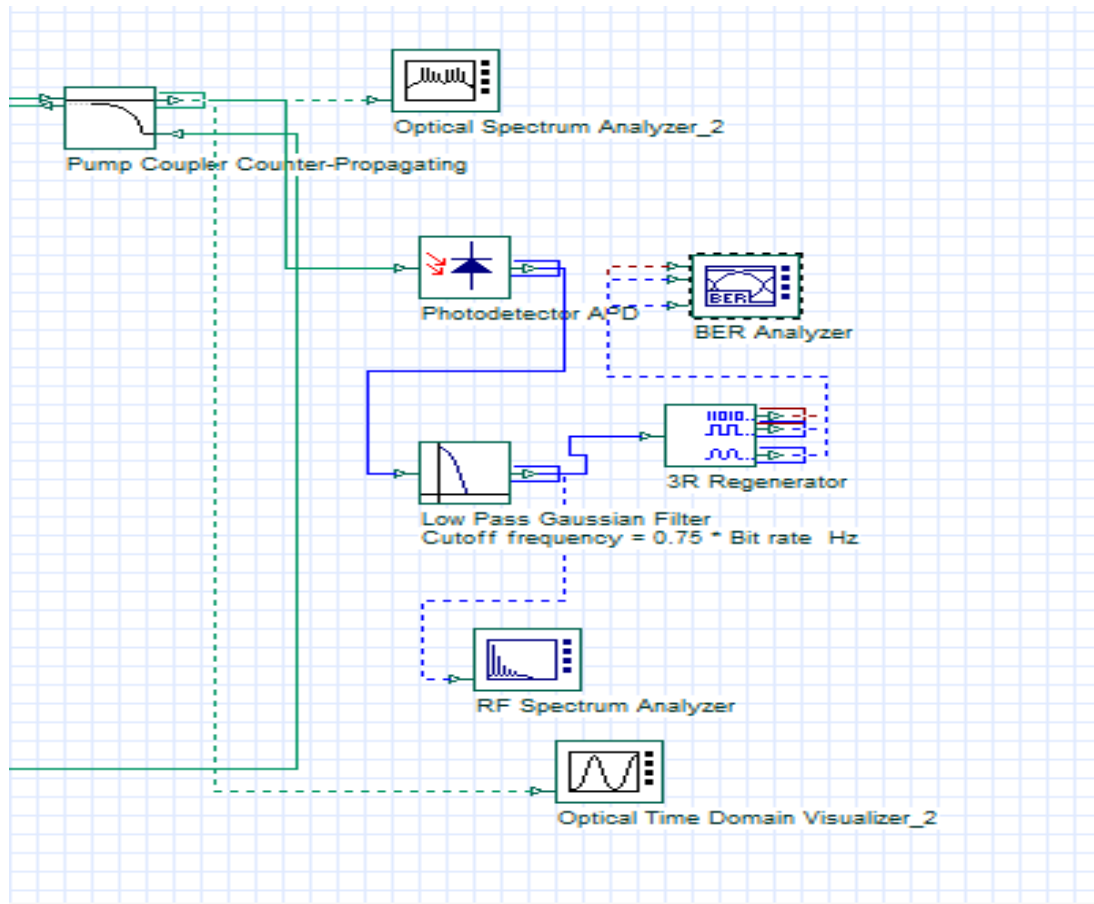


Figure 3.13 The receiving part with coupler.

3.6 Single And Multiple Mode With And Without Coupler Genetic Algorithm

Figure (3.14) depicts the diagrams of the genetic algorithm used in this work. A population's "individual" is a pulsed regime with two genes – the values of the two pumping diode currents. Each person has a distinct set of parameters, including the contrast of the RF spectrum of the fundamental mode, the average power, the duration of the autocorrelation function, and the contrast of the coherence spike. These values can be used to build a fitness function that a genetic algorithm must optimize. The goal (fitness) function is set such that the desired parameters' pulsed regime corresponds to its highest value. The population is first seeded by a random pair of currents in the genetic algorithm. Consequently, each value ranges from 0 to 1. After sorting the population by the fitness function value, individuals are married

by randomly combining their genes. The group of people with the greatest fitness function values—the elite group—remains the same. A segment of the population is transformed by mutation, which is a random change in genes, to avoid the algorithm from clamping on a local maximum of the fitness function. The algorithm cycle can be stopped if the change in the goal function stays below a certain value after a number of cycles. In order for the algorithm to work correctly, it is necessary to provide the population size, the percentage of elite individuals, and the percentage of mutant individuals. All details of the objective function have been described in chapter 2 .

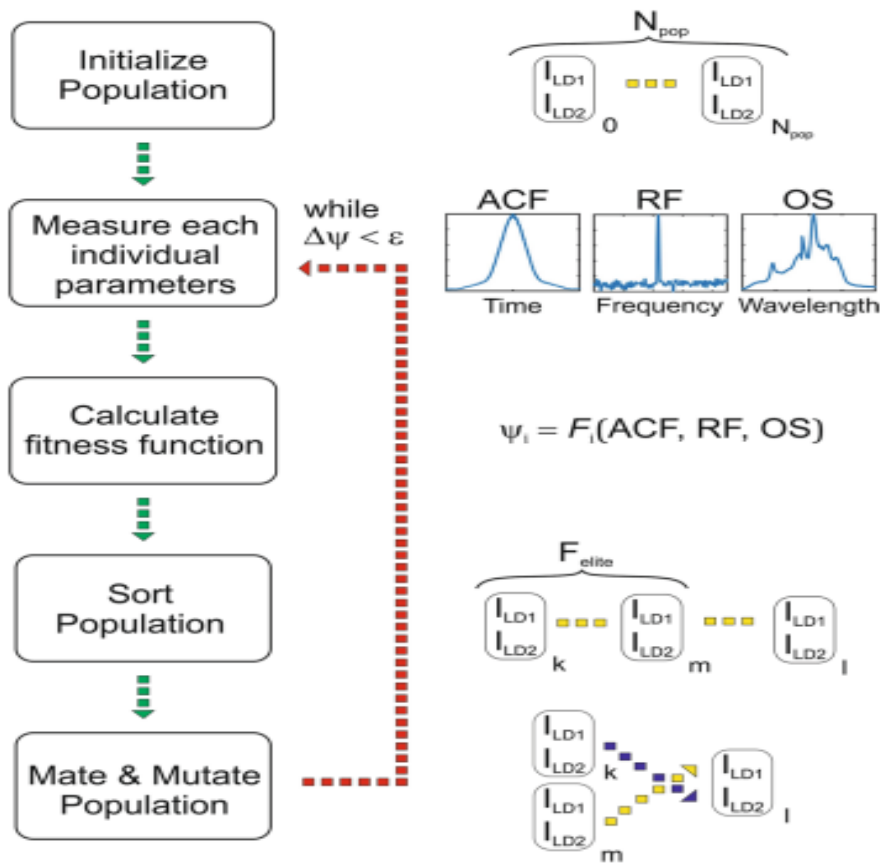


Figure 3.14 schematic diagram for optimal selection of pumping laser diode currents (I_{LD1} , I_{LD2})

3.7 Polarization Angle Proposed System

The Pseudo Random Binary Sequence (PRBS) is generated according to the various operating modes in the Schematic of Angle Polarization (Figure 3.15). From the output of the sine generator, the oscilloscope visualizer creates a signal with a sine waveform that displays the data. A time-domain optical signal visualizer that uses an optical time domain visualizer.

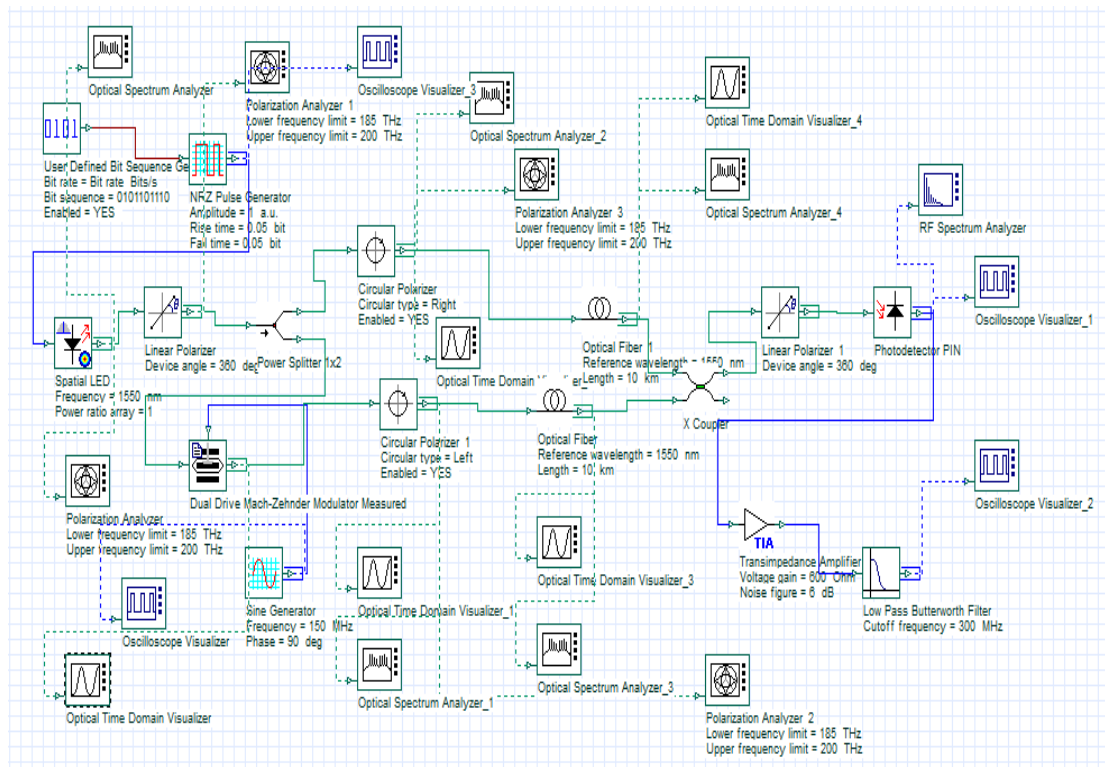


Figure 3.15 Schematic Of Angle Polarization

It is possible to see the laser frequency response on an RF spectrum analyzer. This part is an LED with transverse mode profiles included in the optical output. It is a subsystem that was constructed utilizing the Multimode Generator and the LED component. The polarization analyzer photonic signal polarization characteristics (frequency, sampled). Linear Polarizer is a model of a perfect linear polarizer. Dual Drive Mach-Zehnder Modulator Measured Simulates

a Mach-Zander modulator with dual-drive modulation using measured parameters. Power Splitter (1x2) Ideal power splitter - splits an optical input signal into two output signals. Circular Polarizer Simulates an ideal circular polarizer. The optical fiber component simulates the propagation of an optical field in a single-mode fiber with the dispersive and nonlinear effects taken into account by a direct numerical integration of the (NLS) equation (when the scalar case is considered) and a system of two, coupled NLS equations when the polarization state of the signal is arbitrary. The optical sampled signals reside in a single frequency band, hence the name total field .

Table 3.4 Parameters setup for polarization angle laser fiber proposed system.

No	No. Parameter	Value
1.	Pseudo-Random Bit Sequence Generator	Bit rate
2.	Oscilloscope visualizer	Automatic range(amplitude)
3.	NRZ Pulse Generator	Exponential
4.	Optical spectrum analyzer	Automatic range(power)db.m
5.	Optical time domain visualizer	Automatic range(power)
6.	Spatial LED	850nm

7.	Polarization analyzer (frequency THz)	Polarization properties of optical signals(frequency, sampled)
8.	Dual Drive Mach-Zander Modulator Measured	Phase-Shift, 1.2 v
9.	Linear Polarizer	0 degree
9.	Power Splitter	Loss applied to the signal after splitting (0db)
10.	Circular Polarizer	Right, left
11.	Optical fiber	1550nm
11.	X Coupler	Coupling coefficient (0,5)
12.	Trans impedance Amplifier	Voltage gain, Include Noise, Noise equivalent bandwidth, Noise figure, Input noise density
13.	Low Pass Butterworth filter	Cutoff frequency (0.75 * bit rate)Hz

14.	Photodetector APD	True
15.	Low Pass Gaussian filter	Cutoff frequency (0.75 * bit rate)
16.	RF spectrum analyzer	Automatic range (power)db. m

All that happens is an attenuation of the specified signals and noise bins. A trans impedance amplifier Having a user-defined noise figure, this component is an electrical trans impedance amplifier. Additive thermal noise and linear gain are also present. Coupler optical signal splitting or combining cross coupler. Low Pass Butterworth Filter An optical filter having Butterworth frequency transfer characteristics. Image-detecting PIN the internal filter's centering at the signal's maximum amplitude or a user-defined center, as the case may be. Figure 1 depicts the primary procedures for determining the polarization angle see Figure (3.16).

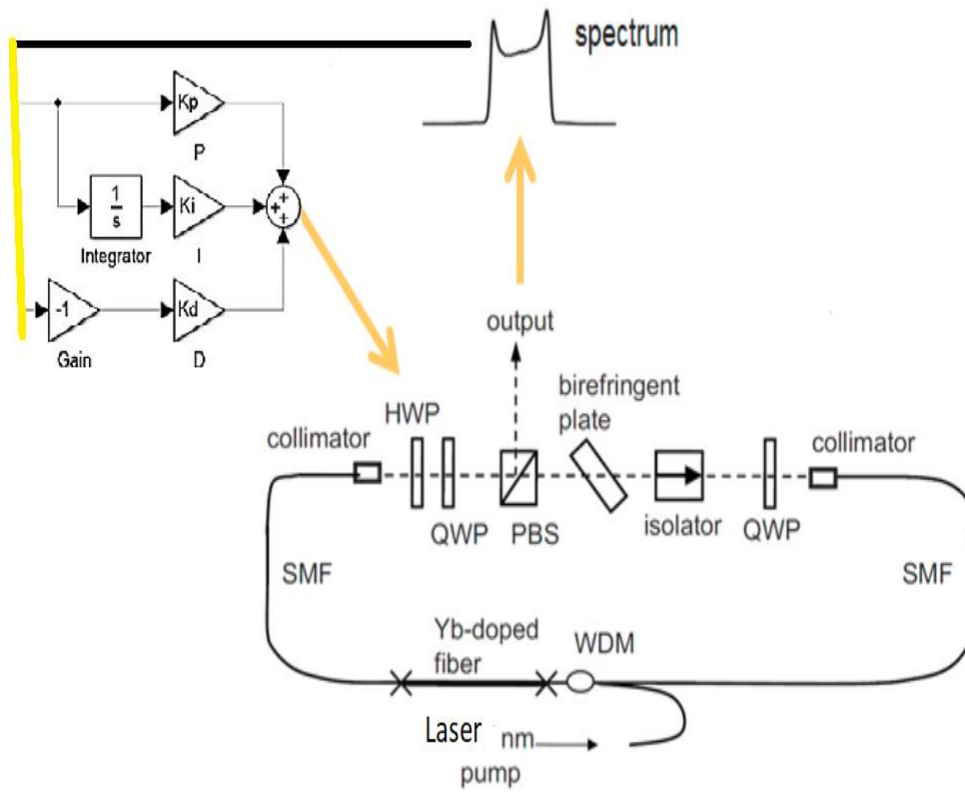


Figure 3.16 Polarization angle controller system.

Chapter Four

Simulation Results

4.1 Introduction

In this chapter, three cases of simulation results have been demonstrated our proposal system. The First consideration of the type of laser mode and then demonstrated the double gain of two laser pumping sources using the genetic algorithm to find the optimal value of the diodes, finally applying the PID controller to find the optimal polarization angles. All simulation results have been found simultaneously by using the op-net program that has been described in chapter (3) and the Simulink Matlab program

4.2 Simulation Results: Type Of Laser Modes Under Bending Effect

A Gaussian beam with an arbitrary wavelength of 800 nm and a beam waist of 2.5 m is launched into a straight, 1 mm-long MMF with a 10 m-radius core, $n_{\text{core}}=1.48330$, $n_{\text{cl}}=1.45330$, and V-number $V=23.3$ in our first validation model. Figures (4.1) and (4.2) show the proximal normalized intensity patterns.

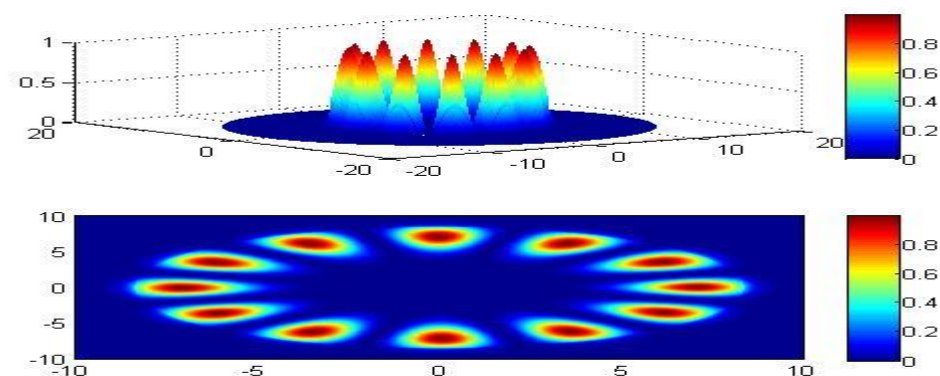


Figure 4.1 Normalized intensity for 12 modes laser.

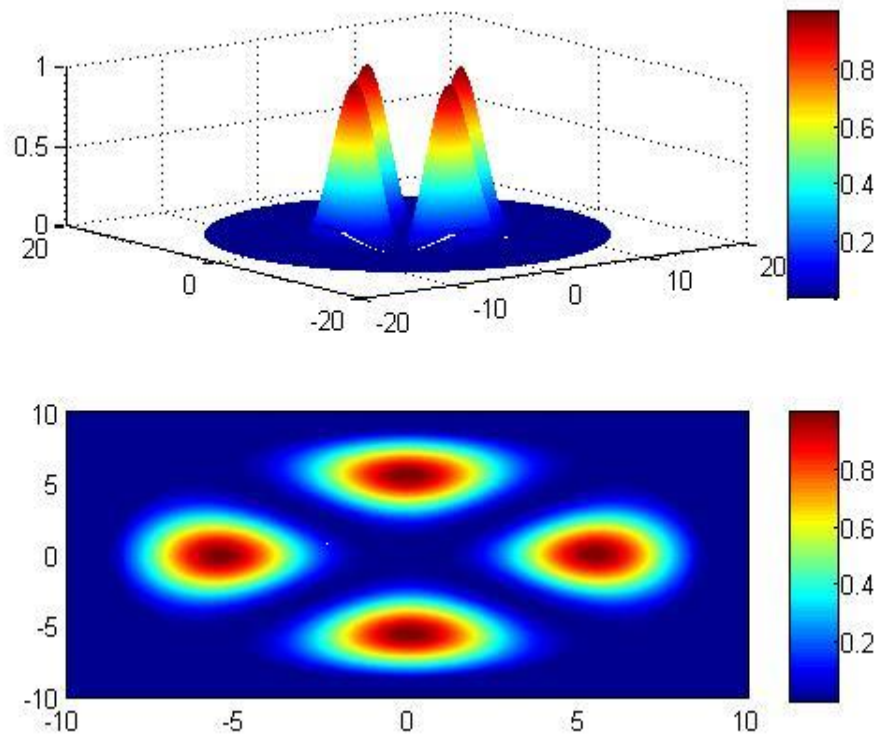


Figure 4.2 normalize four mode laser over the fiber with bending effect.

Most studies show that using MMFs for beam shaping is carried out with a fixed fiber since MMFs are susceptible to bending. Since this cannot be used for endoscopy, it is crucial to research how sensitive fibers are to bending. The actual use of MMF beam shaping depends on understanding which modes are more resistant to bending than others. Using the mode solver in BPM-Matlab, Figure 2 shows the bent and straight simulated mode field intensity patterns for the five lowest order modes of an MMF. The fiber has core radius $a=12.5\mu\text{m}$, cladding refractive index $n_{\text{clad}}=1.52$, and $\text{NA}=0.1$, where $\sqrt{\text{NA}}=n_{\text{core}}^2-n_{\text{clad}}^2$. The bending radius was increased to 1.24 cm, and the wavelength was changed to 1064 nm. The straight MMF's mode profiles shown in Fig. 2(a) are consistent with the profiles obtained analytically based on the well-

established equations employing Bessel and modified Bessel functions .
 Furthermore, the BPM-Mat lab findings for both bent and straight fibers concur
 Figure (4.3), proves that bending is well predicted .

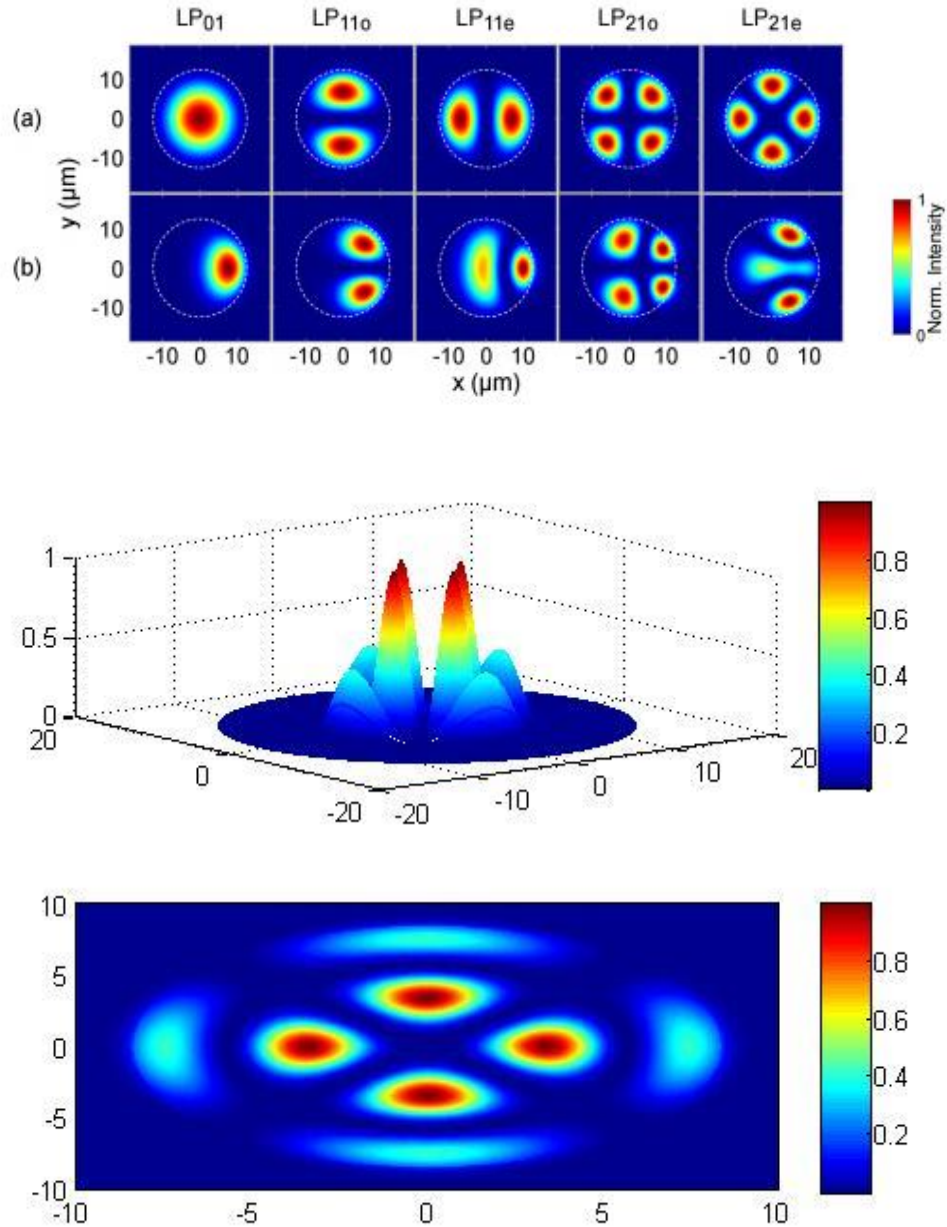


Figure 4.3 Profiles of the five lowest order fiber modes' mode intensities supported by (a) a straight and (b) a bent MMF.

Despite having large mode areas, higher order MMF modes appear to be somewhat insensitive to bend-induced distortions, according to numerical and experimental studies. We replicate this result in figure (4.4), where we calculate the normalized fractional power of the total propagating electric field in each guided mode in accordance with equation (2.1) as a function of propagation distance and for two distinct injected modes, LP01 and LP03. The fiber has $n_{\text{clad}}=1.450$, $n_{\text{core}}=1.46660$, core diameter $a=6\mu\text{m}$ together with an 800 nm wavelength. The initial 0.50 mm is straight, followed by a 1 mm bend in the x direction, a 1 mm curve in the y direction, and then another 0.50 mm of straight space. The curvature's 10 mm bending radius. Despite the fact that the mode overlap for all 30 guided modes has been determined, the graphic only shows the six most exciting modes.

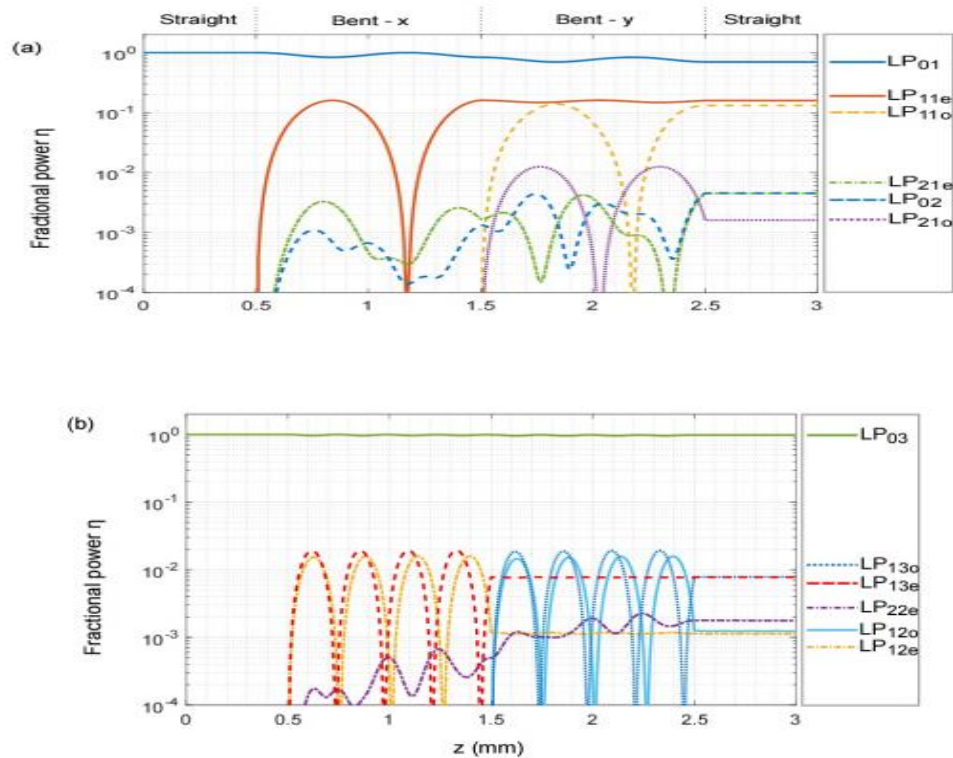


Figure 4.4 Numerical simulations using BPM-Matlab of the normalized fractional power of various LP modes in an excited bent MMF modes (a) LP01 and (b) LP03

It may be observed that the LP03 is more resistant to mode coupling caused by bending. To learn more, read the text. There are a number of things to note. In the first two segments, no modes with odd parity are at all stimulated due to symmetry. However, once the bend in the yy-direction begins, this situation changes. Mode coupling can also be thought of as oscillations back and forth with varying periodicities. Last but not least, the author may see that the fractional power of the higher The bent MMF's order mode LP03 exhibits the relative stability of the higher order mode against bending observed compared to the lower order mode LP01. This is seen by how the order mode LP03 remains comparatively constant during propagation via bends. Rare earth amplifiers play an important role as active devices in fiber optic communication networks since they do not require electro-optical conversion during the amplification process. In 1994, the first active fiber optic amplifier, the erbium-doped fiber amplifier (EDFA), was shown. Thulium-doped fiber amplifiers (TDFAs) are another rare earth doped fiber that are used because of the demand for larger bandwidth. Because their amplification bandwidth is centered at 1470 nm, which is in the silica fibers' low loss zone, TDFAs are a viable candidate for S-band amplification.

4.3 -Single Mode Fiber With Coupler Linear

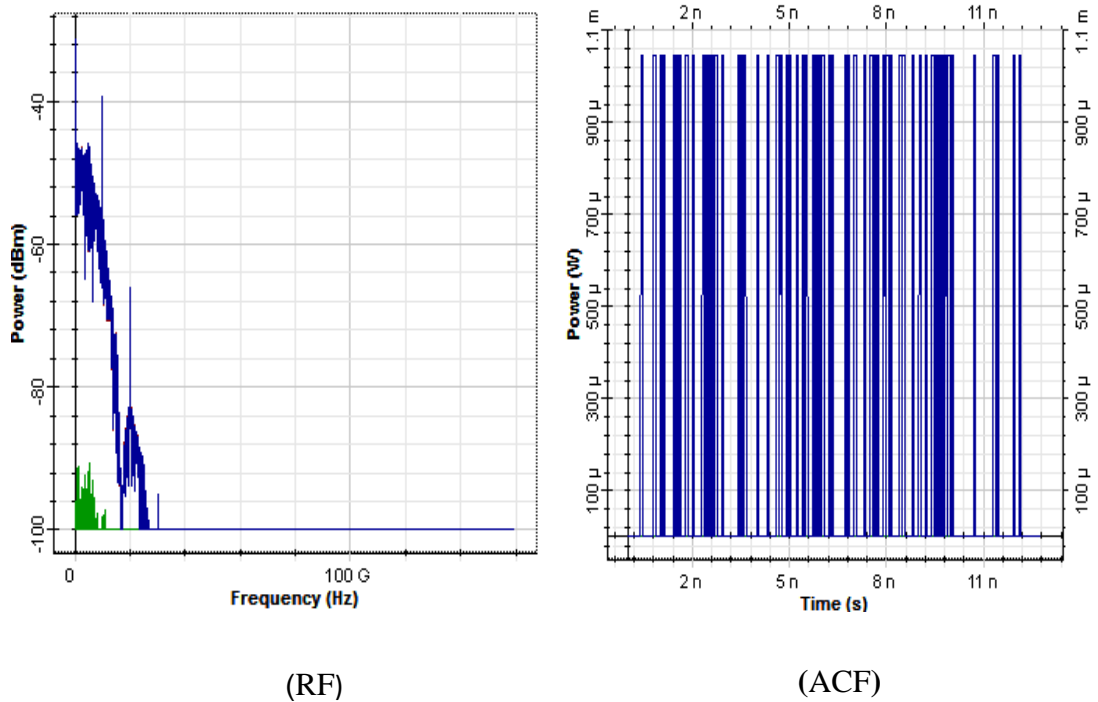
In this section the simulation results presented for single mode with linear coupler fiber are illustrated. Firstly, using the op-net system that is illustrated in chapter three, The author will present the manual change the value of the current of the two pumping diodes in the loop. Table (4.1) lists the value of the current diode current change versa the value of intensity and the RF frequency. Where the

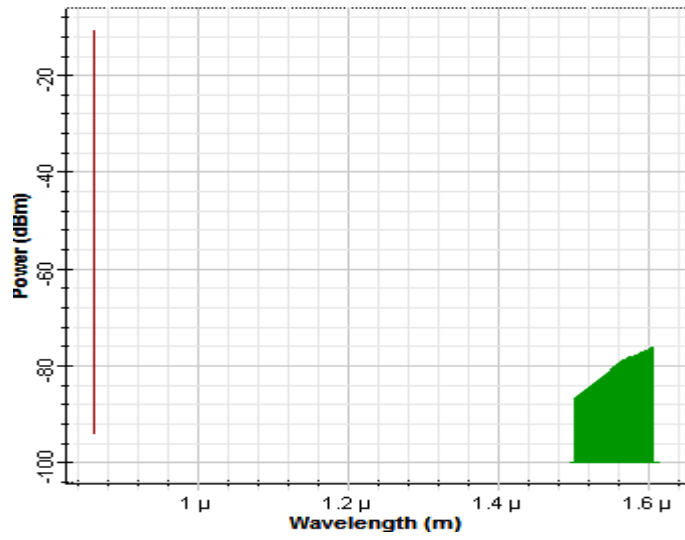
frequency of the two laser pumping sources is (860-nm) and the length of the fiber is 40 Km.

Table 4.1 diode current relationship with RF and intensity.

Id1(m amp.)	300	350	400	450	500	550	600	650	700	750	800
Id2(m amp.)	300	350	400	450	500	550	600	650	700	750	800
Max intensity (power)w	998m	1.8m	2.9m	4.4m	5.8m	9.6m	11.6 m	13.4m	13.94m	15m	17m
Rf(frequency)db magnitude	-46	-42	-38	-35	-32	-28	-24	-24	-24	-24	-22
Wave length (power)db	-76	-72	-68	-64	-57	-46	-36	-41	-42	-40	-38

Figure 4.4 shows one case of the original signal when both diode current is 300 m amp.



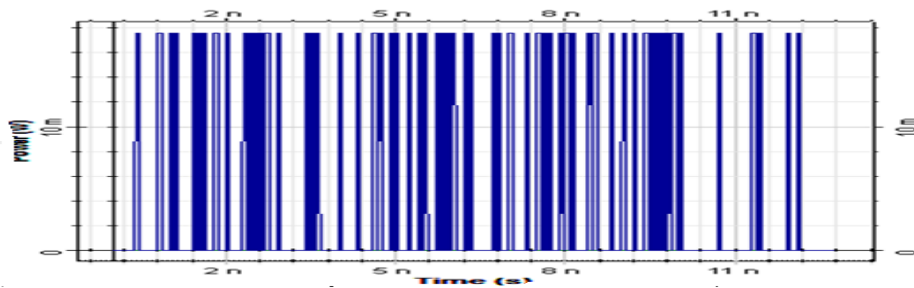
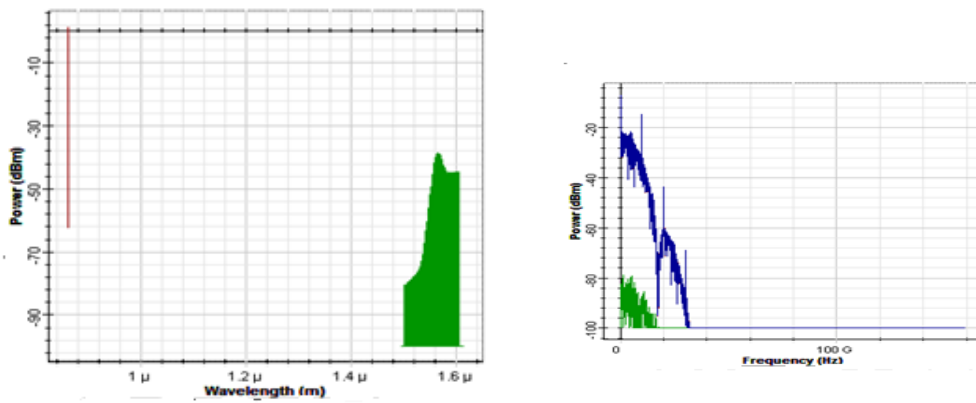


(OS)

Figure 4.5 Actual simulated signals for $id1=id2=300$ m amp.

(OS)

(RF)



(ACF)

Figure 4.6 Signals of simulation results when $id1=id2=800$ m amp.

4.4 Linear Multi-Mode With Coupler:

Now, in this section considered the two laser pumping source id_1, id_2 with frequency of 850 nm, and the power of 1 watt, with short distance which is 1 Km, all the information details can be seen in Table 4

Id1 m amp.	300	350	400	450	500	550	600	650	700	750	800
Id2 m amp.	300	350	400	450	500	550	600	650	700	750	800
Max intensity (power)w	170 M	110 M	40 M	11.6 M	32M	63.4 M	80.3 M	51.3M	14M	- 6.8M	31M
Rf(frequency) db magnitude	-70	-76	-82	-90	-82	-82.4	-76	-81	-89.4	-94.6	-90.6
Wave length (power)db	-39	-40	-44	-46	-44	-42	-41	-43	-48	-50	-46

Table 4.2 shows values for the 1 km fiber linear pair.

For more description and details, we would have considered the signals for initial value of the currents which is $id_1=id_2=300$ m amp (Figure (4.7)).

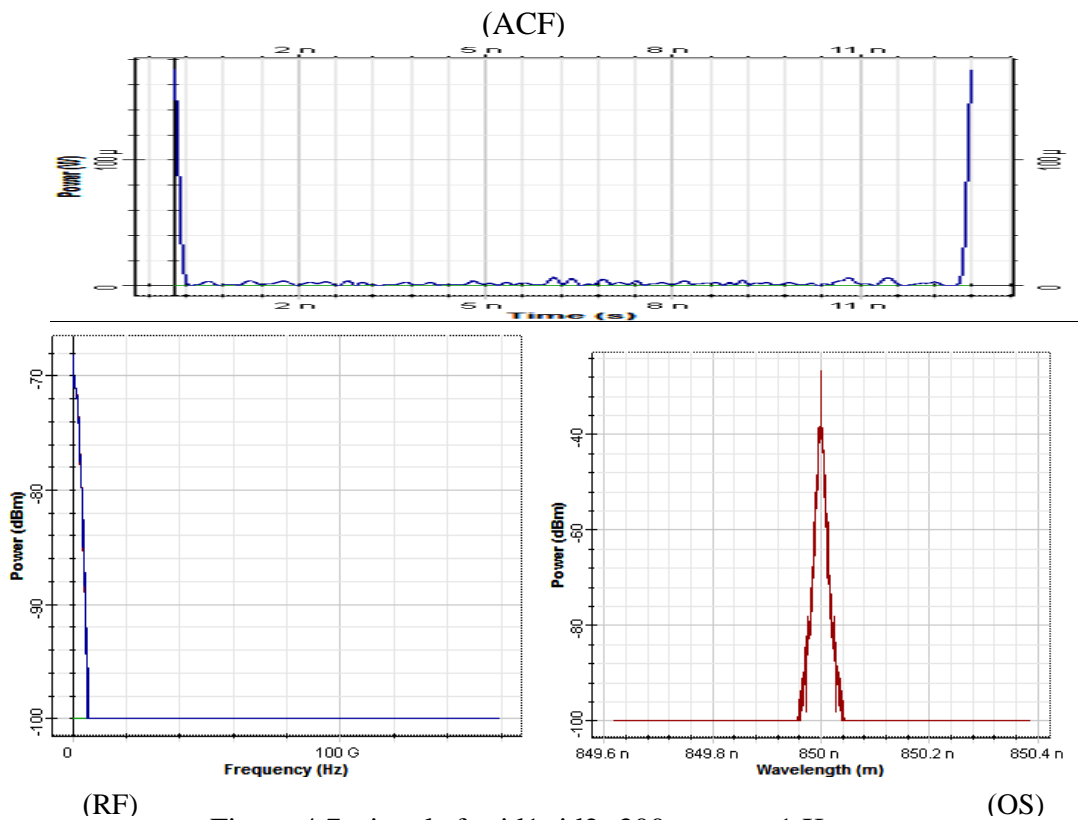
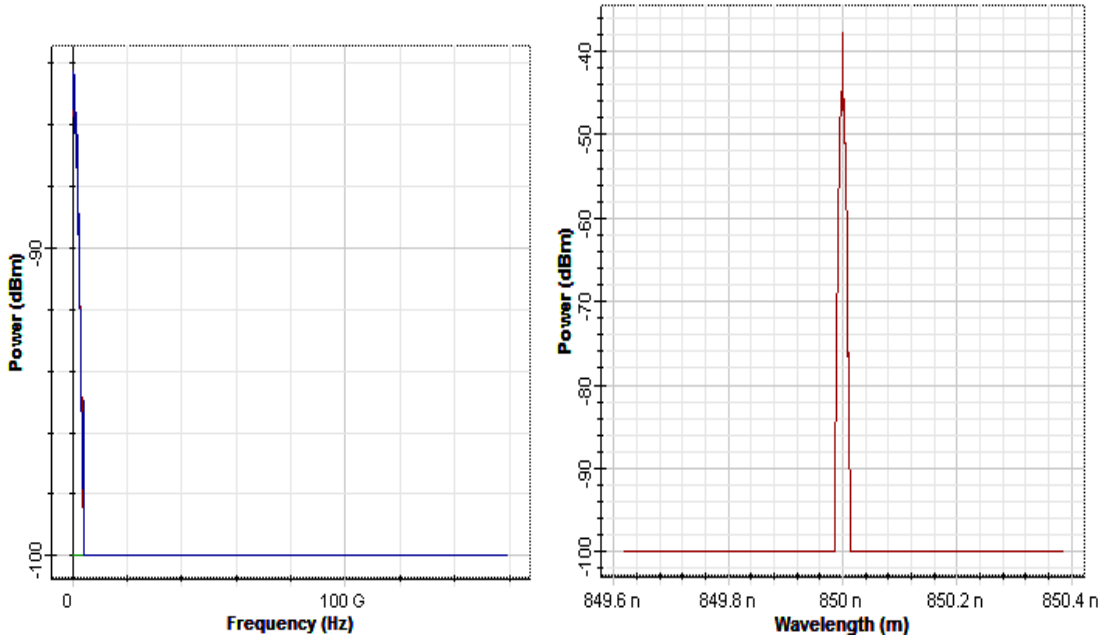


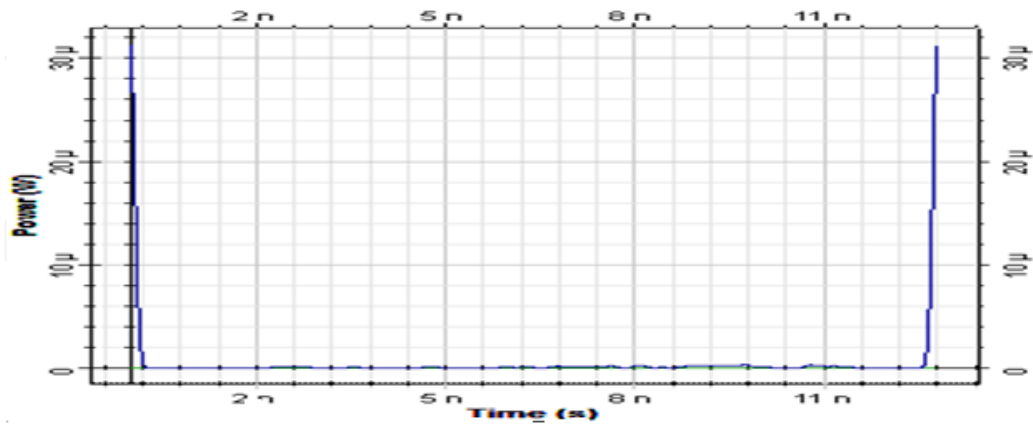
Figure 4.7 signals for $id_1=id_2=300$ m amp, 1 Km.

Finally, the final value of the diode current $i_{d1}=i_{d2}=800$ m amp is considered and has been shown in Figure (4.8).



(RF)

(OS)



(ACF)

Figure 4.8 Illustrated simulation signals $i_{d1}=i_{d2}=800$ m amp., 1 Km.

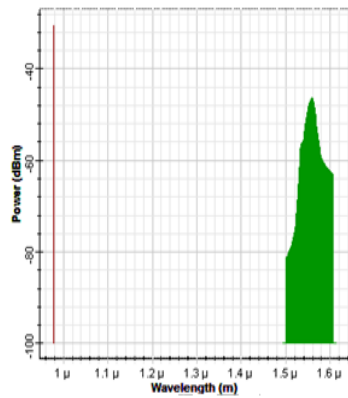
4.5 Linear Single Mode Fiber Without Coupler:

Basically, consider the single mode without a coupler to verify that the coupler connection is one main effect parameters in the signal shapes. Table 4.3 illustrates all the values of the intensity power and the wavelength for the case of id=300 m amp., and the frequency 978 nm for fiber with 10 m.

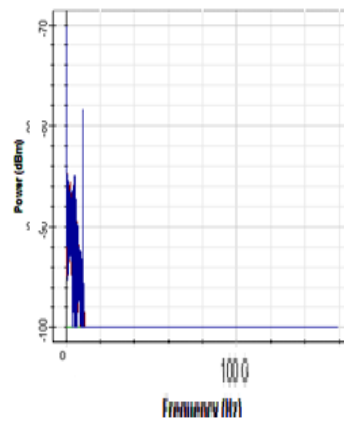
Table 4.3 single mode without coupler.

Id	300	350	400	450	500	550	600	650	700	750	800
Max intensity (power)w	11.6 M	19M	27M	36M	42M	52M	64M	67 M	86M	96M	106 M
Rf(frequency) db magnitude	-86	-81	-78	-76	-75.5	-72	-70	-69	-68	-65.6	-90.6
Wave length(power) db	-47	-44	-42	-39.5	-40	-39	-38	-37.8	-36.5	-36.2	-36

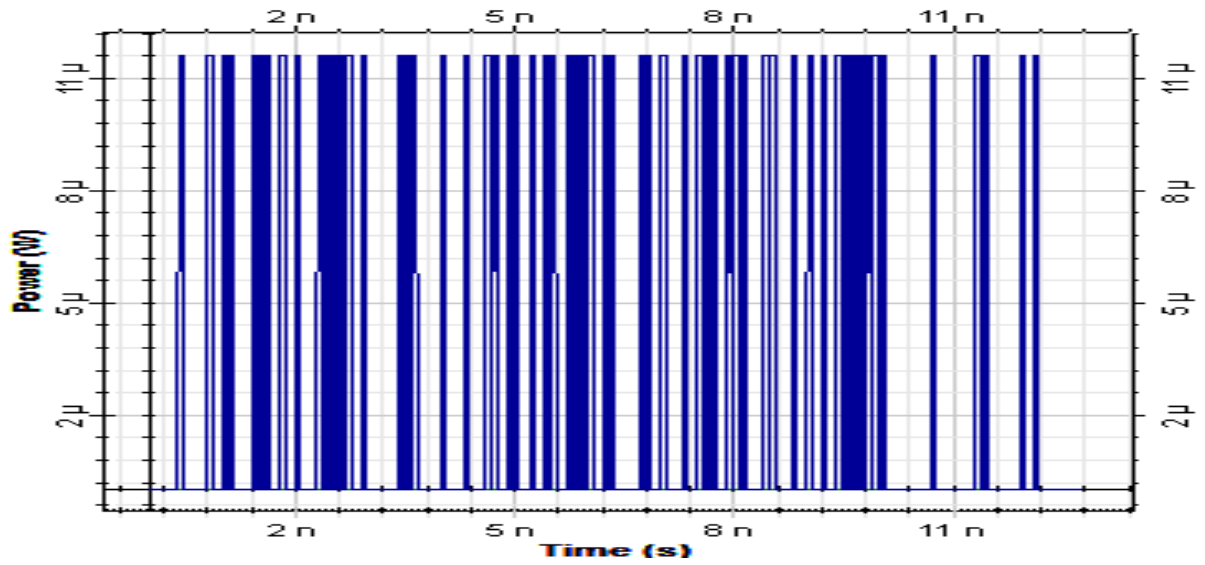
Figure 4.9 shows the simulated signals for the linear single mode without coupler.



(OS)



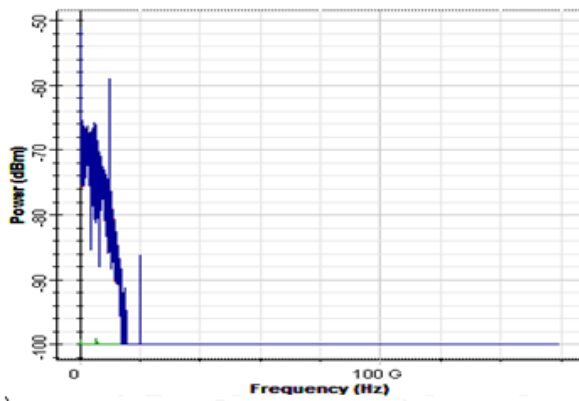
(RF)



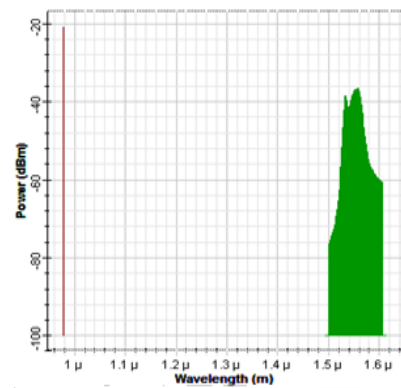
(ACF)

Figure 4.9 single mode without coupler, $i_d=300$ m amp., 10 m

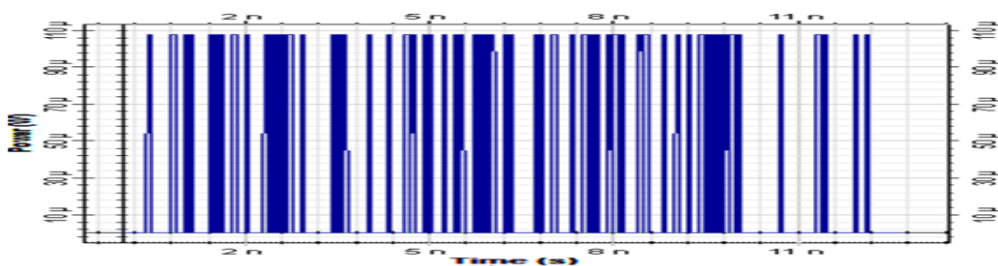
Considering another value of the current with $i_d=800$ m amp., all the signals shape is shown in Figure (4.10).



(RF)



(OS)



(ACF)

Figure 4.10 signals of $i_d=300$ m amp., single mode

4.6 Linear Multi-Mode Fiber Without Coupler:

All the details of the Multi-mode without coupler are shown in Table 4.4., where the frequency is 850 nm and the length of fiber is 60 m. and the power is 1 w.

Table 4.4 The actual value of the intensity and wavelength for multi-mode without coupler.

Id	300	350	400	450	500	550	600	650	700	750	800
Max intensity(power)w	84m	97m	110 m	118 m	140 m	150 m	170m	180m	190m	210 m	220 m
Rf(frequency)db magnitude	-32	-37.8	-32	-32	-31.9	-32	-32	-31.8	-31.8	-31.8	-32
Wave length(power)db	-42	-38	-38	-38	-37.8	-40	-39	-38	-38	-39	-43

Figure 4.11 shows the details of multi-mode without a coupler for id 300 m amp.

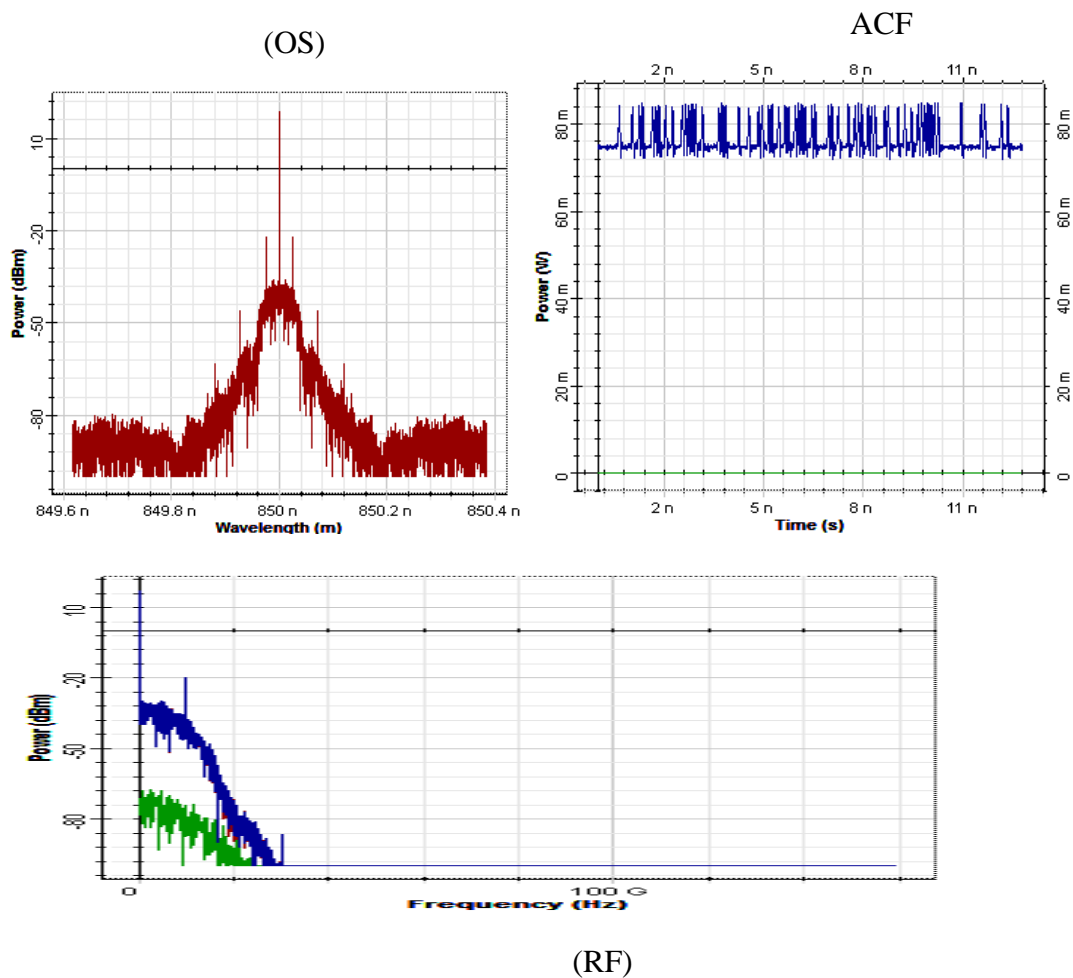


Figure 4.11 signals of multi-mode without coupler, id 300 m amp.

4.7 Simulation Results Of Genetic Algorithm

We examine the mode-locked, figure-eight fiber laser cavity design (see chapter three). A 40/60 coupler connects the two fiber-optic loops that make up the cavity—one on the left, which is unidirectional, and one on the right, which is bidirectional. Multimode laser diodes are used to power the amplifier sections of the two loops that make up the laser resonator. The laser cavity only comprises elements that preserve polarization in order to prevent non-linear polarization development. Thus, the radiation's output is linearly polarized. The two pumps' currents can be controlled separately. For radio-frequency outputs in the pulsed domain, diodes offer a broad range of average output power. Contrast, autocorrelation function length, and coherence level. The evolutionary algorithm's schematics after two rounds are shown in Figure (4.12). The creation of a population from "one person" requires the use of a pulsed regime and two genes that stand in for the values of the two pumping diode currents. Each person's characteristics are unique, including the average power, contrast of the RF spectrum in the fundamental mode, the magnitude of the autocorrelation function, and contrast of the coherence spikes. These figures may be used by a genetic optimization method to build a fitness function that has to be optimized. The goal (fitness) function was set so that the maximum value of the needed parameters for the pulsed regime. First, a pair of random currents are distributed to the phase of genetic to initialize it .

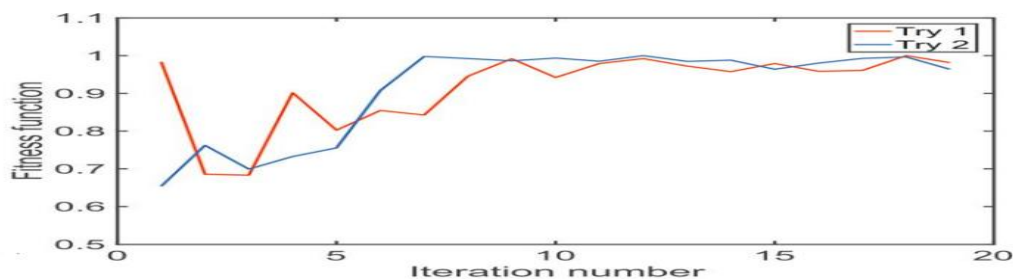


Figure 4.12 Genetic algorithms steps.

Now, it can be seen that from figure (4-13), the tested 10-iteration chromosome with the quickest time for every sort of fitness function that was fully explained in chapters two and three.

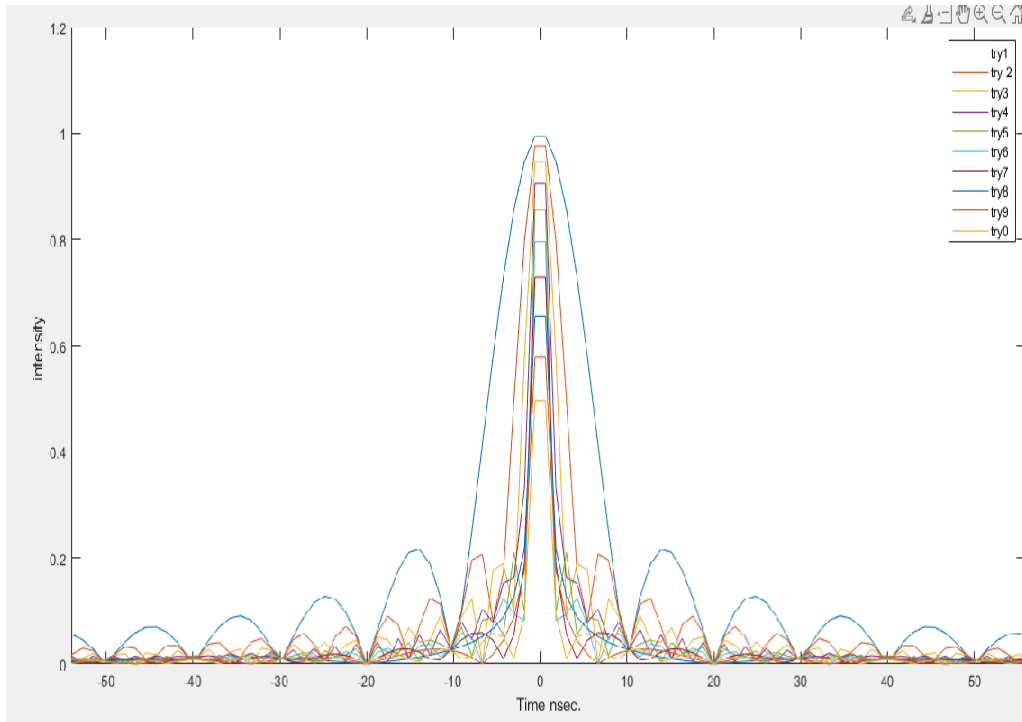


Figure 4.13 All try duration pulses.

In the literature survey researcher's summary of the nonlinearity difficulties that arise from the physical characteristics, global searching for finding the best parameters is characterized as being very helpful.

In figure, the initial and ultimate goal optimum points for the diode pumping current are displayed Figure (4.13). The approach must do 15-20 iterations until it finds the shortest pulses. The objective function then fluctuates in accordance with the pulse parameters and keeps dipping below our 6 percent cutoff.

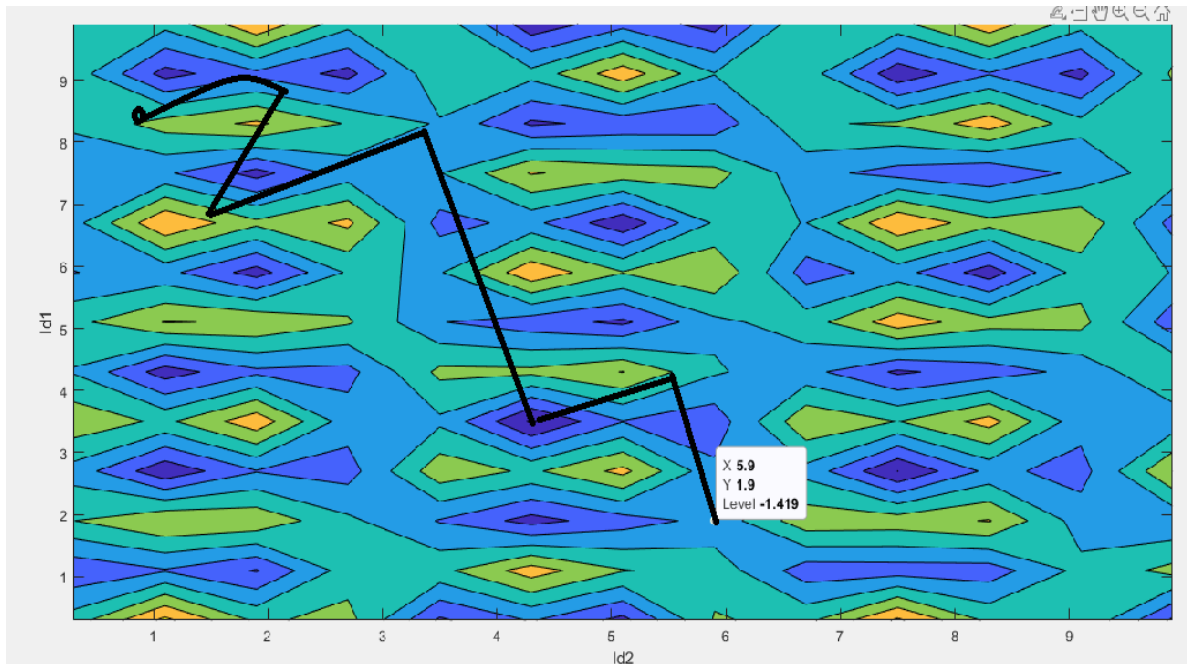


Figure 4.14 target track using genetic algorithm.

We consider the spatial intensity with the wavelength, searching by using the genetic algorithm to find the maximum value as explained extensively in chapter two and chapter three genetic algorithm section. Figure (4.15) shows exactly how could precisely be found the maximum intensity with the shortest pulse duration.

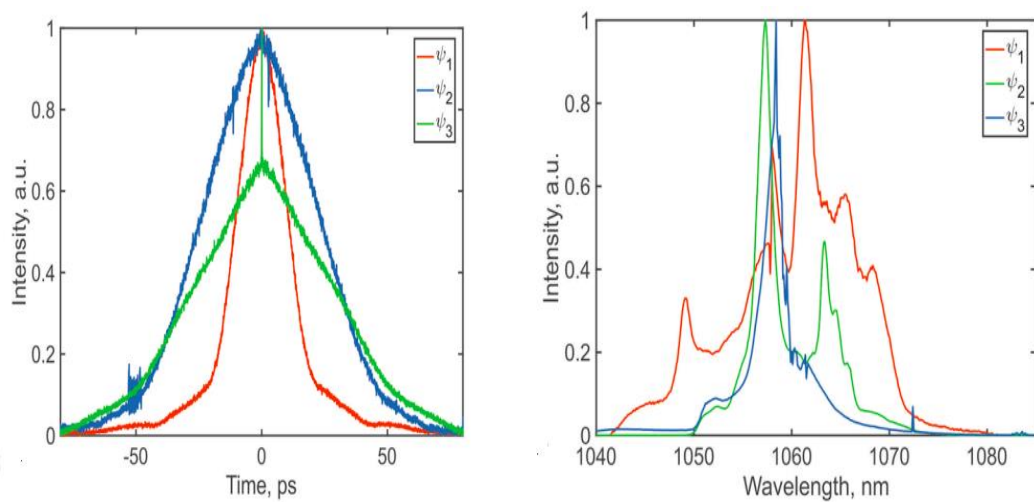


Figure 4.15 Practical op-net and simulated mat lab three objective function using genetic algorithm.

4.8 PID Controller For Polarization Angles

Firstly, going through the manual changing of the polarization angle to figure out how far it affects on the system performances. The First case considered the system setup as: The spatial led frequency 1550 nm, Bandwidth 6 THz Time between (2n-14n). table (4.5) has all the details for changing the angle by 10 and finding the amplitude.

Table 4.5 polarization angle changes.

Device angle (degree)	10	20	30	40	50	60	70	80	90	100	110	120	130	140
Amplitude (m)	340	230	255	400	600	760	805	720	540	340	230	260	400	620
Device Angle (degree)	150	160	170	180	190	200	210	220	230	240	250	260	270	280
amplitude	800	840	720	540	340	230	260	400	600	760	800	720	540	340

For more details, figure (4.16) shows exactly how was the amplitude changes for the a.u mode where the device angle is 10^0 .

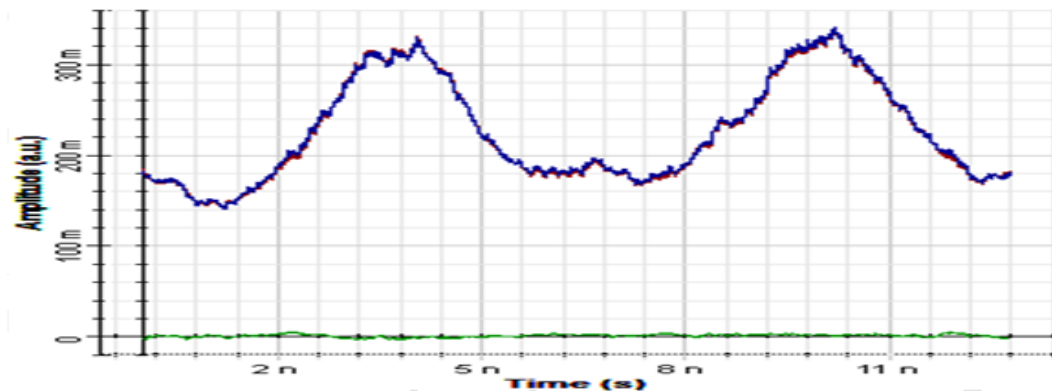


Figure 4.16 Polarization angle 10^0 .

We begin the op-net experiment with the laser in a mode-unlocked state. Once the measurement has been detected by the PC (observer device), it determines that the

laser is not mode locked. SISO Pid controller loop then begins. The HWP is modified by SISO Pid, and the laser eventually achieves its optimal state. Figure (4.17) displays the final outcome. The normalized objective function in Figure (4.17(a)) starts at 0. The objective function rises till it reaches 1 and stabilizes there with SISO Pid modifying HWP. The HWP angle has also been changed from 74 to 87 degrees. After the laser has stabilized, there is an observable oscillation of the objective function due to sinusoidal input change. Because the objective function is sensitive, there is considerable variation. Actually, there is no discernible variation as we watch the output pulse.

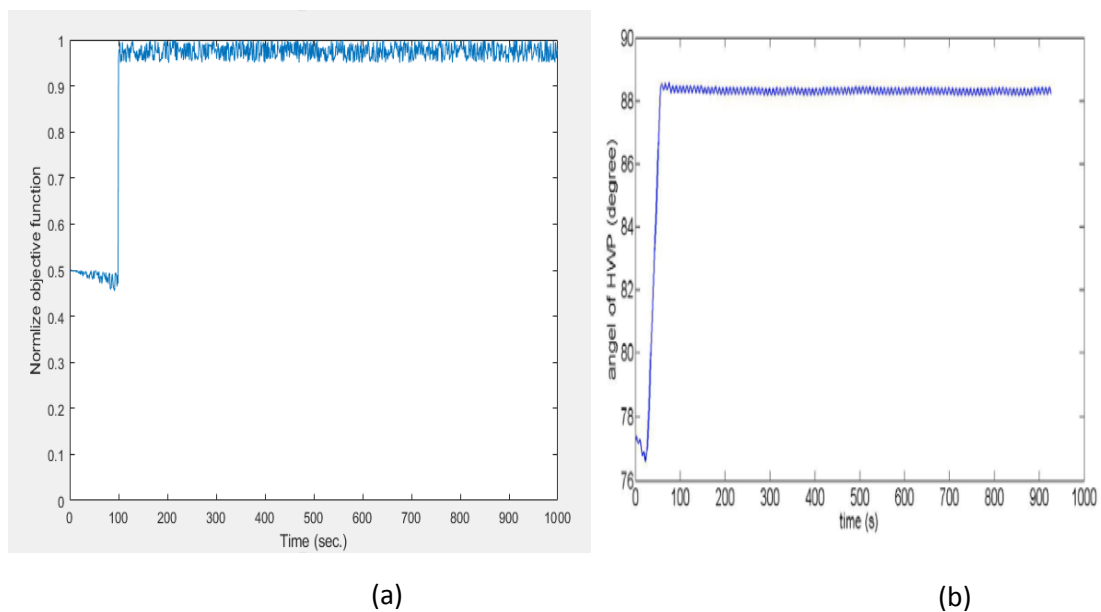


Figure 4.17 Simulation results of polarization angle: (a) Normalized objective function vs time; (b) angle vs time.

Figure (4.18) shows the range of the polarization angle when it is applied with different fiber optics length and attenuation.

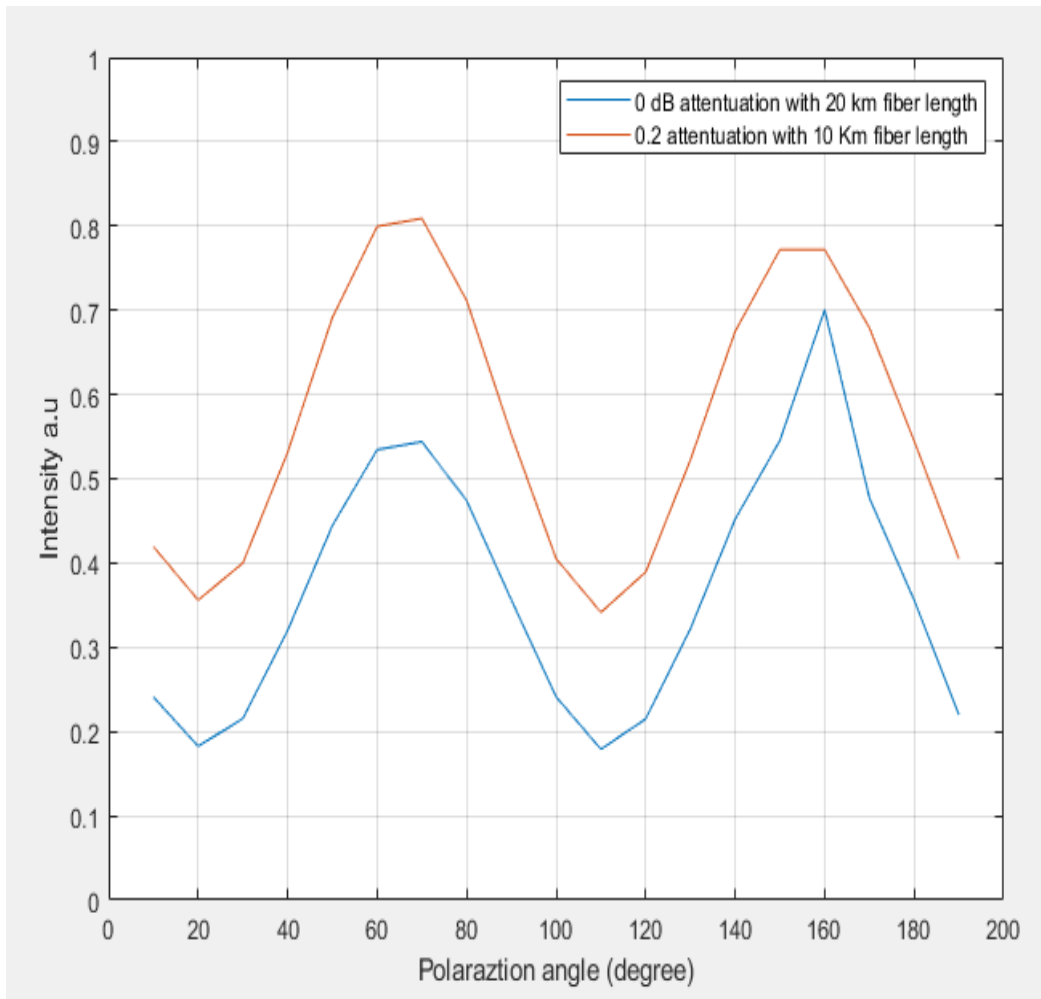


Figure 4.18 Angle with intensity for different fiber optics length.

From Figure (4.18) that it is clear that the maximum intensity happened at angles 62° , and 160° that demonstrated using the PID controller to figure out the optimal value of the polarization angle will be useful.

4.9 Discussion topics

Table 4.6 Gaps And Limitation Of Thesis

No	Limitation	Gaps
1.	Select the wavelength to single and mulimode laser and fiber	Coupler because synchronization
2.	Select the length of fiber to single and multimode	Filter
3.	Select the filter according to input signal band width	Connection the circule as hardware
4.	Gain is select	Gain is change the result unwanted

Chapter five

Conclusion And Future Works

5.1 Conclusion

The current work is the first to operationally and realistically illustrate how machine learning algorithms may be used to govern the pulsed regimes in an all-normal dispersion fiber laser with two separate amplifying fiber loops, the authors write in their conclusion. With two electronically controlled pumps, this particular type of laser is especially suited for the adoption of machine learning techniques. Numerous lasing regimes might coexist in the same cavity, but these operating regimes could be electrically controlled by adjusting the currents of the two pumping diodes.

Self-tuning modification of the laser cavity's two independent gain levels and the use of several target functions allowed for the on-demand synthesis of the three shortest length, highest energy, and best contrast coherence pulses that are all feasible for the same laser cavity. Experimental research has looked at the use of several objective functions to select the pulse length, energy, and degree of temporal coherence of radiation. There are now opportunities for the practical application of lasing regimes with more complex temporal waveform and spectrum patterns due to the limited control offered by conventional laser systems.

Based on ML technology, lasers could develop extremely strong resistance to environmental hazards and self-tuning.

But in order to achieve this, more analysis of simplified approaches must be done, and real-time signal processing is also used, along with ML-driven feedback to the control components.

Our findings, in our opinion, shows the enormous potential for fiber laser lasing regime control and opened the door for future pulsed fiber laser systems with trustworthy electronics-managed control.

Secondly, in this thesis, the author has discussed the data-driven approaches to complex system analysis which are becoming increasingly important in many areas of the physical, engineering, and biological sciences. These techniques can be utilized to give high-dimensional actuation (input) systems with control protocols, in addition to provided us with insights on activity patterns. Such systems can be too cumbersome, unwieldy, or time-consuming to hand tune.

These systems can now be automatically optimized using the techniques shown in this article thanks to the development of machine learning. In fact, we've demonstrated how to moved forward with self-tuning mode-locked lasers and, more broadly, optical systems. These methods are now necessary in the field of nanophotonics, where self-tuning is crucial for integrating such parts in larger networked component structures, i.e. the broader application depends on the reliable performance of the constituent parts The algorithm created here has the appealed

advantage of not requiring any equations, which eliminated the need for the user to have precise quantitative knowledge of the system under consideration. Instead, a suitable objective function is built using data gathered from the system, in this instance optical spectrum and power measurements. It is interesting that the parameter space exploration toroidal search learning algorithm can be evaluated using as many objective functions as needed. For mode-locked lasers and frequency comb applications, this can mean looking for the shortest pulses, the strongest pulses, or the most consistent phase-locking between round trips. Self-tuning might be feasible if a suitable objective function can be created. Our research emphasizes how important it is to combine hardware, software, and algorithms in order to significantly increase the possibility for technological advancements.

5.2 Future Works

The works in this thesis can be extended in many directions, especially as:

- Using the advanced deep learning techniques as an expert system for finding the optimal polarization angles as well as the objective function for the shortest laser duration.
- Using multiple gain loop gain and multiple pumping diode laser current and finding the objective functions.
- Designing and implementation of the multiple gain source pumping current with deep learning tuning system .

References

- [1] Kokhanovskiy, A., Ivanenko, A., Kobtsev, S., Smirnov, S., & Turitsyn, S. (2019). Machine learning methods for control of fibre lasers with double gain nonlinear loop mirror. *Scientific reports*, 9(1), 1-7.
- [2] Massa, N. (2000). *Fiber optic telecommunication. Fundamental of Photonic*, University of Connecticut.
- [3] Richardson, D. J., Nilsson, J., & Clarkson, W. A. (2010). High power fiber lasers: current status and future perspectives. *JOSA B*, 27(11), B63-B92.
- [4] Kutz, J. N. (2006). Mode-locked soliton lasers. *SIAM review*, 48(4), 629-678.
- [5] Kutz, J. N., Fu, X., & Brunton, S. (2014, July). Self-tuning fiber lasers: machine learning applied to optical systems. In *Nonlinear Photonics* (pp. NTu4A-7). Optical Society of America.
- [6] Yang, K., Wang, M., Zhao, Y., Sun, X., Yang, Y., Li, X., ... & Yi, J. (2016). A redox mechanism underlying nucleolar stress sensing by nucleophosmin. *Nature communications*, 7(1), 1-16.
- [7] Chernysheva, M. et al. Carbon nanotubes for ultrafast fibre lasers. *Nanophotonics* 6, 1–30. [https:// doi. org/ 10. 1515/ nanoph- 2015- 0156](https://doi.org/10.1515/nanoph-2015-0156) (2017).
- [8] Kutz, J. N., & Brunton, S. L. (2015). Intelligent systems for stabilizing mode-locked lasers and frequency combs: machine learning and equation-free control paradigms for self-tuning optics. *Nanophotonics*, 4(4), 459-471.
- [9] Fermann, M. E., & Hartl, I. (2013). Ultrafast fibre lasers. *Nature photonics*, 7(11), 868-874.
- [10] Fu, W., Wright, L. G., Sidorenko, P., Backus, S., & Wise, F. W. (2018). Several new directions for ultrafast fiber lasers. *Optics express*, 26(8), 9432-9463.
- [11] Smirnov, S., Kobtsev, S., Kukarin, S., & Ivanenko, A. (2012). Three key regimes of single pulse generation per round trip of all-normal-dispersion fiber lasers mode-locked with nonlinear polarization rotation. *Optics express*, 20(24), 27447-27453.
- [12] Kobtsev, S., Smirnov, S., & Kukarin, S. (2016). Double-scale pulses generated by mode-locked fibre lasers and their applications. *Fiber Laser*, 4, 69.
- [13] Woodward, R. I., & Kelleher, E. J. (2016). Towards ‘smart lasers’: self-optimisation of an ultrafast pulse source using a genetic algorithm. *Scientific reports*, 6(1), 1-9.
- [14] Iegorov, R., Teamir, T., Makey, G., & Ilday, F. Ö. (2016). Direct control of mode-locking states of a fiber laser. *Optica*, 3(12), 1312-1315.
- [15] Baumeister, T., Brunton, S. L., & Kutz, J. N. (2018). Deep learning and model predictive control for self-tuning mode-locked lasers. *JOSA B*, 35(3), 617-626.

- [16] Brunton, S. L., Fu, X., & Kutz, J. N. (2013). Extremum-seeking control of a mode-locked laser. *IEEE Journal of Quantum Electronics*, 49(10), 852-861.
- [17] Andral, U., Fodil, R. S., Amrani, F., Billard, F., Hertz, E., & Grelu, P. (2015). Fiber laser mode locked through an evolutionary algorithm. *Optica*, 2(4), 275-278.
- [18] Andral, U., Buguet, J., Fodil, R. S., Amrani, F., Billard, F., Hertz, E., & Grelu, P. (2016). Toward an autsetting mode-locked fiber laser cavity. *JOSA B*, 33(5), 825-833.
- [19] Winters, D. G., Kirchner, M. S., Backus, S. J., & Kapteyn, H. C. (2017). Electronic initiation and optimization of nonlinear polarization evolution mode-locking in a fiber laser. *Optics Express*, 25(26), 33216-33225.
- [20] Fu, X., Brunton, S. L., & Kutz, J. N. (2014). Classification of birefringence in mode-locked fiber lasers using machine learning and sparse representation. *Optics express*, 22(7), 8585-8597.
- [21] Brunton, S. L., Proctor, J. L., & Kutz, J. N. (2016). Discovering governing equations from data by sparse identification of nonlinear dynamical systems. *Proceedings of the national academy of sciences*, 113(15), 3932-3937.
- [22] Nyushkov, B. N., Kobtsev, S. M., Ivanenko, A. V., & Smirnov, S. V. (2019). Programmable optical waveform generation in a mode-locked gain-modulated SOA-fiber laser. *JOSA B*, 36(11), 3133-3138.
- [23] Nyushkov, B., Ivanenko, A., Smirnov, S., Shtyrina, O., & Kobtsev, S. (2020). Triggering of different pulsed regimes in fiber cavity laser by a waveguide electro-optic switch. *Optics express*, 28(10), 14922-14932.
- [24] Horowitz, M., Barad, Y., & Silberberg, Y. (1997). Noiselike pulses with a broadband spectrum generated from an erbium-doped fiber laser. *Optics letters*, 22(11), 799-801.
- [25] Buckley, J. R., Wise, F. W., Ilday, F. Ö., & Sosnowski, T. (2005). Femtosecond fiber lasers with pulse energies above 10⁷ nJ. *Optics letters*, 30(14), 1888-1890.
- [26] Kieu, K., Renninger, W. H., Chong, A., & Wise, F. W. (2009). Sub-100 fs pulses at watt-level powers from a dissipative-soliton fiber laser. *Optics letters*, 34(5), 593-595.
- [27] Tian, X., Tang, M., Shum, P. P., Gong, Y., Lin, C., Fu, S., & Zhang, T. (2009). High-energy laser pulse with a submegahertz repetition rate from a passively mode-locked fiber laser. *Optics letters*, 34(9), 1432-1434.
- [28] Zhang, H., Bao, Q., Tang, D., Zhao, L., & Loh, K. (2009). Large energy soliton erbium-doped fiber laser with a graphene-polymer composite mode locker. *Applied Physics Letters*, 95(14), 141103.
- [29] Russbuedt, P., Mans, T., Weitenberg, J., Hoffmann, H. D., & Poprawe, A. R. (2010). Compact diode-pumped 1.1 kW Yb: YAG Innoslab femtosecond amplifier. *Optics letters*, 35(24), 4169-4171.

- [30] Molinari, D., & Fratalocchi, A. (2012). Route to strong localization of light: the role of disorder. *Optics Express*, 20(16), 18156-18164.
- [31] Lecaplain, C., Grelu, P., Soto-Crespo, J. M., & Akhmediev, N. (2012). Dissipative rogue waves generated by chaotic pulse bunching in a mode-locked laser. *Physical review letters*, 108(23), 233901.
- [32] Grelu, P., & Akhmediev, N. (2011). *Nat. Photonics* 6, 84 (2012).
- [33] Erkintalo, M., Aguergeray, C., Runge, A., & Broderick, N. G. (2012). Environmentally stable all-PM all-fiber giant chirp oscillator. *Optics express*, 20(20), 22669-22674.
- [34] Bednyakova, A. E., Babin, S. A., Kharenko, D. S., Podivilov, E. V., Fedoruk, M. P., Kalashnikov, V. L., & Apolonski, A. (2013). Evolution of dissipative solitons in a fiber laser oscillator in the presence of strong Raman scattering. *Optics express*, 21(18), 20556-20564.
- [35] Boscolo, S., Finot, C., Gukov, I., & Turitsyn, S. K. (2019). Performance analysis of dual-pump nonlinear amplifying loop mirror mode-locked all-fibre laser. *Laser Physics Letters*, 16(6), 065105.
- [36] Kokhanovskiy, A., Bednyakova, A., Kuprikov, E., Ivanenko, A., Dyatlov, M., Lotkov, D., ... & Turitsyn, S. (2019). Machine learning-based pulse characterization in figure-eight mode-locked lasers. *Optics Letters*, 44(13), 3410-3413.
- [37] Fathi, H., Närhi, M., & Gumenyuk, R. (2021, December). Towards ultimate high-power scaling: Coherent beam combining of fiber lasers. In *Photonics* (Vol. 8, No. 12, p. 566). MDPI.
- [38] Mirza, J., Ghafoor, S., Armghan, A., Elhamrawy, O. I., Jamal, L., Magam, M., ... & Qureshi, K. K. (2022). Performance Enhancement of Ytterbium-Doped Fiber Amplifier Employing a Dual-Stage In-Band Asymmetrical Pumping. *Micromachines*, 13(9), 1488.
- [39] Massa, N. (2000). *Fiber optic telecommunication. Fundamental of Photonic*, University of Connecticut.
- [40] Davis, L., & Coombs, S. (2013, August). Genetic algorithms and communication link speed design: theoretical considerations. In *Genetic Algorithms and Their Applications* (pp. 252-256). Psychology Press.
- [41] Beasley, D., Bull, D. R., & Martin, R. R. (1993). An overview of genetic algorithms: Part 1, fundamentals. *University computing*, 15(2), 56-69.
- [42] Davis, L. (1985, August). Applying adaptive algorithms to epistatic domains. In *IJCAI* (Vol. 85, pp. 162-164).
- [43] Davis, L. (1991). *Handbook of genetic algorithms*.
- [44] Whitley, L. D., Starkweather, T., & D'Ann Fuquay. (1989, June). Scheduling problems and traveling salesmen: The genetic edge recombination operator. In *ICGA* (Vol. 89, pp. 133-40).

- [45] Davis, L. (1987). Genetic algorithms and simulated annealing.
- [46] Forrest, S., & Mayer-Kress, G. (1991). Genetic algorithms, nonlinear dynamical systems, and global stability models. *The Handbook of Genetic Algorithms*, New York: Van Nostrand Reinhold.
- [47] Duling, I. N. (1991). All-fiber ring soliton laser mode locked with a nonlinear mirror. *Optics letters*, 16(8), 539-541.
- [48] Dennis, M. L., & Duling, I. N. (1992). High repetition rate figure eight laser with extracavity feedback. *Electronics Letters*, 20(28), 1894-1896.
- [49] Smirnov, S., Kobtsev, S., Ivanenko, A., Kokhanovskiy, A., Kemmer, A., & Gervaziev, M. (2017). Layout of NALM fiber laser with adjustable peak power of generated pulses. *Optics letters*, 42(9), 1732-1735.
- [50] Richardson, D. J., Nilsson, J., & Clarkson, W. A. (2010). High power fiber lasers: current status and future perspectives. *JOSA B*, 27(11), B63-B92.
- [51] Kutz, J. N. (2006). Mode-locked soliton lasers. *SIAM review*, 48(4), 629-678.
- [52] Kim, J., & Song, Y. (2016). Ultralow-noise mode-locked fiber lasers and frequency combs: principles, status, and applications. *Advances in Optics and Photonics*, 8(3), 465-540.
- [53] Chernysheva, M., Rozhin, A., Fedotov, Y., Mou, C., Arif, R., Kobtsev, S. M., ... & Turitsyn, S. K. (2017). Carbon nanotubes for ultrafast fibre lasers. *Nanophotonics*, 6(1), 1-30.
- [54] Baumeister, T., Brunton, S. L., & Kutz, J. N. (2018). Deep learning and model predictive control for self-tuning mode-locked lasers. *JOSA B*, 35(3), 617-626.
- [55] Chauhan, M. Z., Arcuri, J., Park, K. K., Zafar, M. K., Fatmi, R., Hackam, A. S., ... & Bhattacharya, S. K. (2020). Multi-omic analyses of growth cones at different developmental stages provides insight into pathways in adult neuroregeneration. *Iscience*, 23(2), 100836.
- [56] Dowden, J. (2009). The theory of laser materials processing. *Heat and Mass Transfer in Modern Technology*, 95-128.
- [57] Jh, H. (1975). Adaptation in natural and artificial systems. Ann Arbor.
- [58] Gorges-Schleuter, M. (1989, December). ASPARAGOS an asynchronous parallel genetic optimization strategy. In *Proceedings of the third international conference on Genetic algorithms* (pp. 422-427).
- [59] Davis, L. (1985, August). Applying adaptive algorithms to epistatic domains. In *IJCAI* (Vol. 85, pp. 162-164).
- [60] Juliff, K. (1992). Using a Multi-chromosome Genetic Algorithm to Pack a Truck. Department of Computing, Faculty of Business, Victoria University of Technology.

- [61] DeJong, K. A. (1975). Analysis of the behavior of a class of genetic adaptive systems. PhD thesis, Dept. of Computer and Communication Sciences. University of Michigan, 1975.
- [62] Fu, X., & Kutz, J. N. (2013). High-energy mode-locked fiber lasers using multiple transmission filters and a genetic algorithm. *Optics express*, 21(5), 6526-6537.
- [63] Narayan, J., Brown, W. L., & Lemons, R. (1982). *Laser/Solid Interactions and Transient Thermal Processing of Materials*. Boston, 1983.
- [64] Haus, H. A. (2000). Mode-locking of lasers. *IEEE Journal of Selected Topics in Quantum Electronics*, 6(6), 1173-1185.
- [65] Krstic, M., & Wang, H. H. (2000). Stability of extremum seeking feedback for general nonlinear dynamic systems. *Automatica-Kidlington*, 36(4), 595-602.
- [66] Choi, J. Y., Krstic, M., Ariyur, K. B., & Lee, J. S. (2002). Extremum seeking control for discrete-time systems. *IEEE Transactions on automatic control*, 47(2), 318-323.
- [67] Ariyur, K. B., & Krstic, M. (2003). *Real-time optimization by extremum-seeking control*. John Wiley & Sons.
- [68] Wise, F. W., Chong, A., & Renninger, W. H. (2008). High-energy femtosecond fiber lasers based on pulse propagation at normal dispersion. *Laser & Photonics Reviews*, 2(1-2), 58-73.
- [69] Fu, W., Wright, L. G., Sidorenko, P., Backus, S., & Wise, F. W. (2018). Several new directions for ultrafast fiber lasers. *Optics express*, 26(8), 9432-9463.
- [70] Turitsyn, S. K., Bale, B. G., & Fedoruk, M. P. (2012). Dispersion-managed solitons in fibre systems and lasers. *Physics reports*, 521(4), 135-203.
- [71] Bale, B. G., Okhitnikov, O. G., & Turitsyn, S. K. (2012). Modeling and technologies of ultrafast fiber lasers. *Fiber Lasers*, 135-175.
- [72] Kutz, J. N., & Brunton, S. L. (2015). Intelligent systems for stabilizing mode-locked lasers and frequency combs: machine learning and equation-free control paradigms for self-tuning optics. *Nanophotonics*, 4(4), 459-471.
- [73] Kim, J., & Song, Y. (2016). Ultralow-noise mode-locked fiber lasers and frequency combs: principles, status, and applications. *Advances in Optics and Photonics*, 8(3), 465-540.
- [74] Chernysheva, M., Rozhin, A., Fedotov, Y., Mou, C., Arif, R., Kobtsev, S. M., ... & Turitsyn, S. K. (2017). Carbon nanotubes for ultrafast fibre lasers. *Nanophotonics*, 6(1), 1-30.
- [75] Baumeister, T., Brunton, S. L., & Kutz, J. N. (2018). Deep learning and model predictive control for self-tuning mode-locked lasers. *JOSA B*, 35(3), 617-626.
- [76] Chauhan, M. Z., Arcuri, J., Park, K. K., Zafar, M. K., Fatmi, R., Hackam, A. S., ... & Bhattacharya, S. K. (2020). Multi-omic analyses of growth cones at different

developmental stages provides insight into pathways in adult neuroregeneration. *Science*, 23(2), 100836.

[77] Shtyrina, O. V., Yarutkina, I. A., Skidin, A., Fedoruk, M. P., & Turitsyn, S. K. (2015). Impact of the order of cavity elements in all-normal dispersion ring fiber lasers. *IEEE Photonics Journal*, 7(2), 1-7.

[78] Zouridakis, G. (2003). *Biomedical technology and devices handbook*. CRC press.

[79] Mukherjee, S., Wysock, J. S., Ng, C. K., Akhtar, M., Perner, S., Lee, M. M., ... & Scherr, D. S. (2009, February). Human bladder cancer diagnosis using Multiphoton microscopy. In *Photonic Therapeutics and Diagnostics V* (Vol. 7161, pp. 194-203). SPIE.

[80] Ohkawa, A., Miwa, H., Namihisa, A., Kobayashi, O., Nakaniwa, N., Ohkusa, T., ... & Sato, N. (2004). Diagnostic performance of light-induced fluorescence endoscopy for gastric neoplasms. *Endoscopy*, 36(06), 515-521.

[81] Andresen, E. R., Sivankutty, S., Tsvirkun, V., Bouwmans, G., & Rigneault, H. (2016). Ultrathin endoscopes based on multicore fibers and adaptive optics: a status review and perspectives. *Journal of biomedical optics*, 21(12), 121506.

[82] Winzer, P. J., Neilson, D. T., & Chraplyvy, A. R. (2018). Fiber-optic transmission and networking: the previous 20 and the next 20 years. *Optics express*, 26(18), 24190-24239.

[83] Noordegraaf, D., Skovgaard, P. M., Nielsen, M. D., & Bland-Hawthorn, J. (2009). Efficient multi-mode to single-mode coupling in a photonic lantern. *Optics express*, 17(3), 1988-1994.

[84] Love, J. D., Henry, W. M., Stewart, W. J., Black, R. J., Lacroix, S., & Gonthier, F. (1991). Tapered single-mode fibres and devices. Part 1: Adiabaticity criteria. *IEE Proceedings J (Optoelectronics)*, 138(5), 343-354.

[85] Richardson, D. J., Fini, J. M., & Nelson, L. E. (2013). Space-division multiplexing in optical fibres. *Nature photonics*, 7(5), 354-362.

[86] Seitz, W. R. (1984). Chemical sensors based on fiber optics. *Analytical Chemistry*, 56(1), 16A-34A.

[87] Farahani, M. A., & Gogolla, T. (1999). Spontaneous Raman scattering in optical fibers with modulated probe light for distributed temperature Raman remote sensing. *Journal of Lightwave Technology*, 17(8), 1379.

[88] Van De Giesen, N., Steele-Dunne, S. C., Jansen, J., Hoes, O., Hausner, M. B., Tyler, S., & Selker, J. (2012). Double-ended calibration of fiber-optic Raman spectra distributed temperature sensing data. *Sensors*, 12(5), 5471-5485.

[89] Willner, A. E., Huang, H., Yan, Y., Ren, Y., Ahmed, N., Xie, G., ... & Ashrafi, S. (2015). Optical communications using orbital angular momentum beams. *Advances in optics and photonics*, 7(1), 66-106.

- [90] Popoff, S. M., Lerosey, G., Carminati, R., Fink, M., Boccarda, A. C., & Gigan, S. (2010). Measuring the transmission matrix in optics: an approach to the study and control of light propagation in disordered media. *Physical review letters*, 104(10), 100601.
- [91] Plöschner, M., Kollárová, V., Dostál, Z., Nylk, J., Barton-Owen, T., Ferrier, D. E., ... & Čižmár, T. (2015). Multimode fibre: Light-sheet microscopy at the tip of a needle. *Scientific reports*, 5(1), 1-7.
- [92] Plöschner, M., Tyc, T., & Čižmár, T. (2015). Seeing through chaos in multimode fibres. *Nature Photonics*, 9(8), 529-535.
- [93] Freund, I., Rosenbluh, M., & Feng, S. (1988). Memory effects in propagation of optical waves through disordered media. *Physical review letters*, 61(20), 2328.
- [94] Tzang, O., Niv, E., Singh, S., Labouesse, S., Myatt, G., & Piestun, R. (2019). Wavefront shaping in complex media with a 350 kHz modulator via a 1D-to-2D transform. *Nature Photonics*, 13(11), 788-793.
- [95] Stasio, N., Conkey, D. B., Moser, C., & Psaltis, D. (2015). Light control in a multicore fiber using the memory effect. *Optics Express*, 23(23), 30532-30544.
- [96] Banerjee, J. S., Goswami, D., & Nandi, S. (2014). OPNET: a new paradigm for simulation of advanced communication systems. In *Proceedings of International Conference on Contemporary Challenges in Management, Technology & Social Sciences, SEMS* (pp. 319-328).

الخلاصة

في الأونة الأخيرة ، أدى تطور الاتصالات المعاصرة إلى التوسع الأسيوي في المعلومات والتكنولوجيا. الإتصال من أجل الحصول على سرعات عالية للإشارة ، يتم الآن استخدام الألياف الضوئية ليس فقط في أنظمة المهاتفة ولكن أيضاً في الإنترنت وشبكات المنطقة المحلية. في الألياف الضوئية أحادية الوضع ، تم فحص تأثير الانحناء على الضوء المتماسك. يتم استخدام الألياف الضوئية أحادية النمط المكونة من السيليكا والأسطوانات الدوارة بأقطار مختلفة في هذه الأطروحة. أصبح الليزر مع الألياف البصرية حلقة المرآة المزدوجة مؤخراً أحد أهم الموضوعات. أبلغ العديد من الباحثين عن المشكلة الرئيسية في هذا النوع من الأنظمة وهي عدم الخطية لخصائص التضخيم. يتمثل أحد الحلول لهذه المشكلة الحاسمة في استخدام خوارزمية التعلم العميق والبحث التطوري. في هذه الرسالة تم اقتراح الخوارزمية التطورية الرئيسية لنموذج المحاكاة الضوئية وعرض نتائج المحاكاة لحل هذه المشكلة. لاحظ المؤلف أن بنية البرنامج التي تستخدم التطورات في التحكم التكيفي والتعلم الآلي توفر أفضل منصة تكامل للبصرييات ذاتية الضبط. من أجل تنفيذ وحدة برامج التدريب والتنفيذ القادرة على الضبط الذاتي لتجويد الليزر حتى في حالة وجود اضطرابات ميكانيكية و / أو بيئية ، يمكن دمج وحدات التحكم المؤازرة مع مكونات الاتصالات الضوئية المتاحة تجارياً لأجهزة الليزر ذات الوضع المغلق. يمكن أن يؤدي هذا إلى استقرار لفة التردد. في خطوة تدريب الخوارزمية ، يتم البحث في مساحة المعلمة بدقة لتحديد مجالات الأداء المثلى لوظيفة موضوعية مثيرة للاهتمام أو أكثر. يتم استخدام ثلاثة تنشيطات مع تقنيات التحسين العالمية ، والخوارزمية الجينية للعثور على أفضل وأقصر مدة نبضة ليزر ، وتجد الحل الأمثل 20 جيلًا. المعرف $1 = 5.9$ مللي أمبير و $id2 = 1.9$ مللي أمبير. تعمل وحدة التحكم PI على تحسين الأداء بزوايا مثالية.



جمهورية العراق
وزارة التعليم العالي والبحث العلمي
جامعة الفرات الأوسط التقنية
الكلية الفنية الهندسية – النجف

تعزير أداء ليزر ألياف سلسلة الكسب المزدوج

حيدر يحيى سعيد

ماجستير في هندسة تقنيات الاتصالات

تشرين الثاني / ٢٠٢٢



تعزير أداء ليزر ألياف سلسلة الكسب المزدوج

الرسالة

مقدمة الى قسم هندسة تقنيات الاتصالات كجزء من متطلبات نيل درجة الماجستير

في هندسة تقنيات الاتصالات

تقدم بها

حيدر يحيى سعيد

إشراف

م.د. حسام نعمان محمد علي

أ.د. علي عبد العباس البكري

٢٠٢٢